The extent of mRNA destabilization and genetic factors of rapid *GAP1* mRNA clearance upon a nitrogen upshift.

by

Darach Miller

A dissertation submitted in partial fulfillment
of the requirements for the degree of
Doctor of Philosophy
Department of Biology
New York University
May, 2018

David Gresham

"Science is a match that a person has just got alight. They thought they were in a room — in moments of devotion, a temple — and that this light would be reflected from and display walls inscribed with wonderful secrets and pillars carved with philosophical systems wrought into harmony.

It is a curious sensation, now that the preliminary splutter is over and the flame burns up clear, to see lit just their hands and just a glimpse of themselves and the patch they stand on visible, and around them, in place of all that comfort and beauty they anticipated, darkness still."

- H.G. Wells, 1891,
adapted for 2018

Acknowledgements

Sailing works to juxtapose a variety of forces against each other such that they have no other option than to cause progress. Without sails there's no push, without a keel there's nothing to push off of, and a tiller's important for deciding where the push is to proceed. Without the right constraints and re-direction the system is a mess, and destined for the rocks. A rope does not sail upwind but depends on the cleats, pulleys, mast, hull, and so on. Many human endeavors can be described with this metaphor, with a variety of forces, pressures, and opportunities balancing to make progress. Here, I acknowledge some of the people that have made my progress here possible.

The culture built over these many years at NYU Biology has been important for me completing this work. As Benjy Neymotin pointed out several years ago: "it takes a village", and here one continues to grow. Specifically, I thank the kind folks in CGSB, especially our neighbors in the research group lead by Christine Vogel on the 4th floor. We've shared space and scientific discussions, and I owe much inspiration to the compassionate leadership that Professor Vogel consistently demonstrates (as well as for introducing me to Michi and the Tobraza's). I also thank Ken Birnbaum and his group for helpful conversations and access to the lucky FISH incubator, and Edo Kussell and his group for equipment and discussions. The GenCore, led by Tara Rock, has been valuable with labor and guidance from Nicholas Rouillard, Mohammed Khalfan, Pui-Leng Ip, Gina Viavattene, and Theresa Ten Eyck. Across the street in Brown, I thank Viji Subramanian, Andreas Hochwagen, and his research group for microscope use and tolerating my questions. Also, Tovah Markowitz for making important research progress several years ago. I thank Andres Mansisidor and Matt Paul for helpful reading and comments on the paper, and other help. Additionally, I thank Nick DelRose, Anna Houshangi, Kostya Tchourine for comradery, support, and walking me out of Langone.

I must also thank Sherry Scott and the rest of the administrative staff for running this

department and making sure the academics are taken care of, feed, and able to do what they do. These folks, and the thousands of workers who do the work of the power and utilities, safe structures and equipment, public safety, and logistics that are required to operate any institution but especially a research university, these folks make NYU possible in a fundamental way.

Away from NYU, I thank Evelina Tutucci for demonstrating the mRNA FISH method to me, helping me understand just how finicky it can be. I thank Megan McClean for openly sharing a FISH protocol on OpenWetWare (although we've never spoken). I thank the Cold Spring Harbor Yeast Course, especially the instructors Maitreya Dunham, Marc Gartenberg, and Grant Brown for introducing me to the community and (re)-lighting a fire to help me finish. The experience of that course is one large reason I'm staying in science as long as I can.

From the west coast, I thank Carole Hom, Ian Korf, and Patrice Kohel at UC Davis (in 2012), Nitin Baliga and Aaron Brooks at ISB Seattle (in 2011), Richard Bonneau (NYU, but I meet him at ISB in Seattle), but most importantly Marc Facciotti at UC Davis for giving me a chance at getting into science late. It's amazing the string of opportunities that have been generously extended to me, and lead me to this point.

I thank my committee (Edo Kussell, Saeed Tavazoie, Christine Vogel, and Lionel Christiaen) for the most fun three hours I had each year for the last couple years.

I thank my mentor and advisor David Gresham for his steadfast support. His vision and daring has been essential to push this project through to completion. I also thank him for putting together a great group of people, and I thank past and present members of his laboratory at NYU for their discussions and support. Namely, Niki Athanasiadou, Naomi Ziv, Benjy Neymotin, Stephanie Lauer, Farah Abdul-Rahman, Siyu Sun, Grace Avecilla, Pieter Spealman, Chris Jackson, and especially Nathan Brandt. I am also thankful to past students including Daniel Pham, Alex Ferrena, and Stephen Nyarko.

Teaching and learning are essential for establishing the "Ignorance Gradient" that powers science, and it is hard to imagine efficient progress without someone seeking to learn what has been learned.

I thank Michi, Tai, and Henrici "Henri" Poincaré for getting me get up on time.

I thank Sarah Nguyen for keeping me together to complete the journey. We orbited each other at distance for too long, but the wait has been worth it. I am so very lucky to have meet another soul who shares the same fundamental interests in understanding and organizing the world so that others may see clearly and be cared for. I do not know if I would still be on this path had Sarah not been there to keep me moving forward, but I know that we are now together and I hope that I can have a chance to help Sarah along her path as well.

I thank my mother Sue Miller for devising a clever genetic screen for yeast strains that fail to re-initiate growth programs, as well as for being so unconditionally supportive through the years long before and during this work. I also thank my sister Kendra Miller for inspiring and egging me on, a knowingly efficacious combination of support for folks like me. I thank my father Harry Miller for winding me up to wander, and pushing me to keep looking until something worked for me. In this, he taught me on a fundamental level to never stop learning new things. I do not think my family knew this outcome was possible, but they trusted that I would find something good if I kept looking. This trio is responsible for the zealous tenacity, the Long Game, the hopes and dreams of what we can learn and be and do.

This happened because these many people, and many others, made it happen. Part of those who made it happen are those who may read or use this work. You, the reader, are part of this work, I thank you for it, and I hope that it helps you do what you need to do. If you have questions, you can always contact the author for clarification or discussion.

Abstract

Cellular responses to changing environments frequently involve rapid transcriptome reprogramming, and regulated changes in mRNA degradation rates can accelerate this process. Upon the addition of glutamine to budding yeast (*Saccharomyces cerevisiae*) limited for nitrogen, yeast cells resume rapid growth. Preceding the changes in population growth rate, the transcriptome quickly reprograms through a transition state distinct from either rapid or slow growth. As part of this, the five fastest decreasing mRNA are all Nitrogen Catabolite Repression (NCR)-regulated transporters, decreasing significantly faster than expected from their mRNA stability measured in nitrogen-replete conditions. I determined the stability of the yeast transcriptome preceding and during a nitrogen upshift using 4-thiouracil labeling and found that 78 mRNAs are destabilized, a set enriched for NCR and carbon metabolism mRNAs. To find factors specifying or effecting the destabilization, I developed a novel method combining mRNA FISH, fluorescence-activated cell sorting, and DNA barcode sequencing to screen the pooled deletion collection library for *trans* factors that mediate rapid *GAP1* mRNA repression. Modeling of the data identifies known factors of mRNA degradation, namely all three tested components of the Lsm1-7p/Pat1p complex, as being important for wild-type *GAP1* mRNA levels and dynamics. Deletions of the modulators *EDC3* and *SCD6* have more complex phenotypes including reduced clearance of *GAP1*. Re-analyzing previously collected data, I identified that a *scd6*$\triangle$, *tif4632*$\triangle$ (eIF4G2 delete), and a *GAP1* 5' UTR delete strain all share a similar phenotype of lower *GAP1* expression preceding the upshift, and reduced decay upon the upshift. This suggests a connection between translation initiation and mRNA level in different environments of nitrogen availability, and that the destabilization phenomenon may in fact be the release of a stabilizing effect on these mRNA during growth in nitrogen limitation.

Contents

Acknowledgements iv
Abstract vii

List of Figures **xi**

1 Introduction **1**
1.1 Functional transcriptome reprogramming during a nitrogen upshift 4
1.2 What is the function of rapid transcriptional repression during an increase in growth rate? 7
1.3 mRNA degradation and its regulation 9
1.3.1 Primary 5’ to 3’ pathway of mRNA degradation 9
1.3.2 Alternative pathways of mRNA degradation — 3’ to 5’ and quality control 14
1.3.3 The interaction of translation and mRNA degradation 15
1.3.4 Regulation of mRNA degradation 17
1.4 The role of stability control in transcriptome reprogramming 20
1.4.1 Stress conditions trigger rapid regulation of mRNA stability 20
1.4.2 Nutrient shifts also trigger mRNA stability changes 21
1.5 Measuring mRNA dynamics 22
1.6 Methods for determining the genetic basis of a transcript dynamics phenotype 27

2 Modeling transcript dynamics upon a nitrogen upshift **31**
2.1 Abstract 31
2.2 Introduction 32
2.3 Results 34
2.3.1 Accelerated degradation of mRNAs contributes to remodeling of the transcriptome 35
2.4 Discussion 38
2.5 Materials and methods 40

3 Measuring the extent of mRNA destabilization and screening for genetic factors of *GAP1* repression **43**
3.1 Abstract . . . 43
3.2 Introduction . . . 44
3.3 Characterizing transcriptome dynamics upon a nitrogen upshift . . . 48
3.3.1 Transcriptional reprogramming precedes physiological remodeling 48
3.3.2 Global analysis of mRNA stability changes during the nitrogen upshift 53
3.3.3 Methods and materials . . . 64
3.3.4 4tU label-chase sequencing analysis and modeling . . . 68
3.4 Estimating *GAP1* mRNA for every mutant in a pool . . . 78
3.4.1 A genome-wide screen for *trans*-factors regulating *GAP1* mRNA repression . . . 78
3.4.2 Estimating *GAP1* mRNA abundance for individual mutants . . . 84
3.4.3 Testing the roles of decapping modulators and associated components . . . 90
3.4.4 Methods and materials . . . 94
3.4.5 Methods and materials of Barseq after FACS after FISH experiment 96
3.4.6 Design and analysis of Barseq after FACS after FISH experiment . 99
3.5 Discussion . . . 114
3.6 General methods and materials . . . 118

4 Investigations of physiological remodeling upon a nitrogen upshift **123**
4.1 Changes in poly-adenylated transcript content per cell upon changes in growth rates . . . 124
4.1.1 Introduction . . . 124
4.1.2 The assay design . . . 125
4.1.3 Nutrient limitation and transcriptome size . . . 127
4.1.4 Conclusion and future directions . . . 130
4.2 Screening for genes important for remodeling physiology for growth . . . 131
4.2.1 Introduction . . . 131
4.2.2 Results . . . 133
4.2.3 Conclusion . . . 140

5 Conclusion **141**
5.1 Summary . . . 141
5.1.1 mRNA destabilization hastens functional reprogramming . . . 141

5.1.2 Decapping is important for *GAP1* clearance 143
5.1.3 Physiological changes that occur during nitrogen upshift 143
5.2 Suggested future directions 144
5.2.1 An efficient method for estimating mRNA abundance in barcoded mutant pools 144
5.2.2 All metabolism is connected 145
5.2.3 pH as a possible cause of mRNA destabilization 146
5.2.4 Possible mechanisms of *GAP1* clearance 148

References **153**

List of Figures

1.1 Core nitrogen metabolism in yeast. 5

1.2 Diagram of canonical deadenylation-dependent 5’ to 3’ mRNA degradation . 10

2.1 Accelerated mRNA degradation contributes to gene expression remodeling 36

3.1 The nitrogen upshift of population and cellular growth rate. 49

3.2 Dynamics of transcriptome remodeling during a nitrogen upshift, on a coarse scale. 50

3.3 The coarse long-term transcriptome dynamics of a glutamine upshift. 51

3.4 4tU label-chase RNA sequencing measures mRNA stability changes following a nitrogen upshift. 55

3.5 Global mRNA stability changes following a nitrogen upshift. 57

3.6 Comparison between rates of mRNA degradation and abundance changes. . 58

3.7 Many of the destabilized mRNA are members of the ESR-up regulon. 59

3.8 Significantly destabilized transcripts are not always strongly repressed. . . . 60

3.9 Six examples of individual mRNA whose regulation is more complex than a homo-directional destabilization and synthesis repression. 61

3.10 Enrichment of Hrp1p motif in 5’ UTRs of destabilized transcripts. 63

3.11 The destabilized set is longer and has a higher frequency of optimal codons than the rest of the transcriptome. 64

3.12 The proportion of spike-in counts increase over the course of the experiment. 70

3.13 Several examples of alternative normalization strategies. 71

3.14 Simulation of labeled transcript dynamics shows a slight effect from synthesis changes on a label-chase with recycling. 75
3.15 Distribution of all fit changed rates versus effect size thresholds from modeling. 76
3.16 *GAP1* mRNA dynamics by qPCR normalized to a spike-in shows the rapid clearance of *GAP1* mRNA. 79
3.17 Both the *GAP1* delete and omission of the targeting probe removes signal of GAP1 FISH. 80
3.18 *GAP1* mRNA dynamics measured by flow cytometry. 80
3.19 Example microscopy of cells sorted by *GAP1* mRNA. 81
3.20 Quantification of microscopy of cells sorted by *GAP1* mRNA. 81
3.21 Principal components analysis of the abundance estimates for samples captures variation along *GAP1* abundance. 83
3.22 Data and models for several individual sample genes from the BFF modeling. 84
3.23 Flow cytometry of the *GAP1* mRNA distribution across all mutants, and global distribution of *GAP1* mRNA abundance estimates. 85
3.24 Individual BFF estimates of *GAP1* mRNA abundance for mutants known to play a role in *GAP1* regulation. 86
3.25 Mutants of negative regulators of gluconeogenesis or sulfate assimilation are associated with defects in *GAP1* expression. 87
3.26 *tco89*Δ and *xrn1*Δ show defects in *GAP1* mRNA regulation in the BFF assay. 88
3.27 The pre-upshift mean has a significant but slight relationship in predicting the post-upshift mean. 89
3.28 Disrupting the Lsm1-7p/Pat1p complex impairs clearance of *GAP1* mRNA. . 90
3.29 Processing-body dynamics are not associated with the nitrogen upshift, by Dcp2p-GFP microscopy. 91

3.30 Disrupting core pathways of mRNA degradation, decapping modulators, or the 5' UTR impairs the clearance of *GAP1* mRNA, by qPCR 93
3.31 An example of a dimer. 100
3.32 A schematic of the barcode sequencing strategy. 103
3.33 The expected amplicon, before adding P5 sequences at the 5' end. 104
3.34 Sanger sequencing of the produced library shows the expected degenerate positions. 104
3.35 A comparison of the unique UMIs versus input UMIs for un-corrected and error-corrected UMIs. 107
3.36 Histograms of UMI observations associated with the YOR202W barcode in three samples. 108
3.37 Optimization of mutant quantification methods, looking at simulated data on a whole-lane comparison. 110
3.38 Optimization of mutant quantification methods, looking at deduplicating methods on whole comparisons. 111
3.39 Optimization of mutant quantification methods, looking at deduplicating methods on per-sample comparisons. 112

4.1 Changes in whole cell polyA content in YPD or nitrogen-limitation. 128
4.2 Changes in polyA content upon a nitrogen upshift. 129
4.3 Measuring polyA content across systematically varied growth rates in chemostats, and comparison to a spike-in normalized RNA sequencing method. 130
4.4 Glutamine upshift causes a lost in heatshock-resistance. 134
4.5 Histogram of mutant counts, within each sample. 135
4.6 Histogram of mutant counts, summed across samples. 136
4.7 Diagnostic `limma/voom` plots show the effects of low-count barcodes in confounding the noise model. 136

4.8 A *mae1*Δ mutant is slower in a glutamine upshift, but this is not rescued by supplementation with alanine or pyruvate. 139

5.1 Hypothetical adaptive role for slowed translation under low amino-acid conditions 150

5.2 Hypothetical mechanism by which translation initiation and elongation inhibit mRNA degradation — ribosome extrusion. 152

— 1 —

Introduction

Organisms adapt to their environment by expressing different phenotypes as environments change. We expect this to be an advantageous strategy, depending on the fitness consequences of each phenotype in each environment balanced against the costs of innovating and maintaining the machinery for adaptive differential gene expression (Kussell and Leibler 2005). One way to achieve this is through the regulation of gene expression. If different mechanisms of gene expression act on different properties of gene expression, or have different costs of energy or complexity, then we would expect that as the environment selects for the use of gene expression patterns that advantageously model the environment (Tagkopoulos et al. 2008), we may see the use of different mechanisms used to achieve different regulatory demands. Thus, understanding how different mechanisms can be used to regulate one particular level of gene expression may inform our understanding of these mechanisms and how multiple levels of selection balance in causing an adaptive outcome.

Expression of a protein-coding gene product involves many steps, each with a variety of opportunities for regulation. At the outset, DNA sequences that encode genetic elements are transcribed into corresponding messenger RNA (mRNA). The rate of this transcription is helped by factors that facilitate recruitment of RNA polymerase II (PolII) and is hindered by factors that block this process by physical occlusion or changes in the accessibility to the chromatin (Hahn and Young 2011). The translation of mRNA into a protein product by ribosomes occurs at different rates for different genes and different environments, and this approximately 15-fold variation (Weinberg et al. 2016)

is thought to be regulated by a complex interplay between ribosomes and associated translation factors, RNA binding proteins (RBPs), and intrinsic factors of the mRNA like length or codon-usage (Dever et al. 2016). For both the mRNA and its protein product, stability is also important (McManus et al. 2015; Pérez-Ortín et al. 2013). Additionally, localization or allosteric regulation can change the activity of a gene product. Myriad factors contribute to the expression of a gene product, and determining the functional adaptive basis for particular regulatory mechanisms, if they are indeed adaptive, would help us better understand the diversity of gene regulatory mechanisms.

The budding yeast *Saccharomyces cerevisiae* is a model system for many fields, including gene expression regulation. In response to different nutrient availabilities yeast changes its rate of growth, and this is accompanied by large changes in gene expression (Brauer et al. 2008; Conway et al. 2012) and changes in physiology (Carter et al. 1978; Waldron 1977) including a changed rate of proliferation (Slator 1918), cell size (Jorgensen et al. 2004), RNA content (Waldron and Lacroute 1975), protein content (Kief and Warner 1981), and resistance to stressors (Elliott and Futcher 1993). This integration of diverse metabolic signals into a coordinated program of growth is thought take place with multiple hierarchies of control in response to different particular types of nutrients as well as the general availability of any nutrient source (Broach 2012; Cooper 1982; Winderickx et al. 2003). These signals are integrated into a similar systemic output by well conserved growth signalling pathways of eukaryotic cells, like TORC1, Snf1p/AMPK, or PKA (Conrad et al. 2014; Thevelein 1994). Thus, the study of nutrient limitations to growth, especially with the aim of discerning particular molecular mechanisms and how these may overlap (Oliveira et al. 2015a,b; Péli-Gulli et al. 2015; Stracka et al. 2014; Tate et al. 2017) would shed light on our understanding of how a eukaryotic cell regulates its most essential project of growth in the face of diverse limitations.

Nutrient availability is described in terms of the quality and quantity of the source

provided. Quantity refers to the molar availability of the nutrient that the yeast can take up, while quality is an empirical reference to how rapidly budding yeast can biochemically incorporate the nutrient into their metabolism and grow. One prediction from this understanding is that altering the quantity of the nutrient availability to vary growth rates in a range below which the quality limits growth rates will elicit a common response between various nutrient limitations. Indeed, studies systematically varying nutrient environments have shown that about a quarter of the transcriptome is differentially expressed at different steady-state nutrient-limited growth states, regardless of nutrient used to limit growth (Brauer et al. 2008; Regenberg et al. 2006), and that a small subset of transcripts were regulated particular to the specific type of limitation. Statistical modeling of this process determined that the molecular signature of this growth-rate signalling could be captured in a small number of calibrator genes whose expression was very well correlated with changes in growth rate or perturbation of signalling pathways associated with this process, and importantly also changed during dynamic transitions or upon perturbation of growth signalling pathway PKA (Airoldi et al. 2009). Dynamic transitions to better nutrient environments (nitrogen, carbon, and phosphorus upshifts) shared a similar pattern (Conway et al. 2012), and the pattern of gene expression associated with increased nutrient availability and growth rates is similar but of opposite sign compared to the Environmental Stress Response (ESR) — a shared in co-regulation of $\sim$600 mRNA across dynamic responses to various stressors (Gasch et al. 2000). Together, this shows how yeast has a common molecular response that largely corresponds to the suitability of the sensed environment, in addition to the physiological changes previously described. A better environment translates to faster growth, with more growth associated mRNA and less stress response mRNA, and this holds true in different steady-states and in the dynamics of transitions between steady-states.

1.1 Functional transcriptome reprogramming during a nitrogen upshift

One classically studied transition between growth rates is the nitrogen upshift. Yeast grows quickly when provided with nitrogen sources like glutamine or ammonium, but can make use of various nitrogen sources like proline or urea by expressing overlapping sets of specific and general nitrogen-source permeases that concentrate these sources inside the cell for use (Grenson 1992). Various nitrogen sources are then catabolized to eventually make glutamate and glutamine, with an estimated ∼85% of macromolecular nitrogen coming from the amino nitrogen in glutamate and the rest from the side-chain of glutamine (Magasanik and Kaiser 2002). The addition of glutamine to a nitrogen-limited culture, for example grown with only the non-preferred proline as a nitrogen source, is called an upshift because it is the change from a slow growing condition to one of rapid growth (Kjeldgaard et al. 1958; Waldron 1977). Upon an upshift, a regulatory phenomenon called nitrogen catabolite repression (NCR) ensures that the set of transporters, metabolic enzymes, and regulatory factors are repressed (Cooper 1982, 2002; Magasanik and Kaiser 2002). Through the use of a temperature-sensitive glutamine synthase allele or treatment with methionine sulfoximine, it has been shown that NCR appears to respond to intracellular glutamine availability (Crespo et al. 2002; Grenson 1983; Stracka et al. 2014). However, recent work has specified that while the transient NCR correlates with glutamine abundance, persistent NCR appears independent (Fayyad-Kazan et al. 2016). Additionally, the use of a *gln1-37* mutant to prevent ammonium from glutamine conversion found that ammonium addition triggered swift repression of *GAP1* and *PUT4* despite not changing intracellular glutamine levels (Schure et al. 1998). This suggests that the sensing might not be simply glutamine abundance, but rather some sensor of flux through central nitrogen metabolism (like Gdh1p activity (Fayyad-Kazan et al. 2016)) or some other, heretofore uncharacterized signalling mech-

anism. Whatever the exact mechanism, the degree to which nitrogen sources can support growth by providing substrates of central nitrogen metabolism is sensed by yeast to appropriately and quantitatively repress catabolic genes in conditions corresponding to the degree to which they are unneeded for growth.

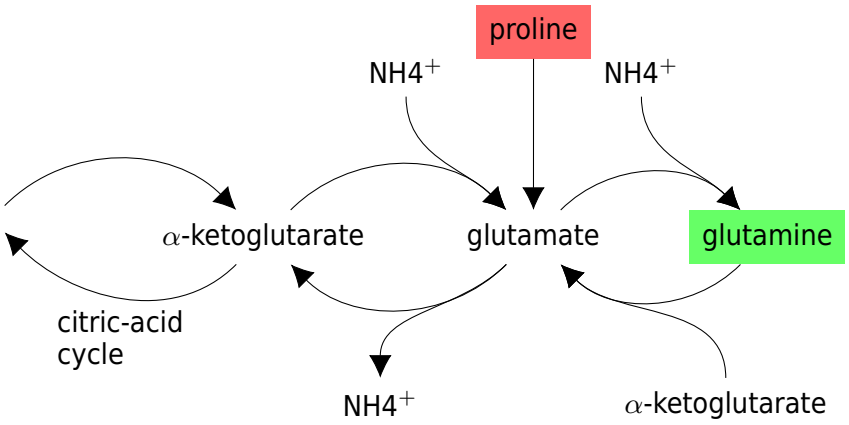

Figure 1.1: **Core nitrogen metabolism in yeast.** Glutamine (green) is a central metabolite, and is thus a preferred nitrogen source for rapid growth. Proline (red) requires specific transport and metabolic enzymes to convert it to glutamate. Redrawn from Magasanik and Kaiser 2002.

One layer of the repression occurs at the level of transcript synthesis. Four of the five GATA factors in yeast coordinate to control transcription of NCR genes, with two factors (Gln3p and Gat1p) activating transcription while two (Gzf3p and Dal80p) repress transcription (Daugherty et al. 1993; Hahn and Young 2011; Scherens et al. 2006; Stanbrough and Magasanik 1995). These factors are also subject to NCR control to different extents, with the activators increasing the expression of the repressive factors (Cunningham et al. 2000). This is thought to be an adaptation to enable quick repression upon a nitrogen upshift, as may be encountered when yeast is introduced to a new abundant nutrient environment of grape or wort. It has been long known that the eukaryotic growth signalling pathway TORC1 largely regulates these factors by controlling the activity of phosphatases and thus localization of these transcription factors, via Ure2p for Gln3p (Beck and Hall 1999; Cox et al. 2000) and unknown mechanisms for

Gat1p (Georis et al. 2008). However, the careful application of genetics has identified that the requirements for phenotypes differ in different environments, with comparisons of nitrogen starvation (8+ hours) versus limitation (<3 hours, or proline) showing that about half of the Gln3-localization regulation (resulting in transcriptional regulation of NCR) was still unexplained by TORC1 signalling alone (Tate and Cooper 2013). By way of a temperature-sensitive tRNA allele, researchers have since identified that Gcn2p impinges in a parallel pathway through the 14-3-3 proteins Bmh1/2 to promote the export of Gln3p and Gat1p (Tate et al. 2015, 2017). Additionally, others have suggested that the amino-acid permease Gap1p may directly signal to PKA (Donaton et al. 2003; Van Zeebroeck et al. 2009). Thus, multiple growth signalling pathways converge to affect the import and export of NCR GATA factors to effect multiply redundant layers of NCR transcript synthesis control.

Gene product regulation can also occur post-translationally. NCR has primarily referred to the control of transcript synthesis rates, but it has been long observed that upon addition of a preferred nitrogen source the enzymatic and permease activities are repressed faster than can be caused by a shut-off of synthesis (Cooper and Sumrada 1983). A classical NCR-regulated gene is the general amino-acid permease *GAP1*. Gap1p transport activity is repressed much faster than the re-localization and degradation of the protein-product (Stanbrough and Magasanik 1995), and we know that this Gap1p shut-off is adaptive (Risinger et al. 2006), perhaps due to an excess of amino-acid transport causing ammonia toxicity (Hess et al. 2006) or excess proton symport driving a depolarization against futile Pma1p proton-export activity. This growth phenotype allowed the early identification of mutants in this process, and this indicates that it is mediated by a ubiquitinyation mark that inactivates the permease and leads to relocalization and degradation (Grenson 1983; Merhi and André 2012; Risinger and Kaiser 2008). Thus multiple layers redundantly repress the NCR-regulated Gap1p.

In Chapters 2 and 3, I show how mRNA degradation also plays a role in this repression, inactivating some NCR mRNA as well as mRNA associated with other metabolic processes.

1.2 What is the function of rapid transcriptional repression during an increase in growth rate?

A landmark integrative study of proteome and transcriptome dynamics (Lee et al. 2011) showed that for most cases of mRNA repression upon osmotic stress, there was not a correlated downregulation of protein products in the same timescale. This asymmetry makes sense, with protein gene-products being approximately 30-50 times more stable than the mRNA intermediate (Christiano et al. 2014). Given the assumption that adaptation implies function (Gould and Lewontin 1979), what purpose might this rapid repression of mRNA fulfill?

An increase in growth rate is associated with a rapid up-regulation of the ribosomal protein (RP) and ribosome biogenesis (RiBi) regulons (Griffioen et al. 1996; Jorgensen et al. 2004). These regulons comprise the protein subunits and biogenesis factors responsible for ribosome biogenesis, and their relative abudnance is well-correlated with growth rate in both dynamic and steady-state conditions (Airoldi et al. 2009; Brauer et al. 2008). While some of the more numerous macro-molecules in the cell, ribosomes are not infinite and the majority are likely engaged in peptide elongation (Boehlke and Friesen 1975; Haar 2008; Shah et al. 2013), and are less abundant (Kief and Warner 1981; Powers and Walter 1999) and with a lower rate of overall translation (Waldron et al. 1977) in slow-growth conditions.

The relative allocation of gene expression resources in the cell is a fundamentally important decision cells must make, and modeling of this phenomenon across various conditions in *E. coli* has led to a simple partitioning model in which the proteome can

be divided into functional sectors (Scott et al. 2010, 2014). While these simple models might explain the balance during steady-state growth, how does the relative allocation of gene expression machinery change during transitions? In particular, what is the best approach to re-balancing this allocation upon the resumption of rapid growth (Erickson et al. 2017)?

Recent work has explored this to identify that an optimal strategy would be to re-invest gene expression machinery activity in the task of expressing more gene expression machinery, at the neglect of an investment in metabolic enzymes (Giordano et al. 2016). This phenomenon, a transient burst of ribosomal over production or a "bang-bang singular" strategy appears to have been observed in yeast before in upshifts (Griffioen et al. 1996; Wehr and Parks 1969) and recently by our lab in nitrogen upshifts (Airoldi et al. 2016). Thus, concordant repression of stress-response and metabolism gene expression is theoretically expected to allow more focus of gene expression machinery on this pulse of production. There is evidence for this in *E. coli*, where Shachrai et al. 2010 induced the expression of a fluorescent protein at different growth stages to show that induction during lag phase had a significant impact on lag duration, while induction during exponential phase did not have a significant effect on growth. This is also true in yeast, where misexpression of transgenic fluorophores has a cost during this period of advantageous focus on producing gene expression machinery (Kafri et al. 2016), although this may be mediated by the maintenance of additional stores of under-utilized ribosomes (Metzl-Raz et al. 2017; Waldron et al. 1977). Thus, the repression of newly unneeded mRNA in yeast may serve a role to reallocate the extant translational capacity of the cell to enact a growth-optimal program (Kief and Warner 1981). Others have suggested that swift repression may instead help to recycle nucleotides (Kresnowati et al. 2006), so identifying the genetic factors responsible for the repression would allow us to test if a particular regulatory event, perhaps a destabilization of mRNA, is indeed

adaptive and by which mechanism.

1.3 mRNA degradation and its regulation

Even when considering only the regulation of mRNA abundance, there are at least two processes that contribute — that of synthesis and degradation. We know much about transcript synthesis, perhaps owing to the fact that virtually all events of mRNA synthesis pass through a well-characterized reaction of synthesis by RNA Pol II, capping and polyadenylation, and export into the cytoplasm. The details may vary, but the common pathway is the same. mRNA degradation does have a main pathway that performs the bulk of mRNA degradation, but mRNA are also subject to divergent redundant pathways that have been challenging to measure. Moreover, the rates of these various processes are subject to control in ways less well-understood. While some similarity is thought to exist in how RBPs may recognize *cis*-element sequences in RNA similar to how TFs recognize upstream activating or repressing sequences in DNA, the single-stranded nature of mRNA complicates this process with that ability to form diverse secondary structures that can block linear *cis*-elements (Li et al. 2010). Additionally, these secondary structures of RNA may be recognized as the *cis*-element (Aviv et al. 2003; She et al. 2017), complicating our approaches to recognize these patterns (Goodarzi et al. 2012).

1.3.1 Primary 5’ to 3’ pathway of mRNA degradation

The canonical protein-coding mRNA is synthesized in the nucleus from a DNA template by RNA PolII, and is capped co-transcriptionally at the 5’ end with a m7G cap. As PolII transcribes sequence 3’ of the stop codon the cleavage factor complex (of which Hrp1p is a sub-unit (Chen and Hyman 1998)) recognizes *cis*-element binding motifs in the RNA to direct cleavage and polyadenylation to specific sites in the mRNA.

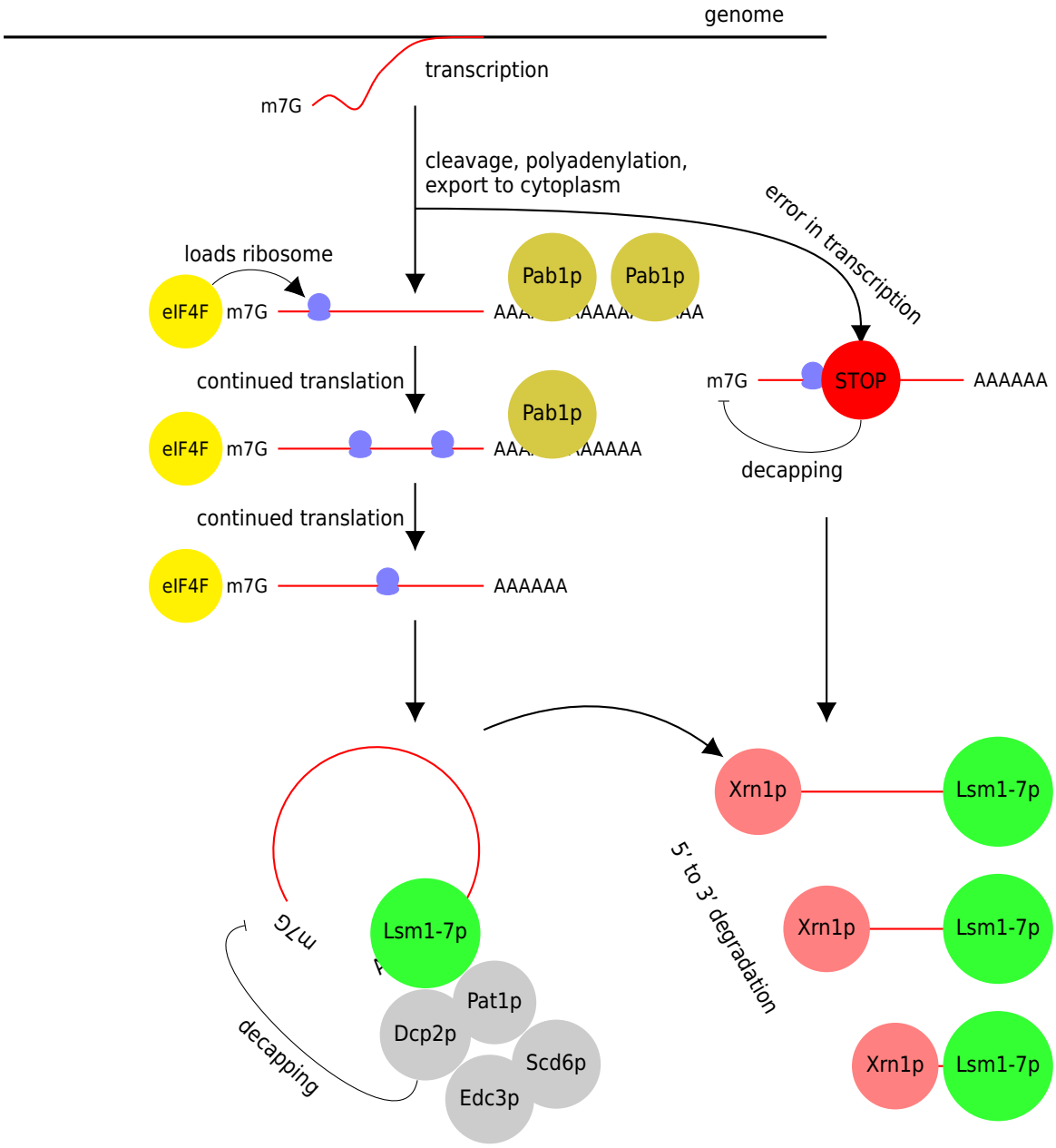

Figure 1.2: **Diagram of canonical deadenylation-dependent 5' to 3' mRNA degradation** Newly transcribed and poly-adenylated mRNA are progressively deadenylated until the Lsm1-7p/Pat1p complex binds to recruit decapping factors and Dcp2p. Co-transcriptional proof-reading surveils the transcript for aberrant translation dynamics. Nonsense-mediated decay, for example, triggers decapping. A decapped mRNA is rapidly degraded from 5' to 3' by Xrn1p.

Upon successful completion of this process, the nascent mRNA is exported to the cy-

toplasm where it enters into the pool of translatable mRNA. Typically, translation begins when initiation factors load ribosomal subunits to scan the 5' leader or untranslated region (UTR) for the start codon, where the process of coding sequence translation begins. These initiation factors (eIF4F) bind the m7G cap to load ribosome subunits (Dever et al. 2016), and thus most translation depends on the cap (with exceptions demonstrated by internal ribosome entry sites (Gilbert et al. 2007)). The m7G cap is also critical for mRNA stability. Xrn1p is a highly-processive combination of helicase and exonucleolytic domains that alone can rapidly degrade transcripts from a 5' to 3' end, recognizing unprotected 5' phosphorylated ribonucleotides as substrates (Parker 2012). Thus, the inverted linkage of the m7G escapes degradation.

During rounds of translation the poly-adenosine tail is shortened from about 65-90 adenosines to about 10 adenosines by a combination of the Pan2/3 and Ccr4/Pop2 deadenylase complexes, with activity antagonized by the poly-A binding protein Pab1p (Decker and Parker 1993; Parker 2012). When the tail is thus shortened, the Lsm1-7p/Pat1p complex binds the remainder of the poly-A tail (Tharun et al. 2000). This complex is a heptameric ring of the Lsm1-7 proteins with the Lsm1p's C-terminal domain elegantly spanning the center (Sharif and Conti 2013), and the last eight residues projecting into this center and critical for binding the shortened poly-A tail (Chowdhury et al. 2016). The critical function of this complex is to recruit and promote activity of the decapping complex to the 5' end of the mRNA, and in cooperation with Pat1p (Chowdhury et al. 2014) the binding of this complex to mRNA and to decapping factors is indeed correlated with decapping of the mRNA (Chowdhury and Tharun 2009). Thus, the complex maps the deadenylated status to the next step in mRNA degradation.

A cytoplasmic mRNA without a 5' m7G cap is not long lived, by virtue of Xrn1p, thus the recruitment and activation of the decapping complex is thought to be the key regulatory step in rates of mRNA degradation (Coller and Parker 2004). Dcp2p carries

out the catalytic activity of the holoenzyme but is promoted by the effects of Dcp1p, and in comparing *in vitro* to functional *in vivo* assays of mutants it appears that the catalytic rate of the enzyme is not the limiting step (Tharun and Parker 1999). Rather it is re-modeling of the mRNP (mRNA-protein) complex that leads to association of the decapping enzyme complex with the 5' cap, and the rate of this process determines the activity of this degradation pathway (Tharun and Parker 2001). This decapping-enzyme-localization process is promoted by the Lsm1-7p/Pat1p complex and inhibited by poly-A binding protein Pab1p (perhaps by competition of Pab1p with Lsm1-7p/Pat1p for the poly-A tail) and eIF4E (Caponigro and Parker 1996; Coller and Parker 2004). eIF4E and eIF4G compose the cap-dependent translation-initiation factor eIF4F (Dever et al. 2016), which gives rise to an elegant model of competition for the 5' m7G cap to explain the observation that translation initiation inhibits decapping (Huch and Nissan 2014). The requirement of sufficient poly-A tail for Pab1p to bind is consistent with the effect of deadenylation in promoting decapping (Parker 2012), and thus a model has emerged wherein deadenylation promotes the association of the Lsm1-7p/Pat1p complex to the shortened poly-A tail, then re-arranges to associate this 3' end of the mRNA molecule with the 5' end, resulting in an interaction that recruits and triggers decapping of the mRNA. The Lsm1-7p/Pat1p complex and Dcp2p/Dcp1p are physically associated (by co-immunoprecipitation) with several factors that genetically modulate the activity of remodeling step —Dhh1p, Edc3p, and Scd6p (Nissan et al. 2010).

Dhh1p is a helicase that associates with polysomes (mRNA with multiple ribosomes bound) and has been recently demonstrated to be genetically required for the relationship between codon optimality and mRNA stability (Presnyak et al. 2015; Radhakrishnan et al. 2016; Sweet et al. 2012). Curiously, tethering Dhh1p to a 3' UTR using the MS2 system resulted in lower translation rate of an mRNA despite causing more ribosomes to be associated with the mRNA (Sweet et al. 2012), suggesting that Dhh1p resolves

slowly translating ribosomes by promoting decapping and mRNA degradation. However, physically tethering Dhh1p may affect its role if topology of interactions is important or movement along the mRNA is important for its function. Dhh1p also appears to play a role in promoting the association of mRNPs into processing bodies.

Edc3p physically associates with the decapping complex and stimulates its activity (Nissan et al. 2010), but it has also been shown to be important (Decker et al. 2007; Huch et al. 2016) but not critical (Rao and Parker 2017) for the formation of processing-bodies. These are microscopically visible foci of mRNA and degradation factors that form in response to stress conditions but are assumed to be condensed from mRNA-protein complexes that exist before stress (Lui et al. 2014; Rao and Parker 2017; Sheth and Parker 2003). A mutant deleted of *EDC3* and the C-terminal domain of the essential *LSM4* is deficient in processing-body formation, and surprisingly this processing-body deficiency also correlates with a deficiency in the stabilization of several mRNA upon osmotic stress (Huch and Nissan 2017). Edc3p plays a role in promoting the association of mRNPs together into processing-bodies, and perhaps its effect on decapping is by virtue of co-localizing degradation factors in processing bodies.

Scd6p inhibits the formation of the 48S pre-initation complex (when the 40S subunit associates with eIF4E cap-dependent initiation factors and begins to scan the 5' UTR) via forming its own cap-binding complex with eIF4G subunit eIF4G1 in an arginine-methylation-dependent manner (Poornima et al. 2016; Rajyaguru et al. 2012). This is thought to physically occlude the normal initiation complex from binding. Scd6p also binds to several other factors in the Lsm1-7p/Pat1p deadenylation-promoting complex (Nissan et al. 2010), and thus may play an indirect role in preventing the pre-initiation complex from binding and stabilizing the mRNA through translation.

1.3.2 Alternative pathways of mRNA degradation — 3’ to 5’ and quality control

Other pathways of mRNA degradation exist. If the poly-A tail is completely removed, the cytoplasmic exosome complex can degrade the mRNA from 3’ to 5’. This redundant mechanism allows a *xrn1*Δ mutant to grow, although slowly, as the 5’ to 3’ pathway is throught to effect the bulk of mRNA degradation (Parker 2012). The balance between the two may be because of the enzymatic rate of digestion, but more likely because the binding of the Lsm1-7p complex to the shortened poly-A tail protects the mRNA from further deadenylation and thus inhibit this 3’ pathway (Tharun 2009).

Three other pathways are known to act as a co-translational layer of quality control, where errors detected by abnormal translation processes result in destruction of the presumably defective mRNA. Nonsense-Mediated Decay (NMD) is the canonical example of this. A mutation, transcriptional error, alternative splicing event, or abnormal translational event (like leaky scanning or a uORF, explained later) can cause an mRNA to have a stop codon well before the usual position, which is recognized for destruction by a deadenylation-independent decapping and 5’ to 3’ decay (Muhlrad and Parker 1994). How the aberrant nature of the misplaced stop codon is detected is still a mystery, but NMD sensitivity is known to be more active at the 5’ end of the coding sequence (after translating a sufficient stretch of amino-acids), with activity reducing towards the 3’ end of the transcript (Losson and Lacroute 1979). Non-Stop Decay refers to the inverse of NMD, no stop codon. Ribosomes that over-run into the poly-A tail recruit degradation by the 3’ exonuclease (Schmid and Jensen 2008). No-Go Decay is named for the phenomenon that triggers it, when ribosomes "no go" (encounter a difficult to elongate sequence). Difficult to translate sequences (such as arginine or lysine repeats) trigger the endonucleolytic cleavage of the offending mRNA, which is then degraded from the cut site towards both ends (Doma and Parker 2006). While the molecular mechanisms

of this process have been not been comprehensively defined, it has been shown that it is likely the ribosome collisions that promote the ribosome ubiquitination associated with the triggering of No-Go decay (Simms et al. 2017), and other work has suggested that the protein Asc1p (Ikeuchi and Inada 2016) or K63 ubiquitination (Saito et al. 2015) may play a role. Thus a model for ribosomal subunits sensing ribosome collisions and activating this quality control pathway through ubiquitination of ribosome-associated factors offers an elegant mechanism to sense locally-stalled ribsomes, although this idea is still beginning to be explored.

Together these pathways surveil translating mRNAs for defects, but it is likely that false positives in the recognition process also contribute to their regulatory effects. Disruption of the NMD pathway is associated with different expression of many transcripts. Recent genome-wide analysis identifying ∼900 mRNA upregulated upon deletion of any of UPF1-3, and subsequent ribosome profiling found this targeting to be associated with out-of-frame translation effects and non-optimal codons (Celik et al. 2017). NMD has been implicated in the regulation of ribosomal subunit protein pre-mRNA (Garre et al. 2013) in different environmental conditions, has been shown to interact genetically with Hrp1p and cis-elements spanning the start codon of PPR1 mRNA to target this mRNA for degradation (Kebaara et al. 2003; Pierrat et al. 1993), and may be triggered by upstream open reading frames (uORFs, discussed later). These could be specific regulatory events, or aberrant probabilistic activation due to the sensitivity of co-translational quality control (Celik et al. 2017).

1.3.3 The interaction of translation and mRNA degradation

Codon-optimality refers to the concept that certain codons are translated by the ribosome more quickly than other codons. This is thought to result in part from changes in tRNA abundance and in part due to intrinsic differences in the decoding rates (Curran and Yarus 1989; Thomas et al. 1988), and is often quantified using the tRNA adaptation

index (tAI) (Reis et al. 2004). The expectation that tRNA availability is associated with increased rates of translation has been tested with more recent ribosome footprint profiling experiments, and consistent with this ribosomes tend to occupy optimal codons less often (Weinberg et al. 2016).

The functional relationship between codon-optimality and mRNA degradation rate had been considered and rejected by a review of single-transcript studies (Caponigro and Parker 1996). However, with the advent of accurate genome-wide measurements of mRNA degradation rates, we are able to explore the generality of this principle in a relatively unbiased way. Several groups (Cheng et al. 2017; Harigaya and Parker 2016; Neymotin et al. 2016; Presnyak et al. 2015) have found that poor codon-optimality and lower ribosome density is associated with a higher degradation rate when considered on a per-transcript basis. This can be explained through multiple models. One model is that translation elongation rates are sensed, with slower elongation accelerating the degradation of mRNA. Jeff Coller's group has worked extensively on Dhh1p, and found that it is genetically required for the clear relationship between codon-optimality and mRNA stability (Presnyak et al. 2015; Radhakrishnan et al. 2016). Although the mechanism is at this point unclear, Dhh1p's genetic association is an important link from which to start.

Alternatively, competition between decapping enzymes and translation initiation factors for access to the 5' m7G cap has long been proposed as a mechanism by which the two processes interact (Schwartz and Parker 1999, 2000). Karsten Weis' group (Chan et al. 2017) reproduced the result that slowing elongation with cycloheximide, sordarin, or 3AT treatment slows mRNA degradation, but conversely inhibition of initiation with hippuristanol or a dominant negative eIF4E increased degradation rates. These measurements were made using 4-thiouracil and RNA sequencing, similar to RATEseq (Neymotin et al. 2014). The connection between the effect of elongation rates and ini-

tiation rates could also be explained by the effect of slow elongation rates inhibiting initiation events, as predicted (Shah et al. 2013) and measured (Chu et al. 2014).

Thus, much evidence points to competition between translation initiation and 5' to 3' degradation initiation at the cap as a major determinant of mRNA stability, although the molecular work with Dhh1p suggests that events after initiation still play a role. Other mRNA degradation pathways like NMD or NGD during elongation (as discussed earlier) could also possibly contribute to the effect.

1.3.4 Regulation of mRNA degradation

mRNA degradation can be affected by various *trans* factors. While micro RNAs are prolific in regulating mRNA in animals and plants, budding yeast do not make use of this mechanism. Instead, in yeast mRNA degradation appears to be determined by a combination of intrinsic properties like length or codon-optimality, and trans factor RNA binding proteins (RBPs) that can bind *cis* element sequences in the mRNA sequence to effect changes in stability (Li et al. 2010). The best example of this is Puf3p, which binds motifs in mRNA with products destined for mitochondrial function and degrades these in the appropriate environment (Miller et al. 2013; Olivas and Parker 2000), perhaps by mapping phosphorylation of Puf3p to association of these mRNA to cytoplasmic granules (Lee and Tu 2015). Secondary structures may complicate the recognition of linear *cis* elements, or be used as *cis* elements in their own right (Li et al. 2010), for example Vts1p (Smaug homolog) recognizes a small sequence motif in the context of the loop of a stem-loop hairpin (Aviv et al. 2003; She et al. 2017). Degradation rates can be affected by many mechanisms. Elements in promoters (*cis* when in DNA but not part of the affected mRNA) can mark transcripts for differential stability (Haimovich et al. 2013). One of the most well known examples of this is Dbf2p loading onto *SWI5* and *CLB2* mRNA to effect destabilization upon mitosis (Trcek et al. 2011). In a direct example, the transcription activation domain of Adr1p fused to a different DNA binding domain has been shown

to be sufficient to mark *ADH2* mRNA for destabilization upon a glucose upshift (Braun et al. 2016). Thus, RBPs may recognize sequence elements in the mRNA or be loaded onto messenger ribonucleo-protein complexes (RNPs) at synthesis (Gupta et al. 2016) to effect control of mRNA stability in response to events in the cytoplasm.

Non-RBP mechanisms can also be used. Upstream open reading frames (uORFs) were originally characterized using the phenotype of post-transcriptional regulation of the Gcn2-regulated Gcn4p (Dever et al. 1992) in part through quality control pathways (Ruiz-Echevarria and Peltz 1996). Canonical and non-canonical start-codons can recruit initiation of scanning ribosome subunits with a variety of effects on the translation of the main coding sequence and the mRNA stability (Spealman et al. 2017). Ribosomes may skip re-initiation at the primary start codon to generate N-terminal diversity by initiating at alternative start codons, or upon termination of a uORF very distant from the 3' end of the transcript trigger the NMD pathway to destroy the mRNA (Dever et al. 2016).

While the primary-sequence of the mRNA is often thought to be the primary source of *cis*-elements, mRNA can be modified in a variety of ways. The most extensively studied modification so far is m6A methylation of adenines, with demonstrated consequences for localization and stability (Gilbert et al. 2016). The role of these, or other modifications, is still being investigated. The critical nature of the 5' m7G cap suggests that the discovery of other capping structures, such as recent identification of NAD+ capped mRNA in yeast (Walters et al. 2017), could provide another type of RNA modifications loading during transcription to affect processes of translation initiation and transcript degradation. Although at a low percentage, these modifications suggest that non-m7G caps could contribute to a sizable fraction of euarkyotic mRNA. Application of improvements in biochemical assays of modifications as well as long-read sequencing technology (both PacBio and Nanopore) may yield a new and informative perspective on

the single molecule extent of base modifications and their impacts on the progression of mRNA through various degradation intermediates.

mRNA localization within the cytoplasm may affect degradation by virtue of regulating the accessibility of degradation factors. Processing-bodies were originally described as cytoplasmic co-localized foci of 5' to 3' degradation factors that formed under stress induction conditions, and on the basis of steady-state genetics and experiments with an MS2 aptamer-based live-imaging system, it was concluded that processing-bodies are foci of active mRNA degradation (Sheth and Parker 2003). These foci are usually studied by microscopy during stresses, entry into stationary phase, and in the use of mutants in degradation pathways, but recent advances in microscopy and nanoscopy particle tracking have identified that these complexes are likely condensations of previously-existing RNPs and depend on a network of redundant interactions between mRNA 5' to 3' degradation protein factors (Lui et al. 2014; Rao and Parker 2017). Additionally, recent adjustments to the aforementioned MS2 aptamer system and explorations during dynamic conditions point towards processing-bodies being sites of degradation factor sequestration (Huch and Nissan 2017; Tutucci et al. 2017). Interestingly, the formation of these processing-bodies are halted upon cycloheximide treatment (Sheth and Parker 2003), suggesting that translational status of the transcriptome and processing-body composition may be related. In recent work, inhibition of translation initiation was demonstrated to increase p-body formation in correlation with increased degradation rates (Chan et al. 2017). Together, these observations indicate that processing-bodies result from a complex balance of mRNA degradation initiation, resolution, and mRNA degradation factor interactions with impacts on the accessibility of degradation factors to mRNA targets of degradation.

1.4 The role of stability control in transcriptome reprogramming

The change in concentration of an mRNA (R_t) depends on the rates of mature transcript synthesis (k_s) and mRNA degradation (k_d). We assume that synthesis is a constant rate dependent on the unchanging concentration of the DNA encoding the gene, and that degradation is a first order process of the mRNA interacting with a fixed and unsaturated factor degradation. We also disregard dilution from cell volume changes because this is approximately 50 times slower than the average rates of mRNA degradation and changes will thus not play a large role in our measurements of mRNA dynamics on this timescale. Thus, the change in mRNA over time is

$$\frac{dR_t}{dt} = k_s - R_t k_d$$

From this, the two rates determine the steady-state equilibrium of $\frac{k_s}{k_d}$. Given a singular regulatory event, the doubling time (or half-life) of the mRNA is dependent on only the degradation rate $\frac{log(2)}{k_d}$ and thus a faster mRNA degradation rate will approach or relax to the new equilibrium value quicker (Hargrove and Schmidt 1989).

While both synthesis and degradation contribute to changes in abundance, changes in degradation rates can cause the changes to occur more rapidly. If we expect that the existence of a mechanism implies a selective pressure specifically for it (Gould and Lewontin 1979), we would expect that studying an example of a transcript subject to both synthesis and degradation regulation might reveal a balance of selection across steady-state and dynamic conditions.

1.4.1 Stress conditions trigger rapid regulation of mRNA stability

mRNA degradation rate changes have been characterized to play a role in responses to heat-shock, osmotic stress, pH increases, and oxidative stress, sharing a similar pro-

gram of destabilization of mRNA coding for ribosomal-biogenesis gene products and stabilization of stress-responsive mRNA (Canadell et al. 2015; Castells-Roca et al. 2011; Garre et al. 2013; Miller et al. 2011; Molin et al. 2009; Molina-Navarro et al. 2008; Romero-Santacreu et al. 2009; Shalem et al. 2011). Simultaneous increases in both synthesis and degradation rates of some of these mRNA are thought to serve to return the transcriptome quickly to a new steady-state after effecting a transient pulse of regulation (Rabani et al. 2011; Shalem et al. 2008), demonstrating a key functional role in stability control in achieving a particular pattern of mRNA dynamics. Interestingly, these stability changes seem to usually be a singular regulatory event (Pérez-Ortín et al. 2013), suggesting that the mechanism is coordinated in its effect across the entire transcriptome during the first response to the stress.

1.4.2 Nutrient shifts also trigger mRNA stability changes

In response to a carbon-source downshift (glucose-grown cells resuspended in media with only galactose available), functionally important regulatory changes in mRNA stability occur (Munchel et al. 2011). Ribosome biogenesis associated mRNAs are destabilized, an effect that can be phenocopied by the addition of rapamycin (inhibitor of the central growth signalling TORC1 pathway). Conversely, a carbon source upshift (galactose to glucose) triggers a destabilization of inducible GAL genes, an effect that appeared to be restricted to the dynamic condition as mRNA transgenically overexpressed in glucose media were stable (Munchel et al. 2011).

Global changes in transcription and mRNA destabilization have been observed before (Jona et al. 2000), and recently systematically measured to be correlated with changes in growth rate (García-Martínez et al. 2016). The involvement of the TORC1 pathway in this process has identified that its effect is specified to differentially regulate the stability of certain transcript sets (Albig and Decker 2001; Talarek et al. 2010). Recently, a phosphoproteomics approach to studying signallng of the AMPK homolog

Snf1p during a carbon upshift identified a role in Xrn1p phosphorylation in the specification by this factor (Braun et al. 2014). Thus, specific signalling pathways appear to effect large changes in mRNA stability in response to different nutrient conditions for growth.

Relieving nutrient limitation with a glucose upshift has been shown to mediate both stabilization of mRNA in the ribosomal protein subunit regulon (Yin et al. 2003) and destabilization of gluconeogenic transcripts (Cruz et al. 2002; Lombardo et al. 1992; Mercado et al. 1994; Scheffler et al. 1998). Mapping the determinants of this effect has been met with mixed success. The destabilization of *SDH2* and *GAL1* mRNA has been mapped to elements in the 5' UTR (Bennett et al. 2008; Scheffler et al. 1998) with destabilization of GAL1 being associated with a growth advantage in switching carbon-source environments (Baumgartner et al. 2011). *JEN1* encodes a lactate/pyruvate transporter that is destabilized in rich carbon-sources like glucose, and this has been determined to result from transcription from a downstream transcription start-state destabilizing the larger isoform, through unknown mechanisms (Andrade et al. 2005). Subsequent work has identified *DHH1* as being a genetic factor of the *JEN1* destabilization (Mota et al. 2014). Some transcripts respond at different levels of glucose addition (Yin et al. 2000), and disrupting signalling through the PKA pathway affects destabilization of some mRNA but not others (Yin et al. 2003). Thus, a systematic measurement of mRNA stability and a broad determination of genetic factors of the transcript dynamics would be useful for making progress at untangling the regulation of mRNA stability in response to the increase in growth rate upon a nutrient upshift.

1.5 Measuring mRNA dynamics

While mRNA abundance measurements for entire transcriptomes are now routine, determining the rates that underlie this molecular phenotype has lagged. Synthesis rate

control has largely been assayed by techniques like Genome Run On (GRO) sequencing (discussed below) to measure transcription rates or measuring intron-exon ratios (Gray et al. 2014) as a proxy for synthesis rates (Pérez-Ortín et al. 2013). Degradation rate measurements have used a variety of methods, but are now applied to the whole transcriptome with enough accuracy to enable systematic modeling of the determinants of mRNA degradation rates (Cheng et al. 2017; Neymotin et al. 2016; Pérez-Ortín et al. 2013).

Pioneering studies used pulse-chase experiments with radioactive nucleotides to study turnover of the whole transcriptome (Petersen et al. 1976). Single gene measurements allowed the characterization of individual gene rates of turnover, but required the use of other methods for tracking the dynamics. One approach is to use promoters with inducible repression characteristics to halt transcription, for example transgenic repressors like the doxycycline-inducible Tet-Off (Gari et al. 1997). Researchers have also made use of the native *GAL1* promoter. Upon addition of glucose, transcription of the *GAL1* mRNA is immediately halted. This property has been exploited to study mRNA stability in a technically simple manner and has formed the basis of much of what we understand about the pathways of mRNA degradation (Coller and Parker 2004; Parker 2012). While the *GAL1* system is a convenient system for studying degradation intermediates, its demonstrated destabilization upon glucose addition makes uncertain its use for studying the native stability of different mRNA in different environments.

A system that does not rely on engineered *cis*-elements would avoid these issues and scale to genome-wide assays, and thus two methods of transcriptional inhibition were applied to study mRNA degradation rates in landmark studies. A temperature sensitive *rpb1*-1 allele was demonstrated to halt most PolII transcription at non-permissive temperatures, while the drugs thiolutin and 1,10-phenanthroline inhibited polymerases including PolII to mostly halt transcription. These have been used widely, and are still used

to this day. However, it has been shown that use of thiolutin or 1,10-phenalanthroline induces some heat-shock genes (Adams and Gross 1991), thiolutin inhibits mRNA degradation in a dose-dependent way (Pelechano and Pérez-Ortín 2008) (perhaps via inducing processing-body formation, Huch et al. 2016), and eliminating the essential RNA PolII complex from the nucleus has complex effects on the transcriptome dynamics (Yu et al. 2016). While it may seem logical that studies of mRNA associated with processes distinct from heat-shocks may be unaffected by these, the complexity of the cell demonstrated itself in vital controls run in Mercado et al. 1994 which demonstrated that gluconeogenic mRNA were subject to destabilization upon a heat-shock. Thus in several examples we see that shutting off transcription has complex and difficult to predict effects on transcript abundance as the cells die.

Orthogonal to these approaches is Genomic Run On approaches (Garcıa-Martınez et al. 2004), including microarray or sequencing based assays (Pelechano et al. 2010). This method uses a cold sarkosyl treatment to fix RNA PolII complexes onto genomic DNA by freezing their elongation, then extraction and a defined in-vitro polymerase extension and profiling the resulting mRNA with microarrays or RNAseq allows for an estimate of the instantaneous transcription rate status for each gene in a population of cells. Interpretation of these numbers must be considered in the context of the in-vitro environment of the elongation step, but this method serves as an valuable orthogonal measure of transcript dynamics — and an instantaneous one.

The development of 4-thiouracil metabolic labeling of RNA (Dölken et al. 2008) has enabled a return to the pulse-chase methodology in the development of genome-wide assays of mRNA dynamics. A thiol-containing analog of uracil, 4-thiouracil is readily incorporated by yeast into their nucleotide metabolism and thus into the mRNA. The label does not perturb growth at low concentrations ($< 50\mu$M) (Burger et al. 2013), and supports normal growth. Fundamentally, these assays work by changing the labelling

frequency of mRNA at a time and tracking the dynamics as the labeled mRNA abundance relaxes towards a new equilibrium of labeling. Below I review the basic model of these assays, then focus on their applications and where the dissertation work is placed.

If we consider mRNA abundance at a certain time as being denoted as M_t, then I expect this number to change as a zeroth order rate of synthesis per time (k_s) and a first order rate of degradation per mRNA (k_d). While mRNA degradation is a multi-step process (above) and more complex models may identify nuances in the rates of progression through these intermediates (Deneke et al. 2013), at steady-state the rate of degradation of mRNA in a population should be well modeled by a single first order rate (Thattai 2016).

$$\frac{dM_t}{dt} = k_s - M_t * k_d$$

Introducing a term L that denotes the fraction of newly synthesized mRNA that are labeled and measured after purifying mRNA for the labeled mRNA (thus M_t is just labeled and captured mRNA), we can now model the changes as simply

$$\frac{dM_t}{dt} = Lk_s - M_t * k_d$$

I introduce the superscript notation of L^o for the old labeling frequency and L^n for the new labeling frequency, and solving for the change of M_t from some steady-state equilibrium $L^o\frac{k_s^o}{k_d^o}$ to a new equilibrium $L^n\frac{k_s^n}{k_d^n}$, and rearranging terms we get

$$M_t = L^o\frac{k_s^o}{k_d^o}e^{-k_d^n t} + L^n\frac{k_s^n}{k_d^n}(1 - e^{-k_d^n t})$$

This matches well with our intuition. On the right, the nascent transcripts are labeled at the new rate and approach this new equilibrium controlled by the term $(1-e^{-k_d^n t})$, while on the left the extant transcripts approach zero in an exponential decrease controlled by the term $e^{-k_d^n t}$. These are both controlled by k_d^n, or the rate of mRNA degradation after chasing the label. Thus, by measuring the transition between the equilibrium we get the mRNA degradation rate.

Measuring specific rates with high confidence requires a steady-state approximation. RATEseq is one method to do so, using many timepoints to accurately model the approach of labeled mRNA abundance to a new equilibrium (Neymotin et al. 2014). This experimental design is theoretically the most accurate, although it requires the assumption that the total mRNA (labeled + unlabeled) is indeed at a steady-state abundance. Dynamic Transcriptome Analysis (Miller et al. 2011) violates this assumption to explore changes in degradation rates during 6 minute windows. While the method sacrifices high-confidence of an exact rate, the temporal resolution of stability changes during osmotic stress has revealed an unprecedented dynamic view of the regulation of mRNA dynamics during complex processes. This approach requires that 4-thiouracil transport and incorporation into nucleotide metabolism occurs during the course of the perturbation experiment, but with the right measurements, normalization, and integration with other datasets an accurate and dynamic picture of transcriptome dynamics can be built. To assess mRNA stability changes during dynamic processes, one can also label the transcriptome to equilibrium and then chase out the label by adding an excess of unlabeled nucleotides. This approach was used by researchers in the Weis group to demonstrate changes in the stability of groups of mRNA in response to environmental changes, namely shifts in carbon sources and with rapamycin treatment inhibiting TORC1 (Munchel et al. 2011)

In Chapter 3 I demonstrate the use of a similar 4-thiouracil label-chase experimental design, with refined analysis to explore per-transcript destabilization upon a nitrogen upshift.

1.6 Methods for determining the genetic basis of a transcript dynamics phenotype

mRNA is an intermediate in the expression of a protein product, and has the key virtue of being easy to measure in bulk. This has become especially true with the advent of massively-parallelized DNA sequencers and the methods to accurately convert transcriptomes to DNA libraries (RNAseq) (Shendure et al. 2017). For this reason, it is often used as a proxy of gene expression at the protein level. Although the relationship is strong when correcting for experimental noise (Csárdi et al. 2015), the quantitative functional nature of this relationship within a particular gene in different environments depends on the particular gene in question (Franks et al. 2017). It is also clear that transcriptomic and proteomic responses greatly vary in the timescales of effect, with the transcriptome subject to rapid impulses of changing abundance that may or may not result in longer term regulation of the protein product (Cheng et al. 2016; Lee et al. 2011). Even then, protein abundance in a cell does not correspond perfectly to its activity, be that regulated allosterically or by localization.

Given this disparity, what can we learn about adaptive gene expression from mRNA abundance regulation? First, the expression of a gene product requires mRNA, thus the binary expression of mRNA is a predictor of the possibility of protein expression. Additionally, cellular processes often impinge upon changes in mRNA abundance, be they direct via regulation of abundance, activity, and localization of activity of specific effectors or by indirect effects on common gene expression machinery or cellular metabolism. In this way, a specific perturbation of a signalling pathway is expected to broadcast to changes in mRNA abundance. Quantification of the thousands of mRNA that are expressed in a cell is a sensitively quantitative measurement on thousands of dimensions, and can thus be used as a relatively-unbiased indicator of cellular status with which to explore the genetic requirements of particular signalling perturbations

(Gapp et al. 2016). Thus, efficient methods to explore the genetic basis of transcript dynamics upon a perturbation should help to accelerate the study of cellular signalling pathways.

Genetic screens in yeast have been a powerful tool to narrow down the immense search space of possibilities to a narrow set of hypotheses about a biological process. Classically, these function by mapping some phenotype of interest to a change in growth rate. For example, mutants in transporters of a particular amino-acid can be isolated by feeding the cells a toxic stereoisomer (like D-histidine). A more complex method in Lee Hartwell's classic screen for cell-cycle mutants used the assay of growth at a low temperature and cessation of growth at a high temperature to identify mutants in critically important pathways (Hartwell et al. 1970), work that contributed to a 2001 Nobel Prize for advancing our understanding of the cell cycle. However, this concept becomes problematic when studying a molecular phenotype which is not known to change growth rates, and thus is not known to be selected.

For example, gene regulation might not have a clear phenotypic outcome, or could be subject to redundant layers of regulation that mask the effect of a mutation. One solution is to engineer a specific reporter into the expressed gene, such that defects in gene expression can be assayed. It becomes more difficult if the phenotype is a transient one, such that a reporter through growth rate (perhaps a toxic peptide) does not have time to accumulate the signal of growth. A fluorescent tag is one approach that is more direct, as cells can be instantaneously assayed for the level of GFP fluorescence at that moment via flow cytometry. The GFP can be fused to the protein of interest or simply placed downstream of an appropriate reporter, such as the strategy employed by Neklesa and Davis 2009. These researchers were able to use a DAL80 promoter upstream of a GFP reporter to explore the genetic requirements for the NCR-regulated expression of this promoter, discovering the SEACIT complex components

Npr2/3p upstream of TORC1. This approach is compatible with a pooled assay using barcode-sequencing technologies, also known as SortSeq (Boer et al. 2017; Kinney et al. 2010; Oikonomou et al. 2014; Peterman and Levine 2016). While appropriate for studying steady-state processes, this approach often uses fluorophores that require that the expression phenotype be relevant at the level of protein expression, and that the GFP tag be a relevant and faithful reporter of the protein abundance — a condition which is not always satisfied given the stability of the cleaved GFP tag in the vacuole (Conibear and Stevens 2002).

GAP1 mRNA degradation, which we identify as being subject to accelerated mRNA degradation in Chapter 2 and 3, occurs much faster than the repression of the protein-product (Hein and André 1997). We also know that Gap1p, the protein product of *GAP1* mRNA, is subject to de-activation and re-localization in response to a nitrogen upshift. Thus, a functional assay of Gap1p is irrelevant to the dynamics of *GAP1* mRNA repression, and requires a novel method to screen for genetic factors of this molecular phenotype.

Ambitious work from the Capaldi group developed a workflow using extensive automation to perform qPCR assays for NSR1 mRNA abundance 19 minutes after induction of an osmotic stress response (Worley et al. 2016). While accurate and reproducible, the extensive automation and reagent usage to perform qPCR on $\sim$4700 mutant strains poses a financial and logistical challenge. To perform the assay in different genetic backgrounds, in larger libraries, in replicates, or in different timepoints requires a pooled approach that can scale genome-wide without greatly increasing costs. To do this, I adapted a mRNA FISH assay to use in budding yeast. While mRNA has been observed by flow cytometry before (Yu et al. 1992 described its use on $\sim$1800 copies of histone mRNA), the use of branched DNA probe sets has made sorting on low copies of mRNA possible (Hanley et al. 2013). In Chapter 3 I discuss in depth the combination of this

technology with the aforementioned SortSeq barcode sequencing and modeling approaches to directly estimate transcript abundance in a high-throughput pooled format, and without genetic modifications.

— 2 —

Modeling transcript dynamics upon a nitrogen upshift

This chapter was published as part of the article "*Steady-state and dynamic gene expression programs in Saccharomyces cerevisiae in response to variation in environmental nitrogen* in *Molecular Biology of the Cell* (vol. 27 no. 8 1383-1396. April 15, 2016. doi.org/10.1091/mbc.E14-05-1013).

Authorship of this article was: Edoardo M. Airoldi, **Darach Miller**, Rodoniki Athanasiadou, Nathan Brandt, Farah Abdul-Rahman, Benjamin Neymotin, Tatsu Hashimoto, Tayebeh Bahmani, and David Gresham.

Below is reprinted the abstract, then excerpts of the introduction, results, and conclusion to which I contributed. The text has been edited for clarity. Supplemental tables, figures, and files are available on the MBoC article website (doi.org/10.1091/mbc.E14-05-1013).

2.1 Abstract

Cell growth rate is regulated in response to the abundance and molecular form of essential nutrients. In *Saccharomyces cerevisiae* (budding yeast), the molecular form of environmental nitrogen is a major determinant of cell growth rate, supporting growth rates that vary at least threefold. Transcriptional control of nitrogen use is mediated in large part by nitrogen catabolite repression (NCR), which results in the repression of specific transcripts in the presence of a preferred nitrogen source that supports a fast growth rate, such as glutamine, that are otherwise expressed in the presence of a nonpreferred nitrogen source, such as proline, which supports a slower growth rate.

Differential expression of the NCR regulon and additional nitrogen-responsive genes results in >500 transcripts that are differentially expressed in cells growing in the presence of different nitrogen sources in batch cultures. Here we find that in growth rate-controlled cultures using nitrogen-limited chemostats, gene expression programs are strikingly similar regardless of nitrogen source. NCR expression is derepressed in all nitrogen-limiting chemostat conditions regardless of nitrogen source, and in these conditions, only 34 transcripts exhibit nitrogen source-specific differential gene expression. Addition of either the preferred nitrogen source, glutamine, or the nonpreferred nitrogen source, proline, to cells growing in nitrogen-limited chemostats results in rapid, dose-dependent repression of the NCR regulon. Using a novel means of computational normalization to compare global gene expression programs in steady-state and dynamic conditions, we find evidence that the addition of nitrogen to nitrogen-limited cells results in the transient overproduction of transcripts required for protein translation. Simultaneously, we find that that accelerated mRNA degradation underlies the rapid clearing of a subset of transcripts, which is most pronounced for the highly expressed NCR-regulated permease genes *GAP1*, *MEP2*, *DAL5*, *PUT4*, and *DIP5*. Our results reveal novel aspects of nitrogen-regulated gene expression and highlight the need for a quantitative approach to study how the cell coordinates protein translation and nitrogen assimilation to optimize cell growth in different environments.

2.2 Introduction

The rate at which budding yeast cells grow is sensitive to the molecular form of nitrogen in the environment. Yeast cells are able to use and discriminate between different nitrogen sources (Cooper 1982; Magasanik and Kaiser 2002). When a variety of nitrogen sources are available, a yeast cell will preferentially transport and metabolize particular nitrogen-containing compounds by decreasing levels of transcripts and pro-

teins required for use of nonpreferred nitrogen sources (Cooper 1982; Magasanik and Kaiser 2002). A study of yeast cells growing in the presence of different individual nitrogen sources provided a genome-wide view of nitrogen-regulated gene expression and suggested that >500 genes are differentially expressed as a function of environmental nitrogen source (Godard et al. 2007). On the basis of differential gene expression, promoter sequence elements, and published literature, Godard et al. 2007 assigned membership of many of these transcripts to five regulons that are responsive to environmental nitrogen: the nitrogen catabolite repression A (NCR-A) regulon, which includes bona fide NCR targets; the potential NCR target (NCR-P) regulon; the general amino acid control (GAAC) regulon; the unfolded protein response (UPR) regulon; and the *SSY1*-PTR3-SSY5 (SPS) regulon.

Transcriptional control of the NCR regulon (i.e., both NCR-A and NCR-P regulons) is mediated by the transcription factors *GLN3*, *GAT1*, *DAL80*, and *GZF3*, which bind to the 5-GATAA-3 consensus sequence in target gene promoter regions (Cooper 1982; Magasanik and Kaiser 2002). Whereas *DAL80* and *GZF3* act as repressors of NCR transcription, *GLN3* and *GAT1* activate the transcription of NCR genes in a nitrogen source-dependent manner. The evolutionarily conserved TOR complex 1 (TORC1) is believed to be an upstream regulator of NCR expression, as it promotes the nuclear exclusion of *GLN3* by physical association with *URE2* in a phosphorylation-dependent manner (Beck and Hall 1999).

To study the dynamics of nitrogen-responsive gene expression, we performed transient perturbation experiments in which different quantities and sources of nitrogen were added to cells growing in nitrogen-limited chemostats. The addition of either the preferred nitrogen source, glutamine, or the nonpreferred nitrogen source, proline, to cells growing in nitrogen-limited conditions results in rapid repression of the NCR regulon in a dose-dependent manner. Surprisingly, a sudden increase in environmental nitro-

gen does not correspond to a detectable increase in biomass production or cell number, consistent with a time delay between activation of the transcriptional growth program and its manifestation in an increased rate of cell growth. To compare global gene expression in dynamic conditions with mRNA expression in steady-state conditions, we used computational estimation of instantaneous growth rate from gene expression profiles (Airoldi et al. 2009; Brauer et al. 2008) and defined gene expression responses to growth rate in both steady-state and dynamic conditions using linear regression. We find that the response of transcripts required for protein translation (RP and RiBi) in cells provided with an increase in nitrogen exceeds the response to growth rate in cells growing in steady-state conditions consistent with a transient overproduction of RP and RiBi transcripts. Finally, we show that accelerated degradation of some NCR transcripts underlies gene expression remodeling in response to sudden relief from nitrogen limitation, indicating the activity of a posttranscriptional mechanism controlling nitrogen-responsive gene expression.

2.3 Results

To obtain a high-resolution view of mRNA abundance changes during the first 10 min after addition of nitrogen, when changes in gene expression are maximal, we repeated the pulse experiments (addition of nitrogen source to yeast grown in steady-state nitrogen-limited chemostat cultures) and assayed global gene expression at 1-2 min intervals after the addition of 40 μM glutamine or 80 μM proline. We observed a rapid increase in expression of the RiBi and RP regulons in response to a pulse of glutamine, with a concomitant rapid decrease in expression of the NCR-A and NCR-P regulons. Consistent with our initial observation, we observed a similar response to a pulse of proline.

2.3.1 Accelerated degradation of mRNAs contributes to remodeling of the transcriptome

The majority of NCR transcripts are strongly repressed in response to a nitrogen pulse. If gene expression is repressed at the promoters of these genes and mRNA synthesis ceases, the decrease in mRNA abundance is expected to be a function of the degradation rate of the corresponding mRNA. Using our high-density time-series data, we estimated the rate of change in abundance for all transcripts, assuming a first-order exponential degradation model (Materials and Methods; Supplemental Table S7), which is the standard method for estimating mRNA degradation rates. We found that in response to a glutamine pulse, 269 genes fit a first-order exponential decay model (FDR < 0.05; Supplemental Table S4), whereas 458 transcripts fit a first-order exponential decay model in response to the proline pulse (Supplemental Table S4).

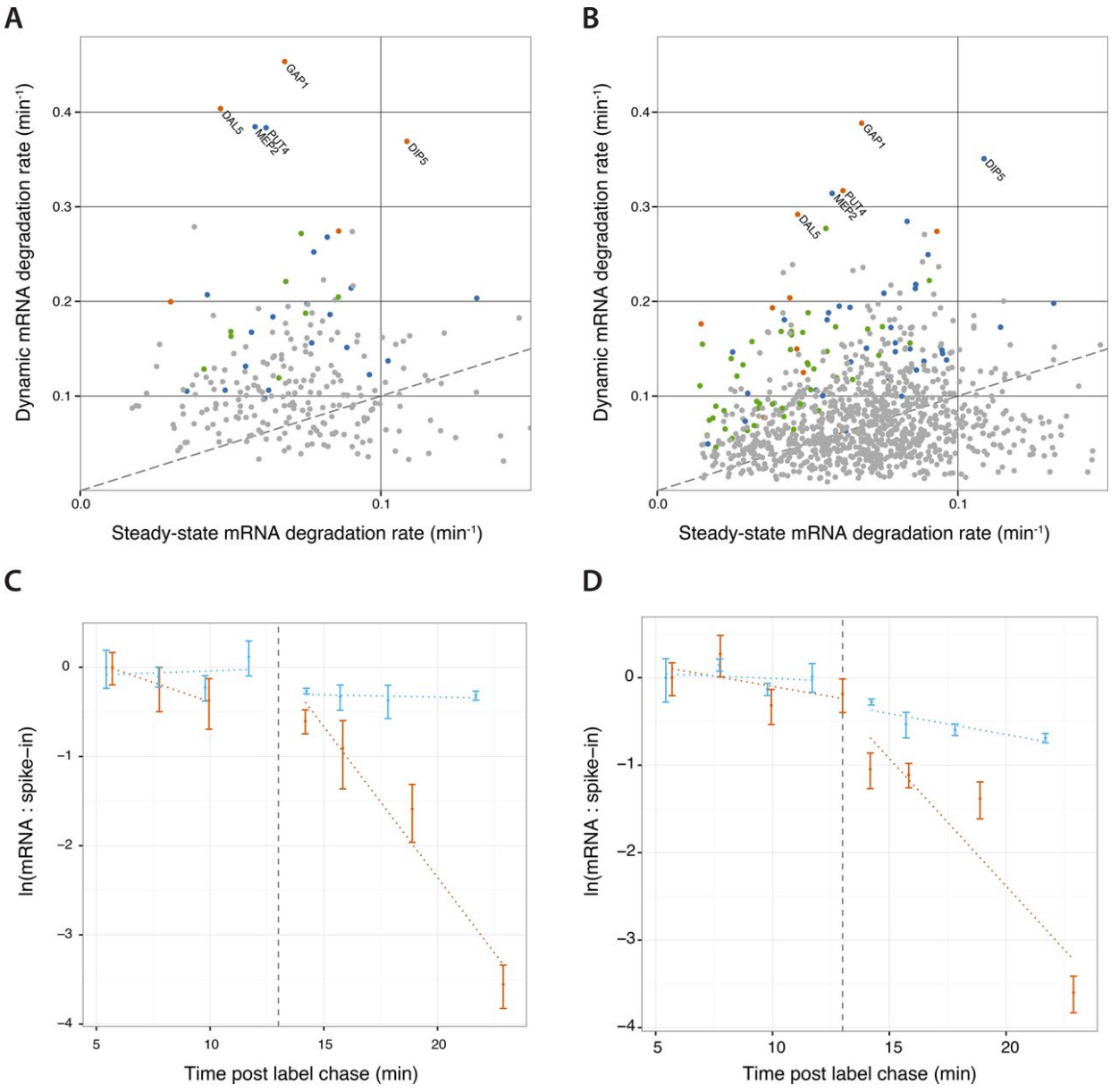

Figure 2.1: **Accelerated mRNA degradation contributes to gene expression remodeling**

Figure 2.1 — Accelerated mRNA degradation contributes to gene expression remodeling. Upon addition of glutamine to NCR-derepressed cells, a subset of transcripts degrade more rapidly than their steady-state degradation rate both (A) in cells grown in ammonia-limited chemostats and (B) in cells growing in proline media in batch

cultures. All points are genes that fit a model of exponential decrease in abundance (FDR < 0.05). Orange points are NCR genes that show significant accelerated degradation, blue points are NCR genes that are not significant, green points are non-NCR genes that show significantly accelerated degradation, and gray points are genes that are neither accelerated nor NCR. The dashed line denotes equal degradation rates in both conditions (i.e., slope equal to 1). Names of nitrogen transporter genes are displayed. We measured the transient changes in the degradation rates of (C) *GAP1* and (D) *DIP5* mRNA using a pulse-chase experiment. Cells were grown for 24 h in the presence of 4-thiouracil, which was chased at t = 0 min by the addition of excess uracil. At t = 13 min, we added either glutamine in water (orange) or equal volume of water (blue). We extracted and quantified the abundance of 4-thiouracil-labeled mRNA relative to a thiolated external spike-in using qPCR. We found significant acceleration of degradation for both *GAP1* and *DIP5* mRNAs ($p < 0.001$). Points are the mean of triplicate qPCR measurements, error bars are the propagated SD of transcript and spike-in measurements, and dotted lines are the log-linear model fit.

We compared the half-lives of rapidly degraded transcripts after the glutamine pulse with half-life estimates in steady-state conditions determined using RATE-seq (Neymotin et al. 2014). We found that some transcripts decay significantly faster than expected, suggesting that their degradation rate is accelerated in response to the glutamine pulse (Figure 2.1A). Batch culture growth in proline also results in derepression of the NCR regulon (Godard et al. 2007). To test whether accelerated mRNA decay is specifically a response to the nitrogen-limited conditions of a chemostat, we added a pulse of glutamine to cells growing in batch cultures containing proline as a sole nitrogen source and measured genome-wide gene expression (Supplemental Table S7). The half-lives

of transcripts that exhibit an exponential decrease is similar in chemostat and batch cultures (Supplemental Figure S7B), and many of the same transcripts show evidence of accelerated degradation rates in batch cultures (Figure 2.1B and Supplemental Table S4). Strikingly, the five nitrogen permease genes *GAP1*, *DIP5*, *MEP2*, *PUT4*, and *DAL5* are the most rapidly cleared mRNAs in both the chemostat and batch culture experiments.

To verify that the addition of glutamine stimulates accelerated degradation of specific NCR transcripts, we performed pulse-chase experiments using the metabolic label 4-thiouracil (4-tU). After several generations of batch culture growth in proline medium in the presence of 4-tU to allow complete labeling of mRNAs, we added unlabeled uracil to the culture. We allowed the chase to occur for 13 min and then added either glutamine or water (mock) to the cells. We purified labeled transcripts and analyzed *GAP1* and *DIP5* mRNAs using quantitative PCR (qPCR) and normalization to external spike-ins. Consistent with our genome-wide assay, the addition of glutamine results in a clear accelerated degradation of both *GAP1* mRNA (Figure 2.1C) and *DIP5* mRNA (Figure 2.1D), confirming that the transition from NCR-derepressed to NCR-repressed conditions results in the accelerated degradation of some transcripts.

2.4 Discussion

Some mRNAs are rapidly degraded when cells transition from NCR-activating to NCR-repressing conditions in both chemostats and batch culture. Comparison with mRNA degradation rates suggests that the degradation of some of these transcripts is accelerated. Using in vivo metabolic labeling with 4-tU, we provide additional evidence that the addition of glutamine to nitrogen-limited cells accelerates the degradation of specific transcripts. A previous study of the transcriptional response to glucose addition in carbon-limited chemostats suggested a role for accelerated degradation of mRNAs

(Kresnowati et al. 2006) , and there is increasing evidence that mRNA stability plays an important role in regulating gene expression programs (Baumgartner et al. 2011; Bennett et al. 2008; Puig et al. 2005). Consistent with a posttranscriptional mechanism underlying the rapid clearing of some NCR transcripts, previous work showed that *GAP1* mRNA transiently decreases in abundance during a nitrogen up-shift in the absence of *URE2* (Schure et al. 1998), which is required for NCR repression by sequestering *GLN3* in the cytoplasm. Several studies have shown that TORC1 can affect transcript stability (Albig and Decker 2001; Munchel et al. 2011). Our results suggest that posttranscriptional regulation of mRNA stability may play an important role in remodeling gene expression in response to changes in environmental nitrogen. Transient stabilization of the RP and RiBi regulons also could contribute to their rapid increase in expression (Yin et al. 2003). Defining the role of regulated changes in mRNA stability in dynamic conditions is an important area for further study.

What is the underlying rationale for rapid induction of RP/RiBi transcripts occurring in parallel with accelerated degradation of NCR transcripts? We propose that accelerated degradation of NCR transcripts may allow for reallocation of ribosomes to transcripts required for growth and proliferation (Kief and Warner 1981; Lee et al. 2011). Our observations are consistent with a model in which TORC1 orchestrates the balance between transcripts required for protein production and transcripts required for the acquisition and assimilation of nitrogen. When nitrogen is abundant, TORC1 activates the expression of the RP and RiBi regulons while actively repressing the NCR-A and NCR-P regulons. Conversely, when nitrogen levels are in growth-limiting concentrations, TORC1 activity decreases, leading to reduced activation of the RP and RiBi regulons and derepression of the NCR-A and NCR-P regulons. In NCR-derepressing conditions, NCR transcripts, including *GAP1*, *MEP2*, and *PUT4*, are the most abundant transcripts (Supplemental Table S5). When a cell encounters a sudden increase in environmental nitrogen, some

highly expressed transcripts may be targeted for accelerated degradation to increase the pool of free ribosomes facilitating rapid translation of newly transcribed RiBi and RP transcripts, thereby accelerating physiological remodeling of the cell for rapid growth.

2.5 Materials and methods

2.5.0.1 Strains and culturing conditions

We used the prototrophic haploid strain FY4 (MATa), which is isogenic to the S288c reference strain, for all experiments. We used minimal defined media for all experiments, using a common base medium for nitrogen limitation, as described previously (Boer et al. 2010; Brauer et al. 2008). The appropriate concentrations of allantoin, glutamine, glutamate, urea, ammonium sulfate, proline, and arginine were added from 100 mM stock. Batch culture experiments were performed in 30°C shaking incubators using 100-ml cultures. Continuous culturing in chemostats using Sixfors bioreactors (Infors, Laurel, MD) was performed as described (Boer et al. 2010; Brauer et al. 2008) using a 300-ml working volume. Culture parameters were determined using either a Klett colorimeter or a Coulter counter after sonication. For perturbation studies, a single bolus of proline, glutamine, or a mix of both was added to the chemostat to a final concentration of 80 or 800 μM nitrogen.

2.5.0.2 RNA analysis

Cell samples for mRNA analysis were preserved by rapid filtration and quick freezing using liquid nitrogen. We isolated total RNA using hot acid-phenol extraction and subsequently purified RNA samples using RNeasy columns. We performed gene expression profiling using Agilent (Santa Clara, CA) 60-mer DNA microarrays and Cy3 and Cy5 incorporation as previously described (Brauer et al. 2008). We used a common reference obtained from a sample growing in an ammonium sulfate-limited chemostat at a dilu-

tion rate of 0.12 hours^{1} for all hybridization experiments and hybridized labeled cRNA to Agilent Yeast DNA microarrays for 20 h at 65°C. We washed arrays and scanned microarrays using an Agilent two-color scanner and extracted hybridization signals using Agilent Feature Extractor Software. Supplemental Table S6 gives the entire data set of processed $\log_2$ ratios.

2.5.0.3 Pulse chase

Cells were grown in 600 ml of minimal medium containing 800 μM proline, 500 μM uracil, and 500 μM 4-thiouracil at 30°C for 24 h. The culture was divided into two 300-ml cultures, and uracil was added to a final concentration of 2mM. We acquired 20-ml samples after the chase using rapid filtration and flash freezing in liquid nitrogen. At 13 min after starting the chase, we added either glutamine to a final concentration of 400 μM or an equal volume of water and acquired additional samples.

After RNA extraction, samples were mixed with an in vitro-transcribed thiolated spike-in (*BAC1*200) at a ratio of 1 ng of spike-in to 25 μg of total RNA and reacted with EZ-Link HPDP-Biotin (ThermoFisher Scientific, Waltham, MA) at 2 mg/ml for 200 min. Reactions were cleaned up by centrifugation and ethanol precipitation and then conjugated with 180 μl of streptavidin magnetic beads (M0253L; NEB, Ipswich, MA). Labeled RNA was eluted using 5% β-mercaptoethanol.

Samples were reverse transcribed with Moloney murine leukemia virus reverse transcriptase (NEB) and random hexamer priming. We performed qPCR in technical triplicate on a LightCycler 480 (Roche, Branchburg, NJ) using the following primers:

GAP1	5'-ACGGTATCAAGGGTTTGCCAAG-3'	5'-GCATAAATGGCAGAGTTAC-3'
DIP5	5'-TGGCGTACATGAATGTGTCTTCA-3'	5'-GGTGATCCAACTCAAGATTC-3'
BAC1200	5'-CTGGACGACTTCGACTACGG-3'	5'-ATCAGCCTTTCCTTTCGTCA-3'

C_p values were calculated for each sample and the spike-in and log-linear regression

performed using the ratio of either *GAP1* mRNA or *DIP5* mRNA to the spike-in in R.

2.5.0.4 mRNA decay estimation

We estimated rates of mRNA decay for all transcripts using high-temporal resolution data. We used ratios (y_t) of hybridization intensities for each transcript obtained from two-color DNA microarrays co-hybridized with a common reference. Data were normalized to the initial data point (y_0) and then log-transformed. We modeled the degradation rate k_deg of each gene:

$$ln\left(\frac{y_t}{y_0}\right) = k_{\text{deg}} \times t$$

where t is the sampling time in minutes. Transcript half-lives were computed as $\frac{ln(2)}{k_{deg}}$. Accelerated degradation was assessed by fitting the model

$$ln\left(\frac{y_t}{y_0}\right) = (k_{\text{transient deg}} + k_{\text{steady-state deg}}) \times t$$

where $k_{steady-statedeg}$ is the specific degradation rate for transcript i as reported in Neymotin et al. 2014. For all linear modeling, we assessed statistical significance of coefficients using a t-statistic and determined empirical p-values by permuting data for each gene 1000 times. The false discovery rate was determined using the `qvalue` package in R. Data availability DNA microarray data are available through gene expression omnibus (GEO) GSE57293.

— 3 —

Measuring the extent of mRNA destabilization and screening for genetic factors of *GAP1* repression

This chapter is similar to an article currently submitted to a journal for review and publication. It is also posted on *biorxiv*, titled: "*Global analysis of gene expression dynamics identifies factors required for accelerated mRNA degradation*". Authorship of this article is: **Darach Miller**, Nathan Brandt, and David Gresham. Darach Miller did most of the benchwork, analysis, and writing. Nathan Brandt did all benchwork to generate mutants and collect qPCR for Figure 3.30. David Gresham helped with discussions and co-writing the article. The *biorxiv* version is at `doi.org/10.1101/254920`.

The below is adapted for the dissertation, incorporating important text from the supplementary methods into the chapter text. Supplemental tables are available from the OSF repository linked with this work (`https://osf.io/7ybsh/files/`), and are reproducible using the `Makefile` and associated scripts in the git repository distributed with the paper (`http://github.com/darachm/millerBrandtGresham2018`).

3.1 Abstract

Cellular responses to changing environments frequently involve rapid reprogramming of the transcriptome. Regulated changes in mRNA degradation rates can accelerate reprogramming by clearing or stabilizing extant transcripts. Here, we measured mRNA stability using 4-thiouracil (4tU) labeling in the budding yeast *Saccharomyces cerevisiae* during a nitrogen upshift and found that 78 mRNAs are subject to significant

destabilization. These transcripts include genes involved in Nitrogen Catabolite Repression (NCR) and carbon metabolism mRNAs, suggesting that mRNA destabilization is a mechanism for targeted reprogramming. To explore the molecular basis of destabilization, we implemented a SortSeq approach using a pooled deletion collection library to screen for *trans* factors that mediate rapid *GAP1* mRNA repression. We combined low-input multiplexed Barcode sequencing with branched-DNA single-molecule mRNA FISH and Fluorescence-activated cell sorting (BFF) to identify that the Lsm1-7p/Pat1p complex and general mRNA decay machinery are important for *GAP1* mRNA clearance. We also find that the decapping modulator *SCD6*, translation factor eIF4G2, and the 5' UTR of *GAP1* are important for this repression, suggesting that translational control may impact the post-transcriptional fate of mRNAs in response to environmental changes.

3.2 Introduction

Regulated changes in mRNA abundance are a primary cellular response to external stimuli. Both the rate of synthesis and the rate of degradation determine the steady-state abundance of a particular mRNA and the kinetics with which abundance changes occur (Hargrove and Schmidt 1989; Pérez-Ortín et al. 2013). Changes in mRNA degradation rates fulfill an important mechanistic role in diverse systems, including development (Alonso 2012; West et al. 2018) and disease (Aghib et al. 1990). In budding yeast, the rate of mRNA degradation is affected by environmental stresses (Canadell et al. 2015), cellular growth rate (García-Martínez et al. 2016), and by improvements in nutrient conditions (Scheffler et al. 1998).

Environmental shifts trigger rapid reprogramming of the budding yeast transcriptome in response to stresses and nutritional changes (Conway et al. 2012; Gasch et al. 2000). mRNA degradation rate changes have been shown to play a role in responses to heat-shock, osmotic stress, pH increases, and oxidative stress (Canadell et al. 2015;

Castells-Roca et al. 2011; Molina-Navarro et al. 2008; Romero-Santacreu et al. 2009). In response to these diverse stresses, destabilization of mRNAs encoding ribosomal-biogenesis gene products and stress-induced mRNA occurs (Canadell et al. 2015). Simultaneous increases in both synthesis and degradation rates of some mRNAs may serve to speed the return to a steady-state following a transient pulse of regulation (Shalem et al. 2008). Addition of glucose to carbon-limited cells results in both stabilization of ribosomal protein mRNAs (Yin et al. 2003) and destabilization of gluconeogenic transcripts (Cruz et al. 2002; Mercado et al. 1994). Destabilization of transcripts can have a delayed effect on reducing protein levels compared to up-regulated genes (Lee et al. 2011). This suggests that accelerated mRNA degradation may serve additional purposes. For example, clearance of specific mRNAs could increase nucleotide pools (Kresnowati et al. 2006) or facilitate reallocation of translational capacity (Giordano et al. 2016; Kief and Warner 1981; Shachrai et al. 2010).

Yeast cells metabolize a wide variety of nitrogen sources, but preferentially assimilate and metabolize specific nitrogen compounds. Transcriptional regulation, known as nitrogen catabolite repression (NCR) (Magasanik and Kaiser 2002), controls the expression of mRNAs encoding transporters, metabolic enzymes, and regulatory factors required for utilization of alternative nitrogen sources. NCR-regulated transcripts are expressed in the absence of a readily metabolized (preferred) nitrogen sources or in the presence of growth-limiting concentrations (in the low μM range) of any nitrogen source (Airoldi et al. 2016; Godard et al. 2007). Regulation of NCR targets is mediated by two activating GATA transcription factors, Gln3p and Gat1p, and two repressing GATA factors, Dal80p and Gzf3p. *GAT1*, *GZF3*, and *DAL80* promoters contain GATAA motifs, and thus transcriptional regulation of NCR targets entails self-regulatory and cross-regulatory loops. When supplied with a preferred nitrogen source such as glutamine, the NCR-activating transcription factors Gat1p and Gln3p are excluded from the

nucleus by TORC1-dependent and -independent mechanisms (Beck and Hall 1999; Tate and Cooper 2013; Tate et al. 2017) and NCR transcripts are strongly repressed. The activity of some NCR gene products are also controlled by post-translational mechanisms (Cooper and Sumrada 1983) such as the General Amino-acid Permease (Gap1p) which is rapidly inactivated upon a nitrogen upshift via ubiquitination (Merhi and André 2012; Risinger et al. 2006; Stanbrough and Magasanik 1995). Recently, we have identified an additional level of regulation of NCR transcripts: cells growing in NCR de-repressing conditions accelerate the degradation of *GAP1* mRNA upon addition of glutamine (Airoldi et al. 2016). Thus, mRNA degradation rate regulation may be an additional mechanism for clearing NCR-regulated transcripts upon improvements in environmental nitrogen availability.

Multiple pathways mediate the degradation of mRNAs. The main pathway of mRNA degradation occurs by deadenylation and decapping prior to 5' to 3' exonucleolytic degradation by Xrn1p; however, transcripts are also degraded 3' to 5' via the exosome, or via activation of co-translational quality control mechanisms (Parker 2012). Deadenylation of mRNAs by the Ccr4-Not complex allows the mRNA to be bound at the 3' end by the Lsm1-7p/Pat1p complex, a heptameric ring comprising the SM-like proteins Lsm2-7p and the cytoplasmic-specific Lsm1p (Sharif and Conti 2013; Tharun et al. 2000), which then recruits factors for decapping by Dcp2p. Recruitment of the decapping enzyme (Coller and Parker 2004) is the rate-limiting step for canonical 5'-3' degradation. Therefore Lsm1-7p, Pat1p, and associated factors play a key role (Nissan et al. 2010).

Regulation of mRNA degradation pathways can alter the stability of specific mRNAs. For example, the RNA-binding protein (RBP) Puf3p recognizes a *cis*-element in 3' UTRs (Olivas and Parker 2000) and affects mRNA degradation rates depending on Puf3p phosphorylation status (Lee and Tu 2015). In addition to *cis*-elements within the transcirpt, promoters have been shown to mark certain RNA-protein (RNP) complexes to specify

their post-transcriptional regulation (Braun et al. 2016; Haimovich et al. 2013; Mercado et al. 1994; Trcek et al. 2011). These mechanisms may be controlled by a variety of different signalling pathways including Snf1 (Braun et al. 2014; Young et al. 2012), PKA (Ramachandran et al. 2011), Phk1/2 (Luo et al. 2011), and TORC1 (Talarek et al. 2010). Thus, regulated changes in mRNA degradation rates includes numerous mechanisms that collectively tune stability of mRNAs in response to the activity of signalling pathways.

Here, we studied the global regulation of mRNA degradation rates upon improvment in environmental nitrogen using 4-thiouracil (4tU) label-chase and RNAseq. We found that a set of 78 mRNAs are subject to accelerated mRNA degradation, including many NCR transcripts as well as mRNAs encoding components of carbon metabolism. To identify the mechanism underlying accelerated mRNA degradation we designed a high-throughput genetic screen using Barcode-sequencing of a pooled library which was fractionated using Fluorescence-activated cell sorting of single molecule mRNA FISH signal (BFF). We screened the barcoded yeast deletion collection to test the effect of each gene deletion on the abundance of *GAP1* mRNA in NCR de-repressing conditions and its clearance following the addition of glutamine. We find that the Lsm1-7p/Pat1p complex and decapping modifiers affect both *GAP1* mRNA steady-state mRNA abundance and its accelerated degradation. This work expands our understanding of mRNA stability regulation in remodeling the transcriptome during a relief from growth-limitation and demonstrates a generalizable approach to the study of genetic determinants of mRNA dynamics.

3.3 Characterizing transcriptome dynamics upon a nitrogen upshift

3.3.1 Transcriptional reprogramming precedes physiological remodeling

Cellular responses to environmental signals entail coordinated changes in both gene expression and cellular physiology. Previously, we studied the steady-state and dynamic responses of *Saccharomyces cerevisiae* (budding yeast) to environmental nitrogen (Airoldi et al. 2016), and found that the transcriptome is rapidly reprogrammed following a single pulsed addition of glutamine to nitrogen-limited cells in either a chemostat or batch culture. To study physiological changes in response to a nitrogen upshift, we measured growth rates of a population of cells. A prototrophic haploid lab strain (FY4, isogenic to S288c) grows with a 4.5 hour doubling time in batch culture in minimal media containing proline as a sole nitrogen source (Figure 3.1). Upon addition of 400μM glutamine the cells undergo a 2-hour lag period during which no change in population growth rate is detected, but the average cell size continuously increases ($\sim$21% increase in mean volume Figure 3.1). Following the lag, the population adopts a 2.1 hour doubling time. By contrast, global gene expression changes are detected within three minutes of the upshift (Airoldi et al. 2016). Thus, transcriptome remodeling precedes physiological remodeling in response to a nitrogen upshift.

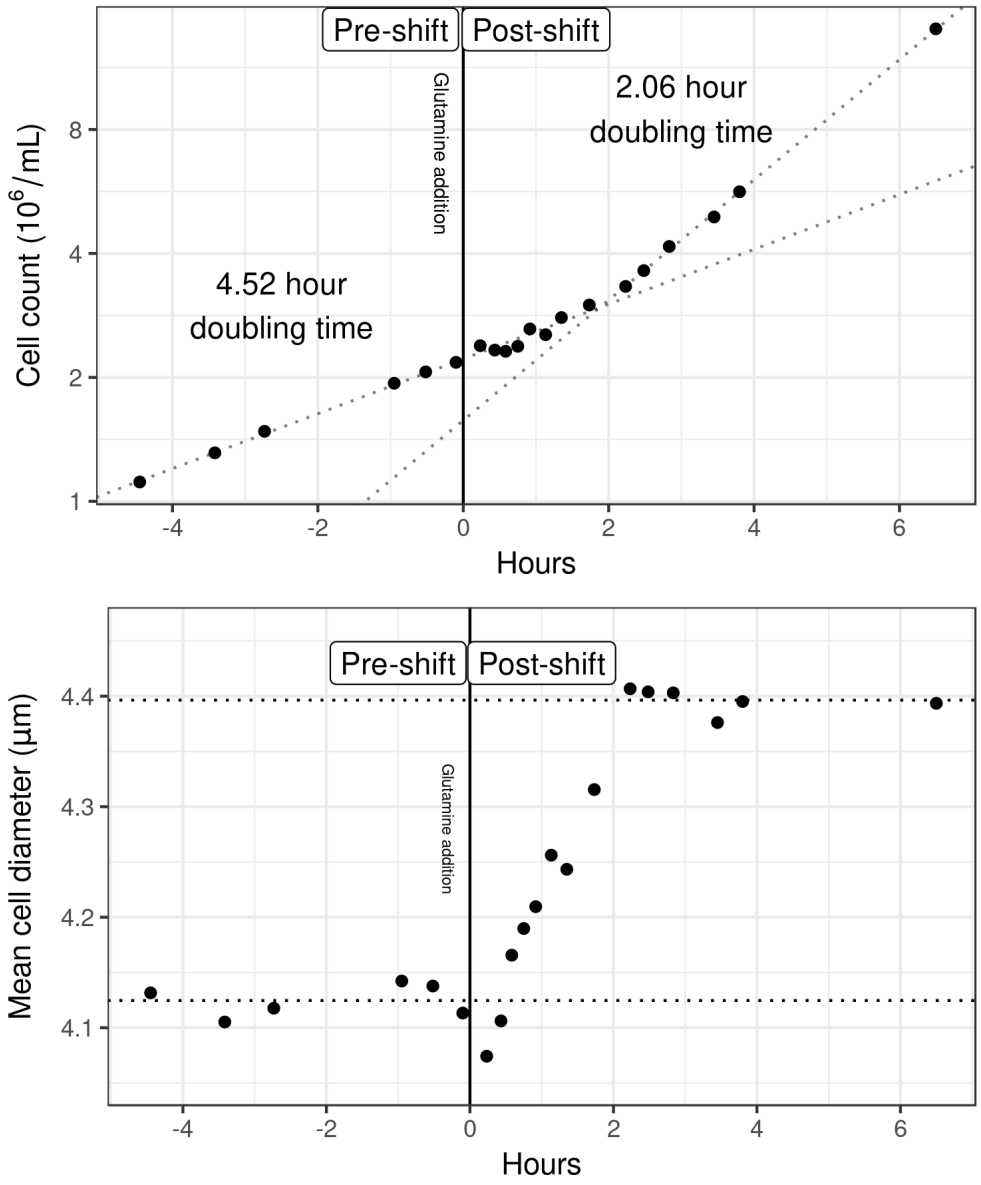

Figure 3.1: **The nitrogen upshift of population and cellular growth rate. (Top)** 400μM glutamine was added to a culture of yeast cells growing in minimal media containing 800μM proline as a sole nitrogen source. Measurements of culture density across the upshift are plotted. Dotted lines denote linear regression of the natural log of cell density against time before the upshift and after the 2 hour lag. **(Bottom)** Average cell size. Dotted lines denote the mean cell diameter before the upshift and after the 2 hour lag.

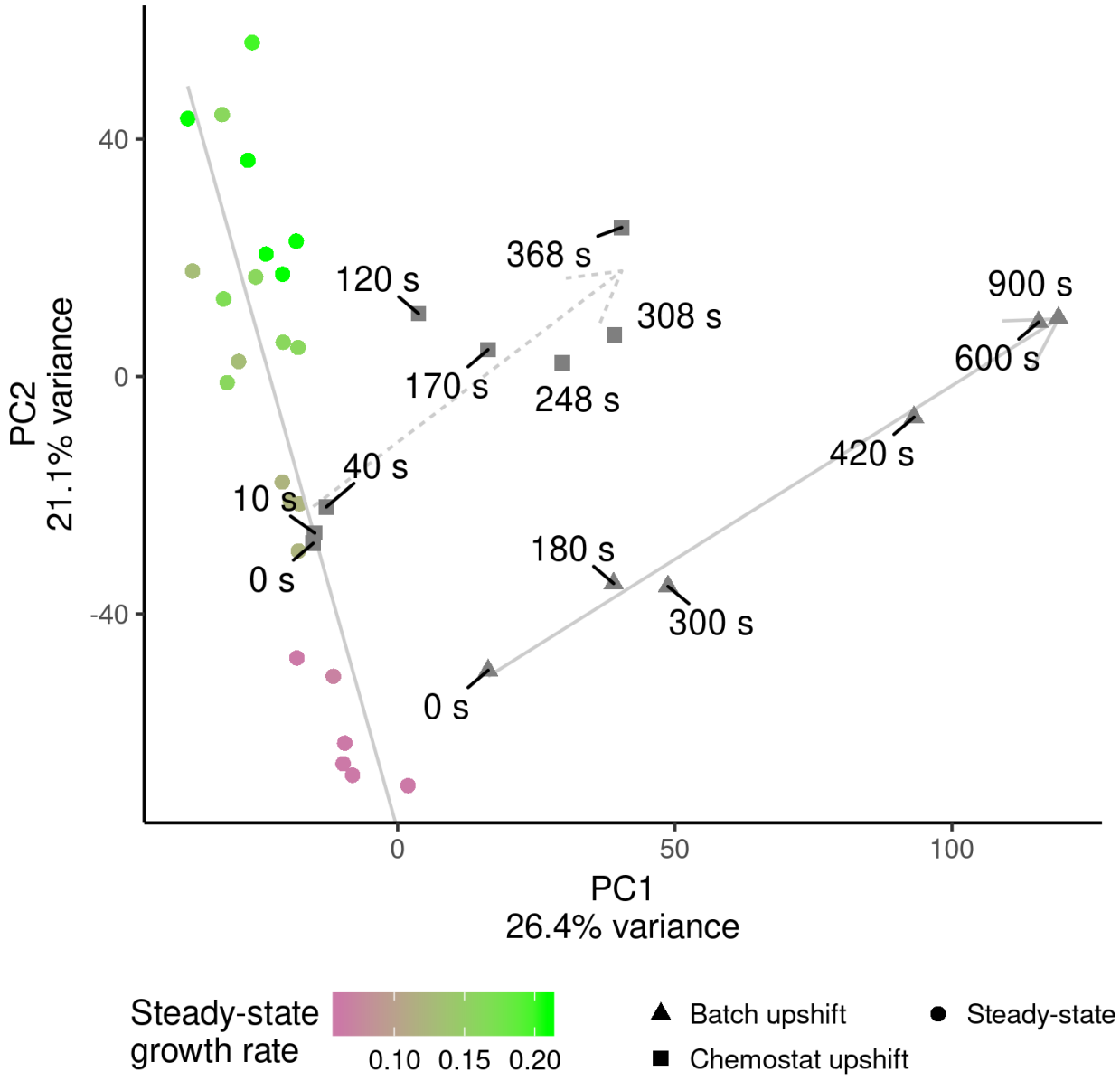

Figure 3.2: **Dynamics of transcriptome remodeling during a nitrogen upshift, on a coarse scale.** PCA analysis of global mRNA abundance in steady-state chemostats and following an upshift (Airoldi et al. 2016). Steady-state nitrogen-limited chemostat cultures maintained at different growth rates (colored circles) primarily vary along principal component 2. mRNA abundance changes following a nitrogen-upshift in either a chemostat (squares) or batch culture (triangles) show similar trajectories and primarily vary along principal component 1. Grey lines depict the major trajectory of variation for the steady-state and upshift experiments.

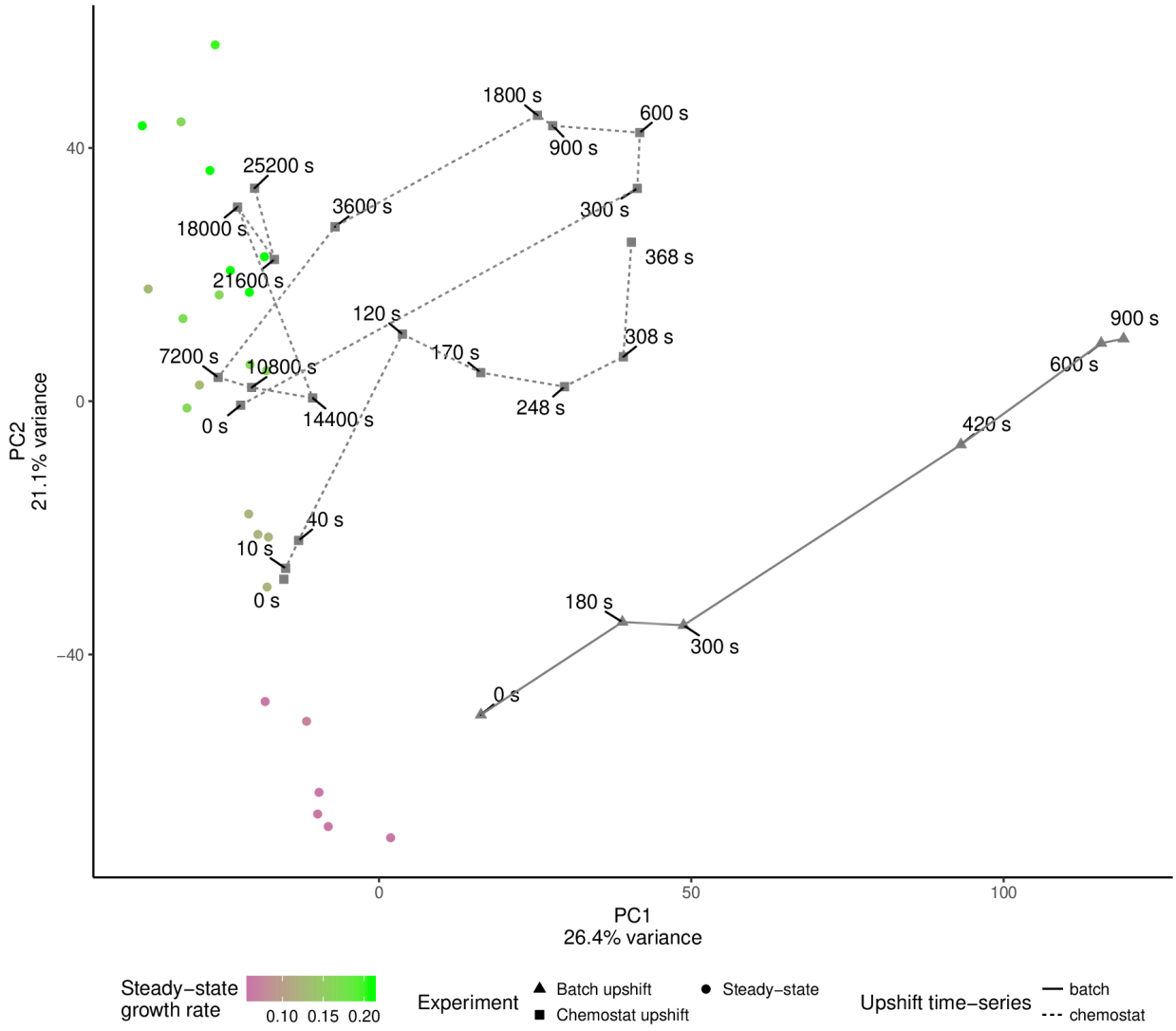

Figure 3.3: **The coarse long-term transcriptome dynamics of a glutamine upshift.** Principal components analysis (SVD) of microarray data from Airoldi et al. 2016. Colored points are from steady-state chemostats grown in nitrogen-limitation with various nitrogen sources, at different growth rates. Time-series experiments are show in grey points, connected by lines, and line-type is the type of upshift (in batch or in chemostat).

To evaluate concordance in transcriptome remodeling between chemostat and batch nitrogen upshifts, and the extent to which they reflect changes in mRNA abundance observed during systematic steady-state changes in growth rates using chemostats, we performed principal component analysis on microarray data (Figure 3.2). The first

two principal components, which account for almost half of the total variation, clearly separate steady-state and nitrogen upshift cultures. Systematic changes in growth rate primarily results in a separation of states along the second principal component, whereas upshift experiments vary along the first principal component. This suggests that the transcriptome is remodeled through a distinct state. In upshift experiments in chemostats, the trajectory ultimately returns to the initial steady-state condition as excess nitrogen is depleted by consumption and dilution (Figure 3.3).

To investigate the functional basis of mRNA abundance changes in the upshift and steady-state conditions, we computed the correlation of each transcript with the loadings on these first two principal components and performed gene-set enrichment analysis (Supplementary tables). Component 1 is positively correlated with functions like mRNA processing, transcription from RNA polymerases (I,II,and III), and chromatin organization, and negatively correlated with cytoskeleton organization, vesicle organization, membrane fusion, and cellular respiration. Both steady-state and upshift trajectories increase with principal component 2, but they diverge along principal component 1. Components 1 and 2 are strongly enriched for terms including ribosome biogenesis, nucleolus, and tRNA processing, and negatively correlated with vacuole, cell cortex, and carbohydrate metabolism terms. Together, this analysis suggests that both upshift and increased steady-state growth rates share upregulation of ribosome-associated components, but the reprogramming preceding the upshift in growth reflects an immediate focus on gene expression machinery instead of structural cellular components. Importantly, dynamic reprogramming is similar in both the chemostat and batch upshift (Figure 3.2). As batch cultures are a technically simpler experimental system, we performed all subsequent experiments using batch culture nitrogen upshifts.

3.3.2 Global analysis of mRNA stability changes during the nitrogen upshift

Previously, we found that *GAP1* and *DIP5* mRNAs are destabilized in response to a nitrogen upshift (Airoldi et al. 2016). We sought to determine if mRNA destabilization is specific to NCR transporter mRNAs by measuring global mRNA stability across the upshift using 4-thiouracil (4tU) labeling and RNA-seq (Munchel et al. 2011; Neymotin et al. 2014). As 4tU labeling requires nucleotide transport, which may be altered upon a nitrogen-upshift (Hein et al. 1995), we designed experiments such that following complete 4tU labeling and metabolism to nucleotides the chase was initiated prior to addition of glutamine or water (mock). We normalized data using *in vitro* synthesized thiolated spike-ins by fitting a log-linear model to spike-in counts across time (Design of Barseq after FACS after FISH experiment), which reduced noise and increased our power to detect stability changes (Supplementary tables). Data and models for each transcript can be visualized in browser using a Shiny appplication (see `http://shiny.bio.nyu.edu/users/dhm267/` or Availability of data and analysis scripts).

We modeled the log-transformed normalized signal for each mRNA using linear regression (Supplementary tables). Of 4,859 mRNAs measured we identified 94 that increased in degradation rate and 38 that decreased (FDR < 0.01, using Storey and Tibshirani 2003). We generated a model of nucleotide labeling kinetics to assess the effect of an incomplete label chase on our experimental design (Normalization of counts into signal for modeling), and found that complete transcriptional inhibition alone could theoretically result in a 17% increase in the apparent degradation rate. In order to eliminate the possibility that rapid synthesis changes could affect our estimates, we only considered destabilization of at least a doubling (100% increase) of apparent degradation rates between pre-upshift and post-upshift. This conservative cutoff left 78 mRNA that are significantly destabilized upon a nitrogen upshift.

The vast majority of transcripts (4,781 of 4,859) do not show individual evidence for stability changes upon addition of glutamine (e.g. *HTA1*, Figure 3.4). The median pre-upshift half-life is 6.92 minutes and the median half-life following the upshift is 6.32 minutes (Table 3.1) suggesting that there is not a global change in mRNA stability. Global stability estimates are considerably lower than previous estimates in rich medium (Miller et al. 2011; Munchel et al. 2011; Neymotin et al. 2014), which may reflect the different nutrient conditions used in our study. The 78 transcripts significantly destabilized upon the glutamine-upshift include mRNAs encoding NCR transporters *GAP1*, *DAL5*, and *MEP2* (blue label, Figure 3.4), the pyruvate metabolism enzymes *PYK2* and *PYC1* (orange label), and trehalose synthase subunits *TPS1* and *TPS2* (yellow label). Destabilized mRNA tend to be more stable before the upshift (Figure 3.5), (median half-life of 9.46 minutes) and exhibit a median 3.06-fold increase in degradation rates (median half-life of 3.02 minutes following the upshift).

Table 3.1: Summary of mRNA stability, median values

	Pre-shift		Post-shift		Change in	Fold-change
	specific rate (min^{-1})	half-life (min)	specific rate (min^{-1})	half-life (min)	specific rate (min^{-1})	specific rate
All transcripts	0.100	6.92	0.110	6.32	0.00865	1.08
Destabilized (n=78)	0.0732	9.46	0.229	3.02	0.158	3.06
Unchanged (n=4781)	0.101	6.89	0.108	6.40	0.00728	1.07

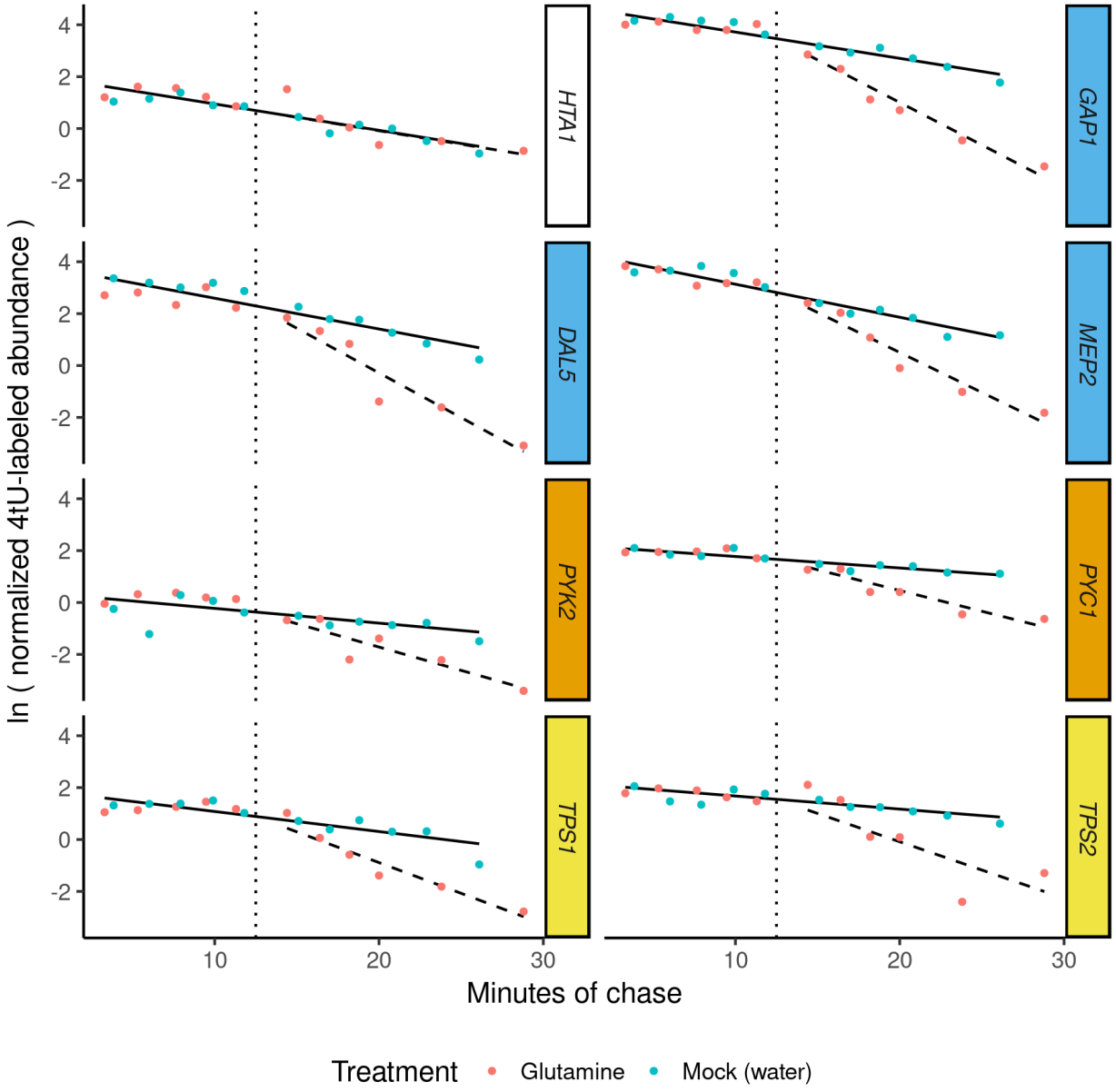

Figure 3.4: **4tU label-chase RNA sequencing measures mRNA stability changes following a nitrogen upshift.** 4tU-labeled mRNA from each gene was measured over time, before and after the addition (vertical dotted line) of glutamine (nitrogen-upshift) or water (mock). Linear regression models were fit to the data with a rate before the upshift (solid line) and a rate after glutamine addition (dashed line). *HTA1* is not significantly destabilized, whereas mRNAs encoding NCR-regulated transporters (*GAP1*, *DAL5*, *MEP2*) or pyruvate (*PYK2*, *PYC2*) and trehalose (*TPS1*, *TPS2*) metabolism enzymes are significantly destabilized.

We tested for functional enrichment among the set of 78 destabilized mRNAs and

found that they are strongly enriched for NCR transcripts (16 of 78, p < 10^{-11}). Almost half of the destabilized transcripts are annotated as ESR-up genes (Figure 3.7), on the basis of their rapid induction during the environmental stress response (Gasch et al. 2000). These 78 destabilized mRNA are enriched (FDR < 0.05) for GO terms and KEGG pathways (Supplementary tables) including glycolysis/gluconeogenesis (6 genes), carbohydrate metabolic process (24), trehalose-phosphatase activity (3), pyruvate metabolic process (6), and secondary active transmembrane transport (8, a subset of the enriched 11 ion transmembrane transport genes). Thus destabilized mRNA upon a nitrogen upshift regulates, but is not restricted to, NCR-regulated mRNA and reflects broader metabolic changes in the cell.

To investigate the extent to which mRNA stability changes contribute to transcriptome reprogramming, we compared degradation rates to abundance changes following the upshift (Airoldi et al. 2016, Figure 3.5). Changes in mRNA degradation rates and mRNA abundance change rates are anti-correlated (Pearson's r = -0.598, p-value < 10^{-15}, Figure 3.6), consistent with stability changes impacting mRNA abundance dynamics. However, they are not entirely co-incident, as some destabilized transcripts do not exhibit decreases in abundance (red points in Figure 3.5, Figure 3.8, and Figure 3.9). This analysis shows that increases in degradation rates play a significant role in the rapid reprogramming of the transcriptome upon a glutamine upshift, but that in some cases they are counteracted by increases in mRNA synthesis rates (Canadell et al. 2015; Shalem et al. 2008).

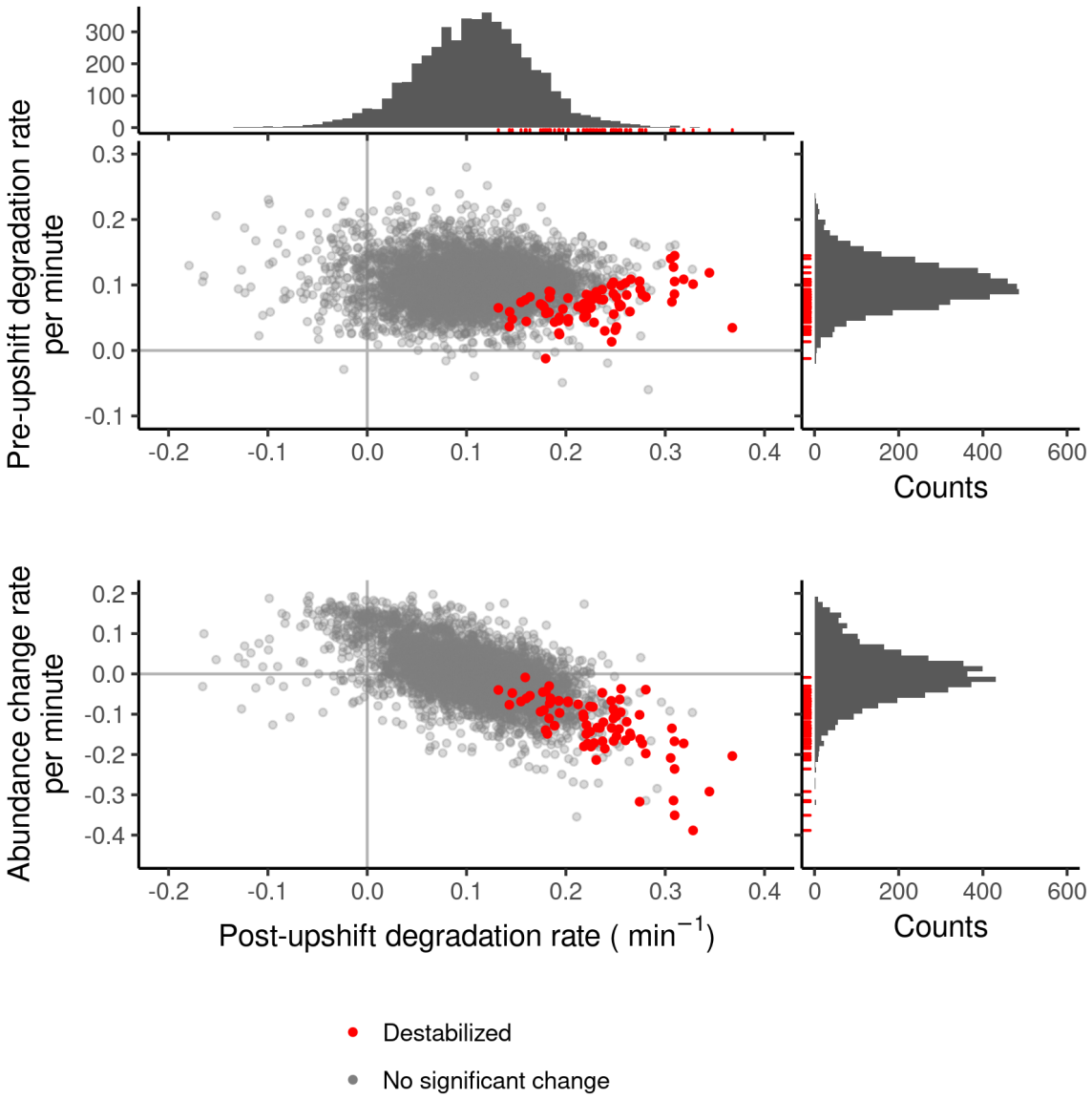

Figure 3.5: **Global mRNA stability changes following a nitrogen upshift.** Comparison between the pre-upshift mRNA degradation rate (y-axis) and the post-upshift mRNA degradation rate (x-axis). Negative values result from noise on the slope estimate. Comparison between changes in mRNA abundance following upshift (Airoldi et al. 2016) (y-axis) and the post-upshift degradation rate (x-axis). Both plots share the same x-axis. Transcripts that are significantly destabilized are colored red, and shown with red rug-marks in the marginal histograms.

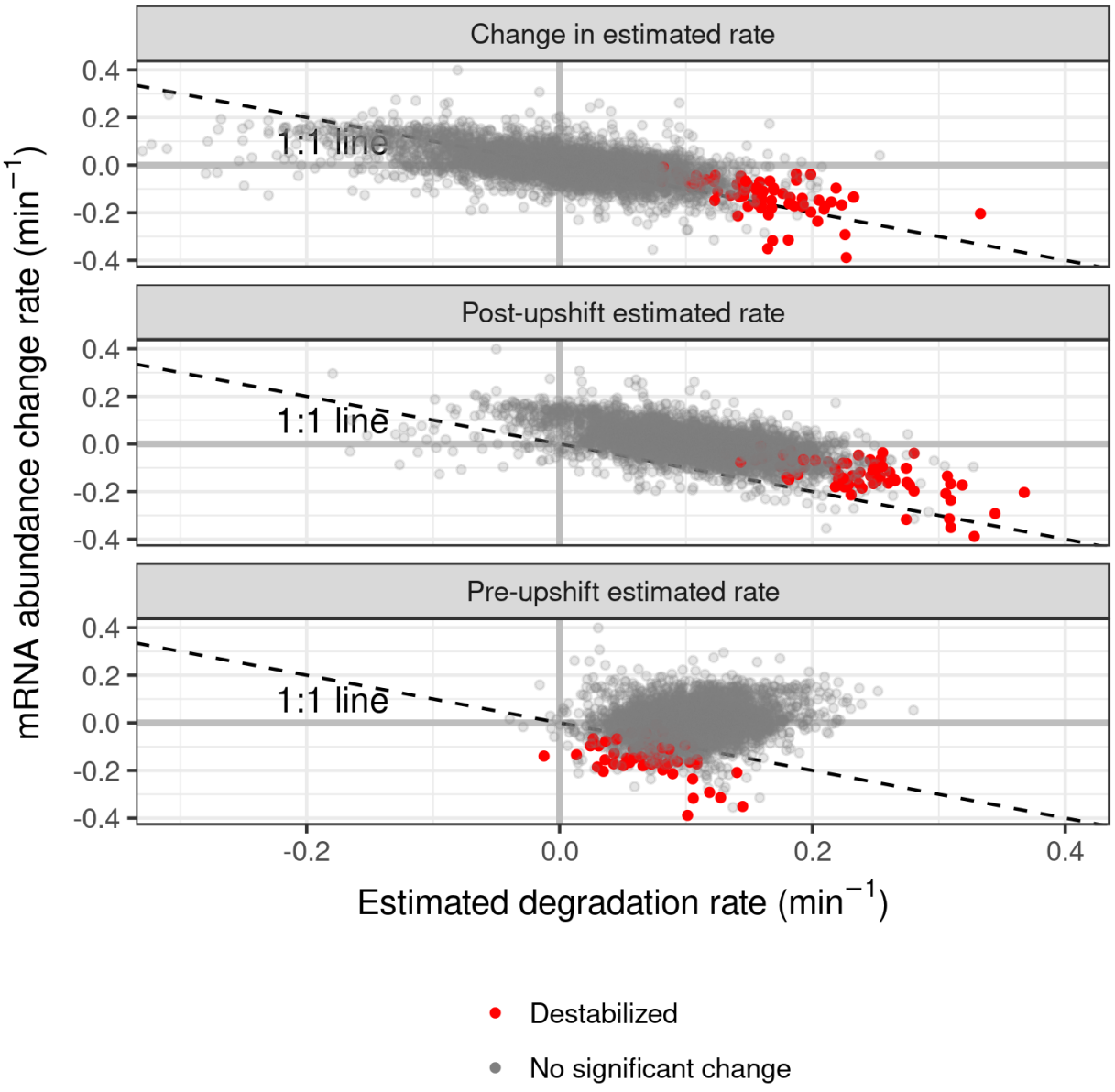

Figure 3.6: **Comparison between rates of mRNA degradation and abundance changes.** Pre-upshift decay rates **(top)** don't explain the abundance change. The degradation rate changes (**middle**, difference between pre and post upshift) and the post-upshift rates **(bottom)** are anti-correlated with the abundance changes.

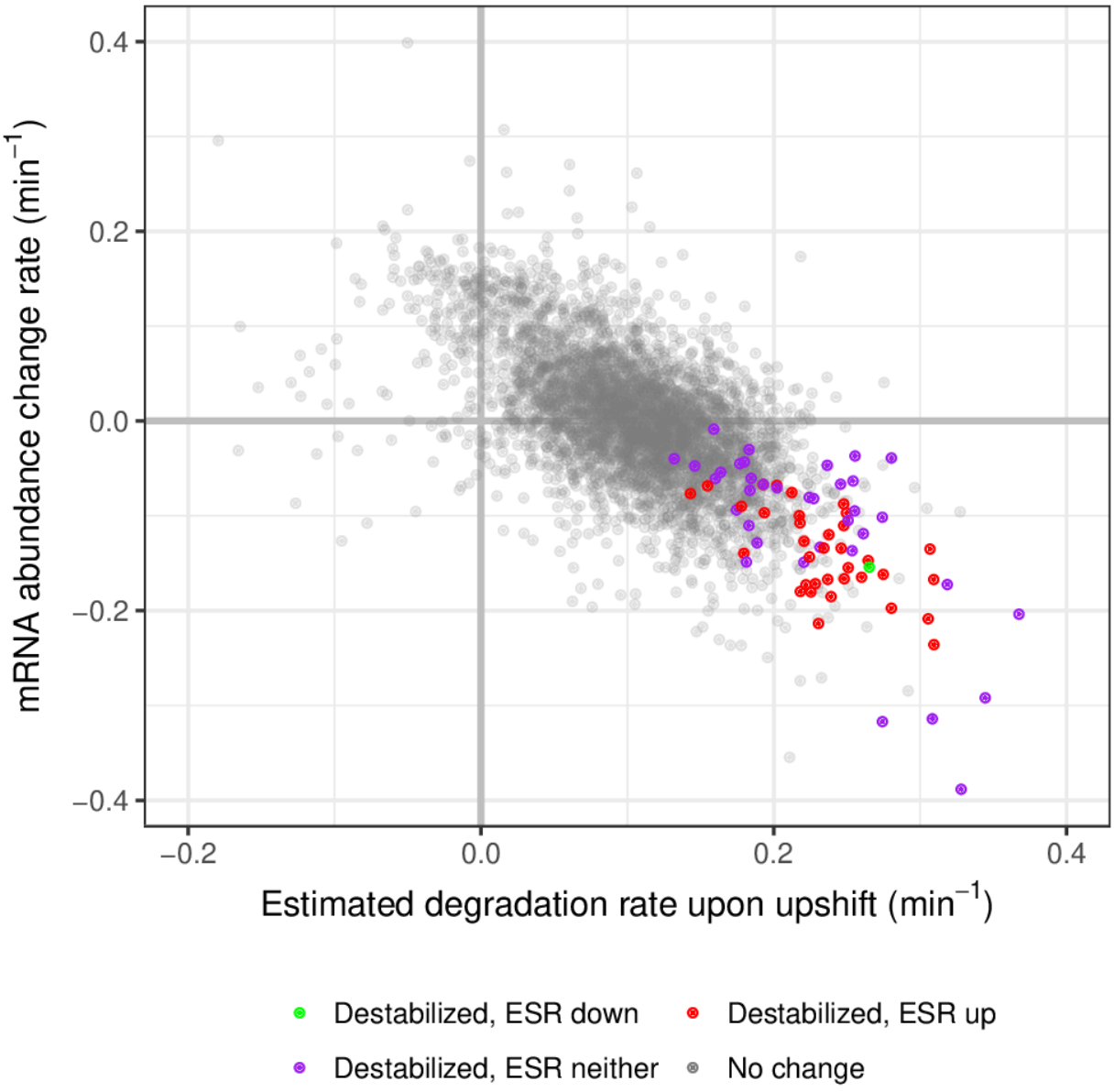

Figure 3.7: **Many of the destabilized mRNA are members of the ESR-up regulon.** Comparisons of degradation rates from this study with mRNA abundance change rates from Airoldi et al. 2016. Destabilized transcripts are colored based on their membership in the ESR gene set (Gasch et al. 2000), as described in the supplement of Brauer et al. 2008. Many of the destabilized set are ESR "up" genes, as they are increased in expression in response to stresses.

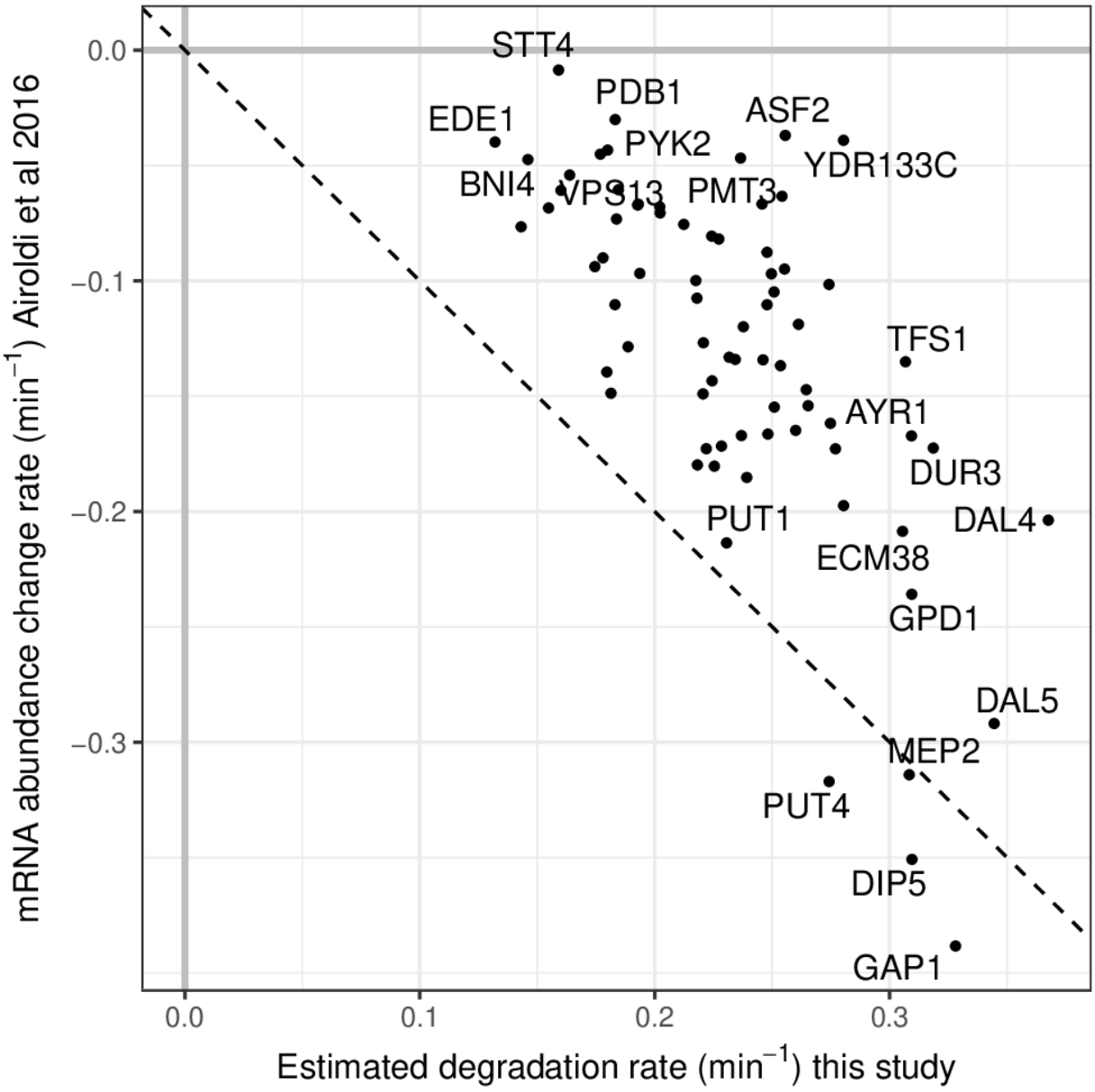

Figure 3.8: **Significantly destabilized transcripts are not always strongly repressed.** For each, the x-axis is the fit rate of degradation rate post-upshift. On the y-axis is the mRNA abundance change rate (Airoldi et al. 2016) after the upshift. These values were modeled to normalized sequencing signal (x-axis) and normalized microarray ratio (y-axis). The dashed line is a 1:1 line of equality.

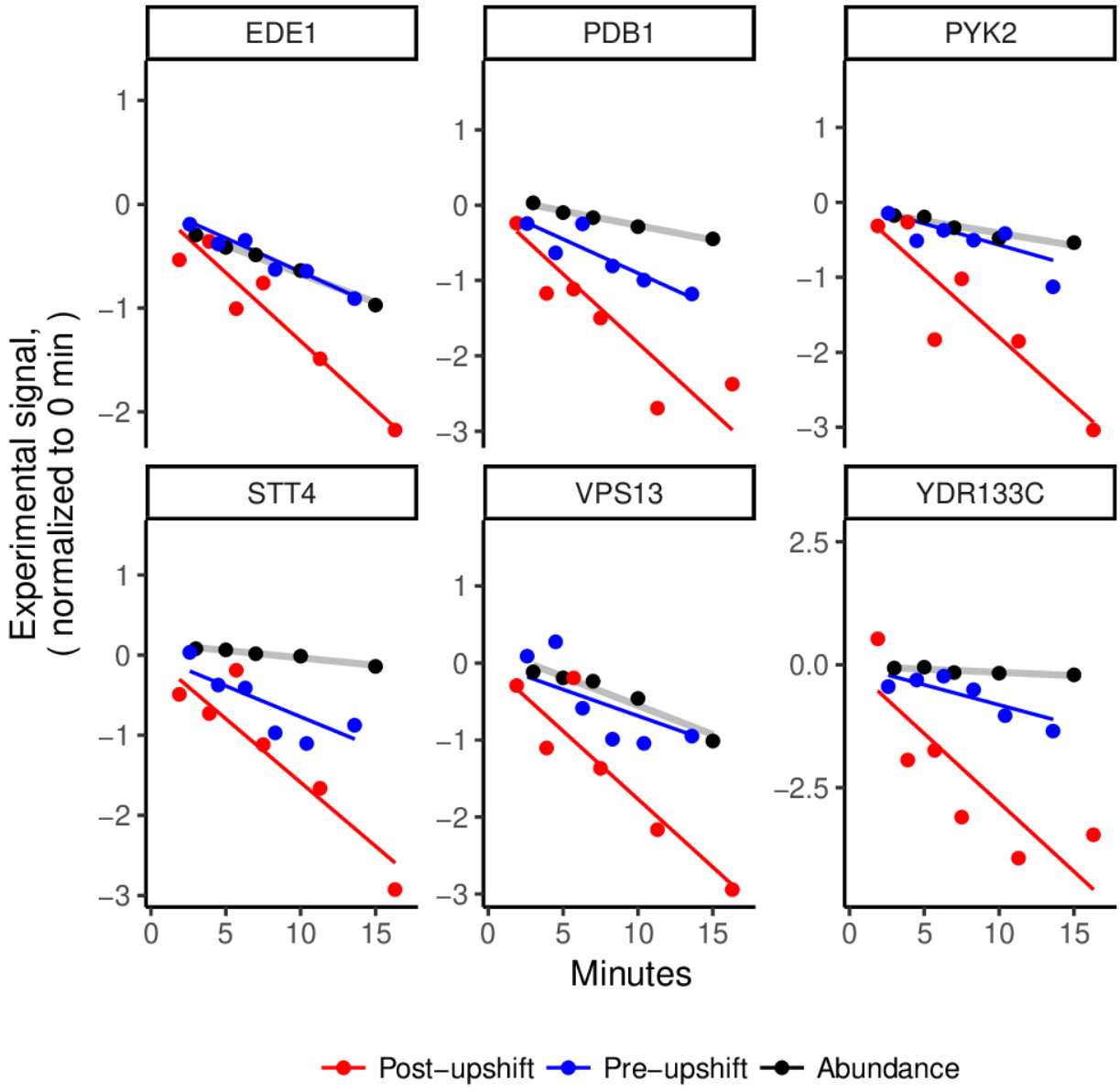

Figure 3.9: **Six examples of individual mRNA whose regulation is more complex than a homo-directional destabilization and synthesis repression.** For several examples of the slowest decreasing (in the microarray fits) transcripts, we plot the microarray (abundance) and sequencing (decaying labeled abundance) data normalized to be on the same relative y-axis scale (subtracted t_0 y-intercepts of fits). Destabilization does not necessarily result in a rapid clearance of the mRNA.

Functional coordination of mRNA stability changes suggests a possible role for *cis*-element regulation. We analyzed UTRs and coding sequence for enrichment of new

motifs or known RNA binding protein (RBP) motifs. 3' UTRs of destabilized transcripts are depleted of Puf3p binding sites, and we found no enriched sequence motif in the 3' UTRs. 5' UTRs are enriched for a GGGG motif, which may be explained by convergence between mRNA stability changes and transcriptional control by Msn2/4 on the ESR up genes (Figure 3.7, Canadell et al. 2015; Gasch et al. 2000). 5' UTRs are also enriched for binding motifs reported for Hrp1p (Figure 3.10), a canonical member of the nuclear cleavage factor I complex (Chen and Hyman 1998). However, this protein has been shown to shuttle to the cytoplasm where it may play a regulatory role (Guisbert et al. 2005; Kebaara et al. 2003; Kessler et al. 1997). On average, destabilized mRNAs are longer and contain more optimal codons (Figure 3.11, Khong et al. 2017). Together, this analysis suggests that the mechanism of destabilization may act through cis elements in the 5' UTR or biased codon usage. Both of these may affect the density or elongation kinetics of the process of translation, which may directly interact with components involved in mRNA degradation or indirectly affect the accessibility of the mRNA to these components in the cytoplasm Huch and Nissan 2017.

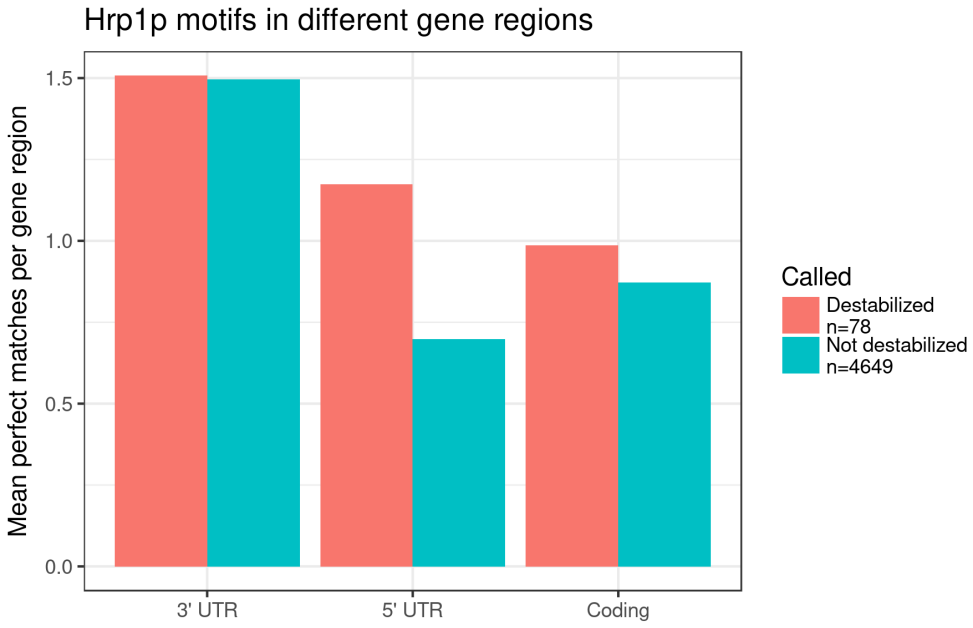

Figure 3.10: **Enrichment of Hrp1p motif in 5’ UTRs of destabilized transcripts.** Sequences of destabilized and unaltered mRNAs were analyzed for RBP binding motif enrichment using the AME program in MEME, then significant hits were confirmed by using a logistic model predicting destabilization based on motif content per sequence length. Hrp1p is significantly ($p<0.0001$) enriched in the 5’ UTRs of destabilized transcripts. For this plot, motif matches were counted using the GRanges package (Lawrence et al. 2013) for the 5’ UTRs, 3’ UTRs, and coding sequence of transcripts using the largest isoforms detected in Pelechano et al. 2014.

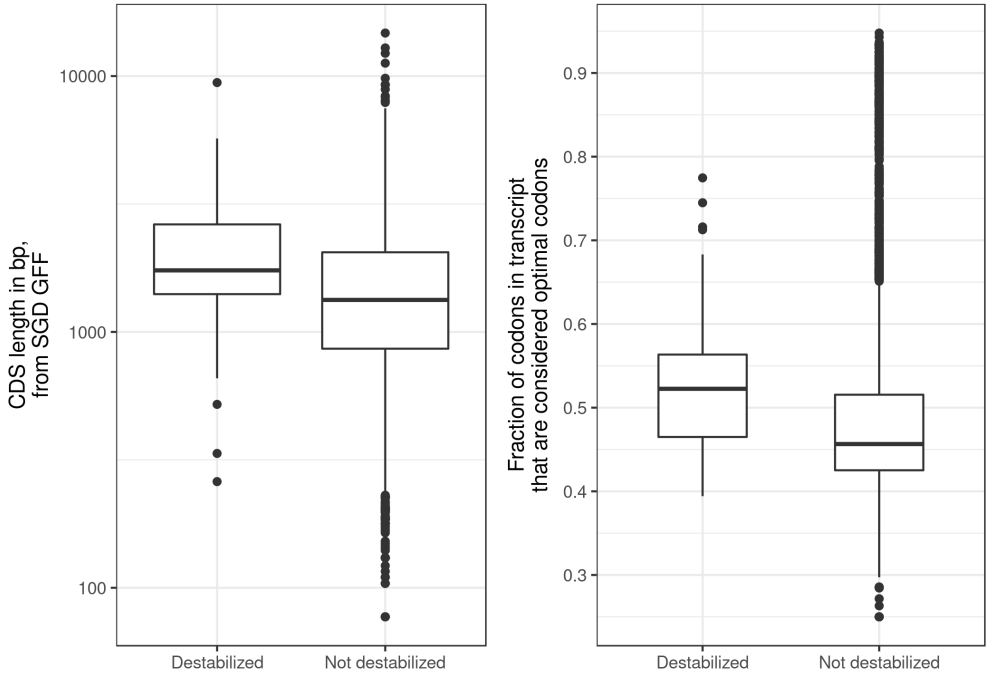

Figure 3.11: **The destabilized set is longer and has a higher frequency of optimal codons than the rest of the transcriptome.** Comparisons of destabilized mRNAs with the rest of the transcriptome. **(Left)** Destabilized transcripts tend to have longer CDS lengths (p-value < 2e-5 by Wilcoxon rank sum test). **(Right)** The destabilized transcripts tend to have a greater fraction of codons that are considered optimal codons than the non-destabilized transcripts (p-value < 2e-8 Wilcoxon rank sum test). The fraction of optimal codons per feature was obtained from the supplement of Khong et al. 2017 using definitions from Presnyak et al. 2015.

3.3.3 Methods and materials

3.3.3.1 Measurement of growth during upshift

A single colony of FY4 was inoculated in 5mL proline-limited media and grown to exponential phase, then back diluted in proline-limited media in a baffled flask. Samples were collected into an eppendorf, sonicated, diluted in isoton solution, and analyzed with a Coulter Counter Z2 (Beckman Coulter).

3.3.3.2 Re-analysis of microarray data

Supplemental files from Airoldi et al. 2016 were downloaded, read into `localc` (an open-source spreadsheet software), a small Excel-generated auto-correction error was fixed ("Oct-1" -> "OCT1"), and the file saved as a CSV. Microarray intensity ratios were processed with `pcaMethods` to perform a SVD PCA on scaled data.

3.3.3.3 Synthetic RNA spike-in generation

Poly-adenylated RNA molecules were synthesized *in vitro* using a Promega Riboprobe SP6 kit (P1420) with 4-thiouridine, as previously described (Neymotin et al. 2014), to serve as spike-in calibrators for RNAseq normalization across samples. Ampure XP beads were used to clean up the reaction. Products were quantified using the Qubit HS RNA assay, and equivalent mass amounts of spike-ins were pooled to create a 8ng/μL stock containing all four 4-thiouridine-labeled spike-ins.

We also prepared total 4-thiouracil labeled *E. coli* RNA to use as another spike-in. We grew strain MG1655 (a gift of Edo Kussell) overnight in 5mL of LB with 20μM of 4-thiouracil, then outgrew this for 2.5 hours in the presence of 4-thiouracil, then extracted by boiling the pellet with 1% SDS, 100mM NaCl, and 8mM EDTA for 5 minutes with intermittent vortexing, before cleaning up with a phenol chloroform extraction. The product was quantified using qubit and diluted to a 5ng/μL solution of thiolated total *E. coli* RNA.

3.3.3.4 Culturing and sampling

FY4 was grown in nitrogen-limitation conditions overnight (26 hours) with a mixture of 50μM:50μM of 4-thiouracil:uracil. The culture was split into two 450ml cultures 5 hours before the label chase began. During exponential phase growth ($\sim 5 \times 10^6$ cells per mL), uracil from a 400mM DMSO stock was added to a final concentration of 4mM (41-fold ex-

cess) to chase the label. 30mL samples from the culture were collected by filtration and flash-freezing within a minute of removal from the flask, and sampling time is recorded as the time of flash-freezing. After letting the chase proceed for 12.5 minutes, I added glutamine from 100mM stock (dissolved in water) to a final concentration of 400μM to one flask, or an equal volume of water to the control flask.

Timepoints were chosen to sample five times before the intervention, but timepoints actually used are the times that the sample was dropped into liquid nitrogen for fixation. For mock treatment (water at 13 minutes), this was 3.85, 6.02, 7.92, 9.90, 11.8, 15.1, 17.0, 18.8, 20.8, 22.9, 26.1, and 50.5 minutes. For nitrogen upshift (glutamine at 12.5 minutes), this was 3.30, 5.32, 7.65, 9.47, 11.3, 14.4, 16.4, 18.2, 20.0, 23.8, 28.8, and 49.1 minutes.

3.3.3.5 RNA Extraction

Since equal volume (30mL) of culture was taken for each sample, an equal volume of synthetic spike-ins was added to each RNA extraction reaction (hot acid-phenol method). The extraction yielded at least 3.3 μg of RNA per 10^7 cells.

3.3.3.6 Biotinlyation and fractionation

The total RNA (yeast and spike-ins, mixed) was reacted by adding a total of 20μg MTSEA-biotin diluted in DMF to 200μL of HEPES buffered total RNA solution, and incubating for 2 hours. Biotinylated total RNA was fractionated with streptavidin bead pulldown, using 200μL of NEB (S1420S) streptavidin beads. These were bound for 20 minute incubation, then pulled down and solution discarded, then washed four times with bead buffer, three times at room-temperature and once at 65C. Labeled mRNA was eluted using beta-mercaptoethanol, twice, then precipitated.

3.3.3.7 rRNA depletion

Fractionated RNA was depleted of rRNA using the RiboZero kit (Illumina RZY1324) according to manufacturer instructions, except that for every reaction of 2μg input RNA, we used half-reactions (half of every supplied reagent). Final RNA was ethanol precipitated, as above. Agilent Tapestation measurements of the RNA size histograms confirmed that virtually all of the rRNA was removed, and later computation analysis found very few rRNA reads in the sequencing results.

3.3.3.8 Preparing sequencing libraries

RNA samples were converted into Illumina sequencing libraries using a strand-specific (UNG) protocol. Briefly, 1st strand cDNA was synthesized using a SuperScript III kit (Invitrogen), primed with random hexamers. RNA was fragmented by 98C hybridization for 1 minute in 4.17mM $MgCl_2$, then actinomycin and the SuperScriptIII enzyme were added after annealing. This was incubated to extend first strand in a series of increasing temperature steps over the course of an hour. This reaction was ethanol precipitated and resuspended for a second-strand reaction that incorporated dUTP in the place of dTTP, using a cocktail of DNA PolI, Ecoli ligase, and RNAseH. This was reacted at 16C for 2 hours, then cleaned up on MinElute nucleic acid purification columns (Qiagen 28004). This product was eluted, end-repaired using T4 DNA polymerase and PNK, then cleaned up on MinElute columns. This product was eluted, A-tailed with Klenow (exo-), then cleaned up on MinElute columns.

This product, fresh from A-tailing, was ligated with "TrUMISeq" adapters made by a former graduate student in the lab (Hong and Gresham 2017). These are TruSeq adapters, but the sample index has been incorporated as the first six bases sequenced from the sequencing priming site and a final T exists to help with ligation. In place of the sample index (interior to the adapter), a degenerate sequence is incorporated during

synthesis. These adapters, theoretically, mark each unique ligation event with a DNA barcode sampled from a degenerate pool of $4^6 = 4096$ different barcodes. This greatly reduces the chance that two molecules that appear to be PCR duplicates (false double-counting by virtue of the amplification scheme) are actually considered to be duplicates in the analysis. For a more in-depth discussion of UMIs, please see Designing an analysis pipeline to filter dimers and extract UMIs from indeterminate locations.

These ligations were all of the A-tailed product with 20nM annealed adapter, each reaction with a different sample index. These were reacted using Quick Ligase (NEB), reacted at 22C for 15 minutes before immediate clean-up with Ampure XP beads (BeckmanCoulter). These were selected twice on beads to remove small adapters. To amplify libraries and select the strand-specificity, I prepared a master-mix of NEB Phusion buffer with primers DGO366 and DGO367, reacted this with UNG (Thermo EN0361) to digest the dUTP containing strand, then added NEB Phusion polymerase and PCR amplified for 18 cycles. These reactions were cleaned up using a MinElute column, then diluted and concentration estimated using qPCR on a Roche 480 (using KAPA Library Quant Kit Illumina REF 07960281001), and submitted as a 1nM pool to the NYU GenCore system for sequencing on a NextSeq using the 75bp format in High-Output mode.

3.3.4 4tU label-chase sequencing analysis and modeling

3.3.4.1 Quantifying sequencing reads

Following base-calling and demultiplexing by NYU GenCore, the sequencing reads were quantified using the following pipeline:

1. Raw reads were trimmed using `cutadapt` (Martin 2011)
2. Trimmed reads were aligned using `tophat2` (Kim et al. 2013) to a reference genome that included the yeast reference genome (assembly R64), the Ecoli genome (assembly GCF_000005845.2), and the four synthetic in-vitro transcribed spike-ins

(termed BES and available in the `data.zip` archive of the OSF archive associated with this paper). This was done with parameters optimized against *in silico* data generated by Flux Simulator `http://sammeth.net/confluence/display/SIM/Home` from this reference genome, in replicates.

3. Reads with mapping quality above 20 and with at least 50 matched bases with `samtools` (Li et al. 2009) were processed with `umi_tools` (Smith et al. 2017) in "dir" mode to de-duplicate possible PCR duplicates.

4. The demultiplexed `.bam` file was processed with the `htseq-count` (Anders et al. 2015) script to generate counts files per gene feature (according to the GFF file in the `data/BES` directory).

3.3.4.2 Normalization of counts into signal for modeling

In order to accurately estimate degradation rates, I must accurately estimate labeled mRNA abundance within each timepoint. This is achieved by normalizing the signal of the mRNA (counts) to the signal of a spiked-in reference transcript pool (the four spike-ins added during extraction).

The simplest normalization is to divide each feature counts by the sum of the counts of all the spike-ins (personal communication, Daniel Tranchina). However, the low RNA abundances of several samples in this experiment had poor quantification of the spike-in which required me to remove outlier measurements to prevent systematically noisy data from disrupting the quantification.

I decided to smooth the normalization across the samples, as we expect the proportion of counts that are the spike-ins to increase over time. This assumes that the whole transcriptome decays with exponential kinetics (Petersen et al. 1976).

In the sequencing data, we clearly see that the proportion of counts that are the spike-ins increases with time. Figure 3.12. We modeled this increase using the `lm` func-

tion to linearly regress this in natural-log-space. We see that the residuals are randomly distributed around the fit across time for both treatments Figure 3.12. Using an ANCOVA (`aov`/`lm`), I found the effect of treatment was associated with a p-value < 0.301 and the p-value associated with time estimated as "1", so it does not appear that the residuals particularly depend on time or treatment.

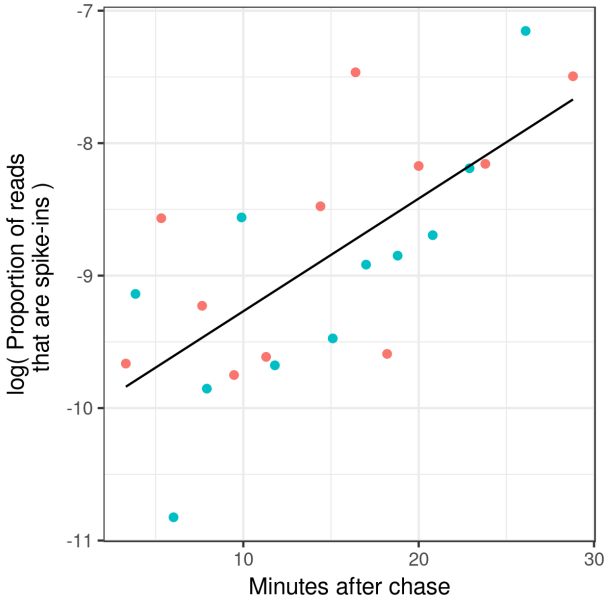

Figure 3.12: **The proportion of spike-in counts increase over the course of the experiment.** The observed proportion of counts that are synthetic spike-ins is each point. The line is a regression fit to both treatment datasets.

How do the normalizations compare on a per-gene basis? 3.13 compares this.

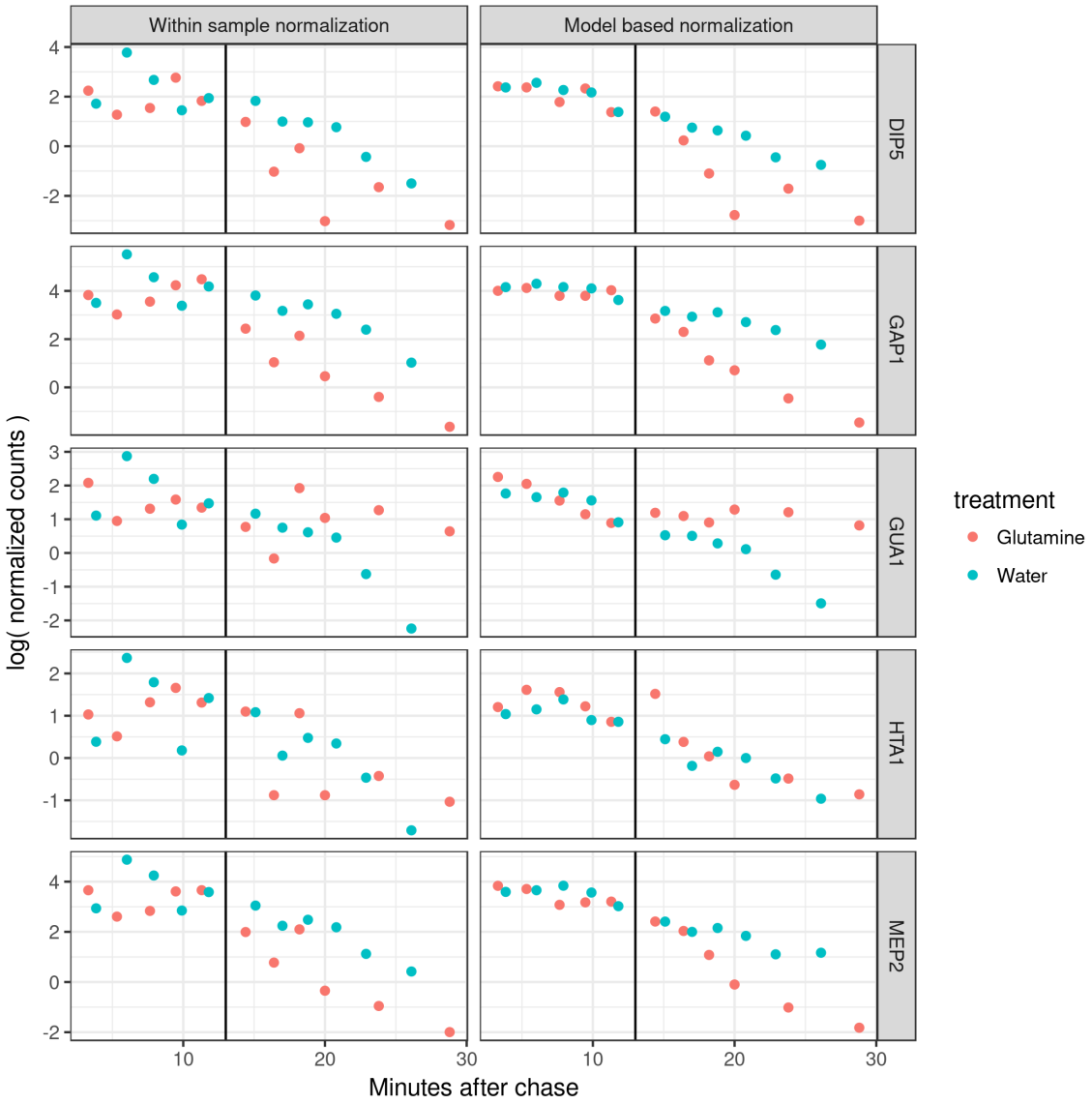

Figure 3.13: **Several examples of alternative normalization strategies.** The results of the two strategies are shown on the left (direct normalization) and on the right (model-based). For several example genes, we see that the model-based smoothing reduces the noise.

The direct normalization of each gene in each timepoint combines the noise of both the measured gene and the measured spike-ins. By smoothing across timepoints, given our expectation of whole-transcriptome exponential decay dynamics, we can deliver a more reliable estimate for each gene feature. Thus more observations can be reliably analyzed without single sample spike-in errors systematically skewing the fits across all

features.

We also tried to spike-in labeled *E. coli* total RNA; however, we found that those counts were low, noisy, and did not behave as expected from previous work (Neymotin et al. 2014). We hypothesize that this was due to lower addition of *E. coli* total RNA than synthetic spike-ins, combined with noise associated with amplifying a random sub-sample of a more complex spike-in pool of total *E. coli* RNA. Each sub-sample may have very different GC-content, and thus may be amplified to a different degree. Thus, we normalized all yeast mRNA to the synthetic spike-ins as previously demonstrated. Sampling from a complex spike-in library may be an important consideration for their use in normalization, and may warrant further technical experimentation.

3.3.4.3 Model of transcript dynamics as a function of dynamics and labeling parameters

To analyze this data, I fit a model of labeled transcript dynamics. I used this model to analyze the dataset for expected label-chase dynamics, and also to exclude effects that may result from a confounding of new synthesis with changes in degradation rates.

m_t is the labeled mRNA at time t. It changes according to the equation:

$$\frac{dm_t}{dt} = Lk_s - k_d m_t$$

where L is the fraction of new mRNA that is labeled and pulled down, k_s is the rate of synthesis, and k_d is the rate of degradation. Our experimental design is to change L from an initial fraction of transcripts that are pulled down by a 4tU-incorporation-dependent mechanism of L^o (old) to a new fraction L^n (new). Note that I use the notation as a superscript, so that I can also share that notation with the synthesis rates as k_s^o and degradation rates as k_d^o.

I assume that the culture begins at a steady state of $L^o \frac{k_s^o}{k_d^o}$, from solving the above equation. I assume this because I grow the cells for 24 hours in conditions of labeling,

and they are well below saturating conditions. Solving the above differential equations with the assumption that everything changes once, which is a simplifying assumption but supported by previous studies of transcript stability changes during shifts (Pérez-Ortín et al. 2013), I expect that m_t should behave as,

$$m_t = L^o \frac{k_s^o}{k_d^o} e^{-k_d^n t} + L^n \frac{k_s^n}{k_d^n}(1 - e^{-k_d^n t})$$

Nicely, the solution is similar to what I would expect intuitively - extant transcripts decay (left), and nascent transcripts approach the new equilibrium (right). The equilibriums are set by all parameters, but the change between them is dictated by the new degradation rate operative during the transition.

In the case were either L^o or L^n is 0, then the transcript behaves just as one side of the equation. With the label-chase, I are trying to get L^n as low as is possible without perturbing the system being measured by killing the cell. To analyze this dataset for potential changes in transcript stability, I approximated this by fitting a linear regression model to the normalized signal. I explore the sufficiency of this model later in this document using simulations. This model was fit using the `lm` function in R, with the formula

```
log( NormalizedSignal ) ~ Minutes + Minutes:Treated + 1
```

where "`NormalizedSignal`" is the signal of the gene feature normalized as described in the previous section, "`Minutes`" is minutes relative to the glutamine (or water) addition, `Minutes:Treated`" is an additional slope of the observations after glutamine addition, and "`+ 1`" denotes to fit a single intercept for the model (data are centered around the moment of treatment, t_0 is the addition of glutamine or water). From this fit, I took the p-values associated with the t-statistic of the additional slope fit to the glutamine treated samples, then adjusted the p-values using the `qvalue` package from BioCon-

ductor using default settings. I chose to use a FDR cut-off of less than 0.01 for this analysis.

3.3.4.4 Estimating possible effects of synthesis changes on labeled abundance

In our experimental design I initially grow the cells in a 50μM:50μM mix of uracil and 4-thiouracil, so I will set as a labeling ratio L^o of 1 for simplicity. I add 4,000 μM uracil to begin the chase, so this is a shift to a L^n of $\frac{50\mu M}{4100\mu M}/\frac{50\mu M}{100\mu M}$, or $\frac{1}{41}$. Since I am not reducing this number to zero, there is still residual labeling incorporated into nascent transcription. $\frac{1}{41}$ is a small number, but is still not zero and should not be neglected. Thus, there is a potential that residual label could confound our estimate of degradation rates. This is an inherent tradeoff in a label-chase design (Pérez-Ortín et al. 2013), especially since the low RNA content of the cells and low cell density in these nitrogen limited conditions make necessary the use of a more efficient pull-down reagent (MTSEA-biotin). This could be circumvented by comparing abundance and synthesis measurements, but the uracil transporter responding to glutamine in the media makes this technically difficult with 4tU incorporation. Comparing abundance and mRNA synthesis by other means is feasible, but introduces a compounding of errors from both methods. Thus performing one direct assay is preferable for precision, and the drawbacks described here are unavoidable with current technology (although progress is being made (Chan et al. 2017)).

Therefore, I used simulations to investigate how varying the labelling parameter changes the expected dynamics if we also vary the synthesis parameter. Figure 3.14 (left) shows a plot of the modeled labeled transcript abundance, with no change in synthesis parameter. How does this estimate of change in degradation look if we decrease the k_s? For example, the NCR regulon is expected to be shut-off at the synthesis level quickly upon glutamine addition, so how would that swift repression affect the apparent change in labeled mRNA dynamics? Figure 3.14 (right) shows a plot of the modeled la-

beled transcript abundance, with a k_d of 0.1 (similar to the median rate of degradation Figure 3.5) and an instantaneous shutoff of transcript synthesis.

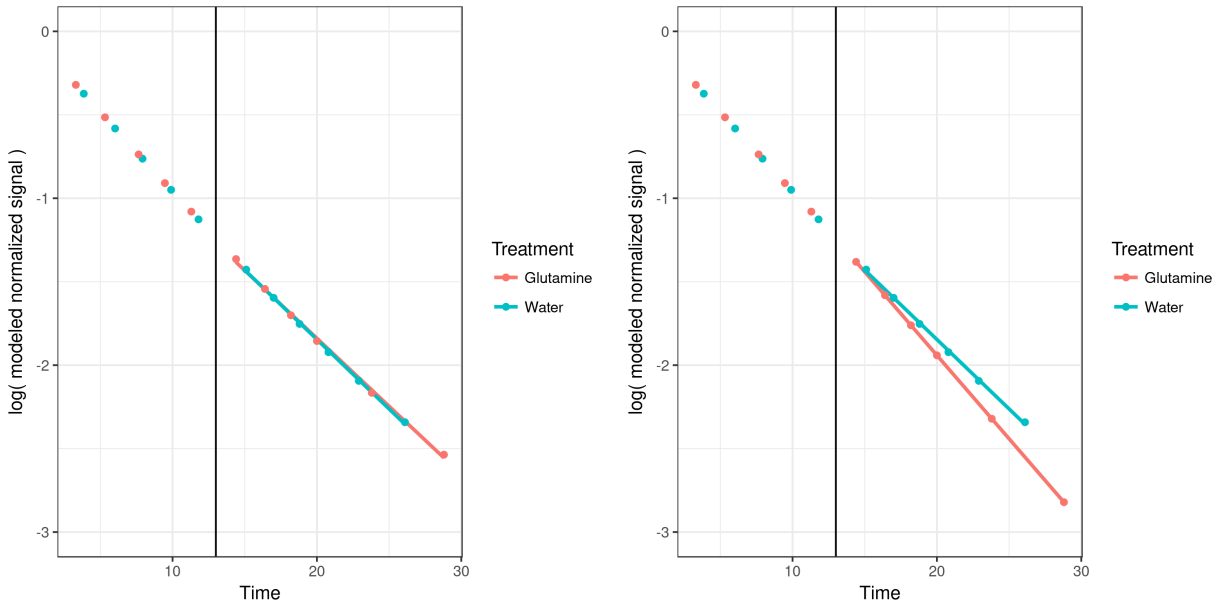

Figure 3.14: **Simulation of labeled transcript dynamics shows a slight effect from synthesis changes on a label-chase with recycling.** The timepoints along the bottom are the exact timepoints used in the actual label-chase RNA sequencing experiment. **(Left)** is with no change in synthesis. **(Right)** is with a complete halt in synthesis. We see a 13.3% decrease in the slope of change in labeled abundance over time.

The effect of reduced synthesis on apparent slope change of the labeled RNA here is a 13.3% increase in the rate. I conclude that there's a slight effect from synthesis rate changes. For transcripts that are putatively stabilized, the effect is much larger ($\sim$60%), likely because of the delay in pertubation until 13 minutes after the label chase begins.

What does this mean for our estimates of destabilization? What effect sizes are estimated, and how do they compare to this effect size? Figure 3.15 shows the distribution of the fold changes in stability:

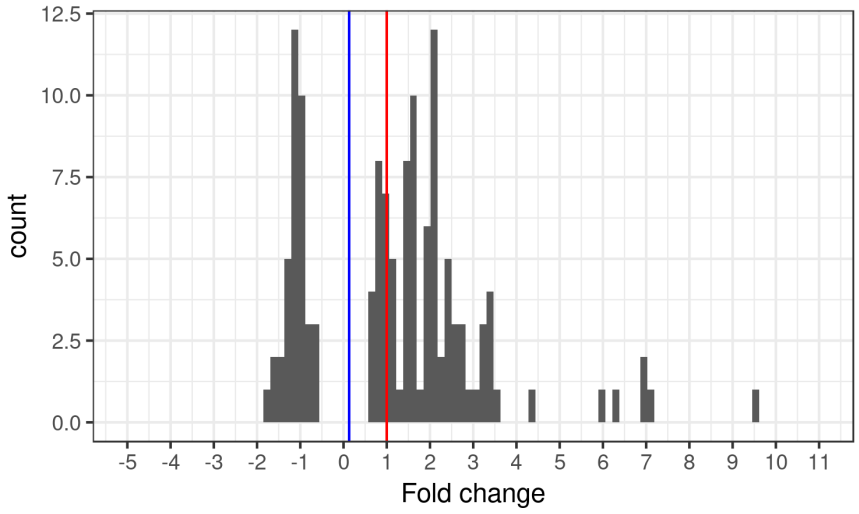

Figure 3.15: **Distribution of all fit changed rates versus effect size thresholds from modeling.** Histogram of the fold-changes in rate of labeled transcript clearance upon glutamine treatment, determined as significant by adjusting the parametric (t-statistic of slope) with a multiple-hypothesis correction (`qvalue` package Storey et al. 2015). The blue line denotes a 13.3% increase in the rate of clearance, the red line denotes a doubling of the rate. Some transcripts appear stabilized (left of 0), most are destabilized, many are destabilized more than the red cutoff.

I see that all of the significant changes are in great excess to that blue line. I choose a strict cut-off of a 100% increase, a doubling, of apparent degradation rate to call a feature destabilized (right of the red line). Since I cannot place an upper bound on the synthesis rates after a glutamine upshift, I cannot definitively say that the potentially stabilized transcripts (left of 0) are stabilized without additional experiments. Could these fits just be on the right side of the blue line by chance? Given that the t-statistics (ratio of effect size over standard error) for the fits of ones over this line are a median of -5.66, I'm not going to have fits within several standard errors of crossing that threshold by a reasonably expected error.

I conclude that the RNA from 78 gene features are degraded more quickly than can be reasonably explained by labelling carry-over, and are thus accelerated in degradation upon the nitrogen upshift. Stability changes upon the nitrogen upshift generally exhibited the expected relationship with rates of abundance change (anti-correlation,

R^2 =-0.376). However, I caution that this data is not suitable for direct interpretation with regards to the fraction of transcriptome reprogramming attributable to degradation rate changes, as an unknown fraction of the correlation could be explained by large changes in synthesis rate systematically confounded into the degradation rate estimate. I encourage the interested reader to go to `http://shiny.biology.nyu.edu/users/dhm267` to explore examples of the data under both normalizations and for a range of features.

3.3.4.5 *Cis* element analysis

To detect if *de novo* or known *cis* elements were associated with destabilization upon a nitrogen upshift, I used a variety of bioinformatic methods. For each transcript, I used a GFF file to extract the coding sequence of each annotated mRNA and four different definitions of its untranslated regions — 200bp upstream of the start codon or downstream of the stop codon, the largest detected isoform in TIF-seq from (Pelechano et al. 2014), or the most distal detected gPAR-CliP sites in exponential-phase or nitrogen-limited growth in (Freeberg et al. 2013). A more rigorous definition using 5' and 3' end sequencing methods in this particular condition would be necessary for best exploring *cis*-element enrichment with certainty.

To find putative cis-elements, I used DECOD (Huggins et al. 2011), FIRE (Elemento et al. 2007), TEISER (Goodarzi et al. 2012), and the #ATS pipeline (Li et al. 2010), I also scanned for RBP binding sites from CISBP-RNA (Ray et al. 2013) using AME from the MEME suite (McLeay and Bailey 2010).

The enrichment for the Hrp1p motif is described in Figure 3.10. It is worth noting that this is the core-element of Hrp1p (also known as Nab4p) described in Chen and Hyman 1998; Guisbert et al. 2005, but is mistakenly recorded in the CISBP-RNA database as being the motif for Npl3p. Guisbert et al. 2005 did not find a motif for Npl3p.

3.4 Estimating *GAP1* mRNA for every mutant in a pool

3.4.1 A genome-wide screen for *trans*-factors regulating *GAP1* mRNA repression

We sought to identify *trans*-factors mediating accelerated mRNA degradation in response to a nitrogen upshift. We selected *GAP1* as representative of transcript destabilization, as it is abundant in nitrogen-limiting conditions and is rapidly cleared upon addition of glutamine (3.24-fold increase in degradation rate, Figure 3.16, Supplementary tables). Previous approaches to high-throughput genetics of transcriptional activity have used protein expression reporters (Neklesa and Davis 2009; Sliva et al. 2016) or automation of qPCR (Worley et al. 2016). However, for our purposes, we required direct measurement of *GAP1* mRNA changes on a rapid timescale. We decided to focus on a single mRNA readout to explore the efficacy of this approach. While multiple readouts is theoretically more informative, the practicality of expanding the SortSeq paradigm to another marker poses technical challenges beyond our current capabilities (moving from 4 bins to 16 bins dilutes the library greatly, available sorter does 4 bins maximum). Therefore, we applied single molecule fluorescent *in situ* hybridization (smFISH) to quantify native *GAP1* transcripts in yeast cells in the pooled prototrophic yeast deletion collection (VanderSluis et al. 2014). Using fluorescence activated cell sorting (FACS) and Barseq (Giaever and Nislow 2014; Robinson et al. 2014; Smith et al. 2009), we aimed to quantify and model the distribution of *GAP1* mRNA in each mutant (Kinney et al. 2010; Peterman and Levine 2016).

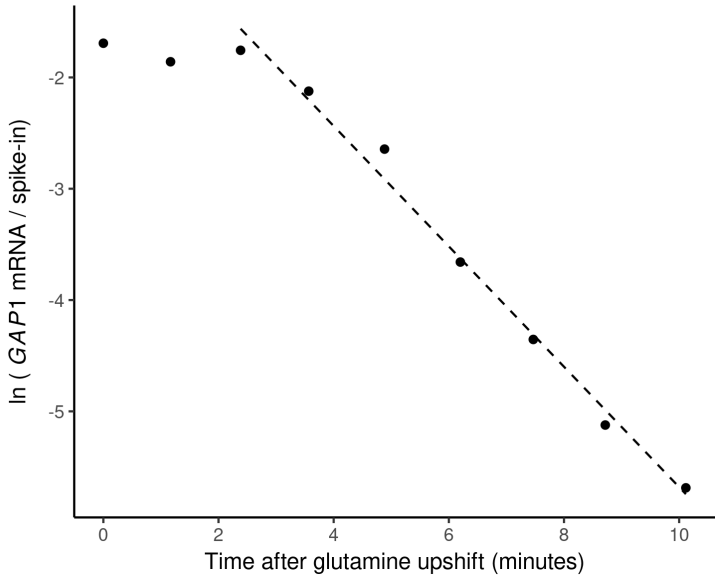

Figure 3.16: ***GAP1* mRNA dynamics by qPCR normalized to a spike-in shows the rapid clearance of *GAP1* mRNA.** *GAP1* mRNA following upshift measured using RT-qPCR, relative to an external spike-in mRNA standard. The dashed line is fit to points after 2 minutes.

We found that individually labeled probes tiled across *GAP1* mRNA (Raj et al. 2008) were insufficiently bright for *GAP1* mRNA quantification using flow cytometry (data not shown), likely due to the small cell size of nitrogen-limited cells and the low transcript numbers in yeast cells compared to mammalian cells (Klemm et al. 2014). Therefore, we used branched DNA probes (Quantigene), which serve to amplify the FISH signal (Hanley et al. 2013). We developed a fixation and permeabilization protocol (Design of Barseq after FACS after FISH experiment) that enabled detection of the distribution of *GAP1* mRNA in steady-state nitrogen-limited conditions and its repression following the upshift (Figure 3.18). In control experiments, we found that the signal is eliminated in a *GAP1* deletion or by omitting the targeting probe (Figure 3.18 and Figure 3.17). To validate sorting, we sorted a sample of cells into quartiles and used microscopy to count fluorescent foci per cell (Figure 3.19) . We found that increased flow cytometry signal is associated with an increase in the number of foci in the cells (Figure 3.20, R^2 = 0.607,

$p < 10^{-11}$).

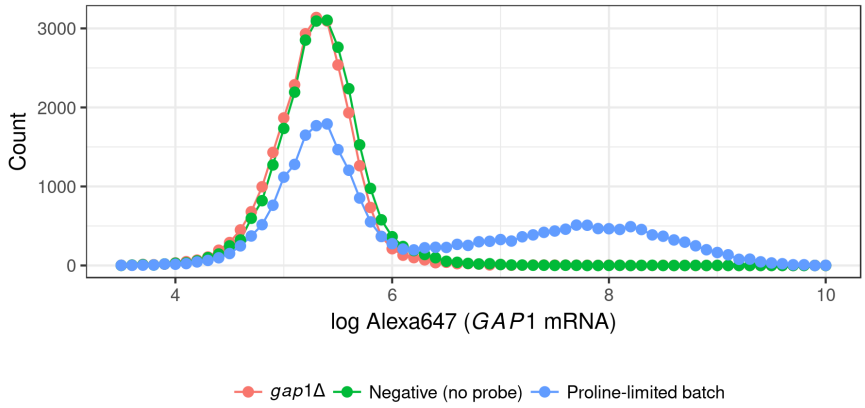

Figure 3.17: **Both the *GAP1* delete and omission of the targeting probe removes signal of GAP1 FISH.** Wild-type or *gap1*Δ cells were grown in proline-media, which induces expression of *GAP1*. As seen in the positive control, there is heterogeneity in the induction. This is likely due to technical issues, namely over fixation. Importantly, *gap1*Δ does not have any positive signal.

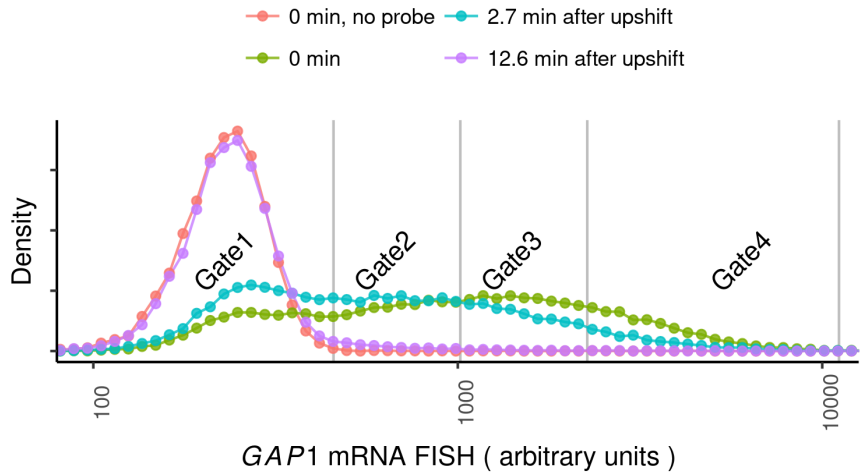

Figure 3.18: ***GAP1* mRNA dynamics measured by flow cytometry.** Flow cytometry of wild-type yeast in nitrogen-limited conditions and following an upshift. The vertical grey lines indicate FACS gate boundaries used for cell sorting, for Figure 3.19 microscopy.

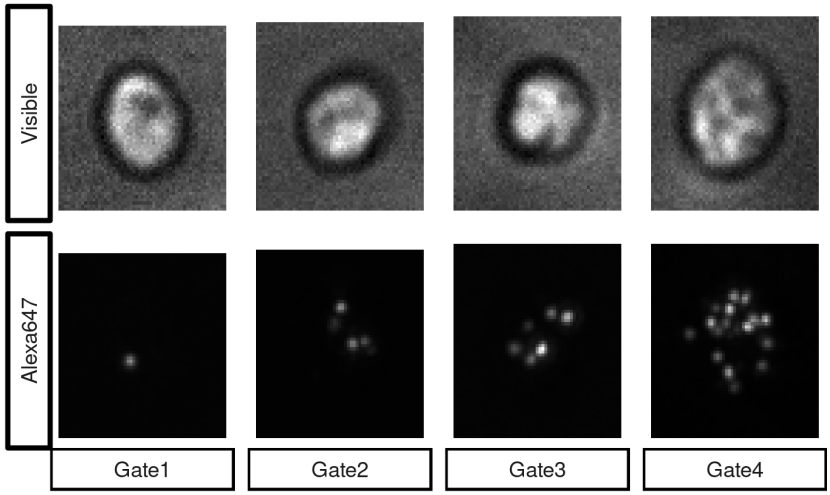

Figure 3.19: **Example microscopy of cells sorted by *GAP1* mRNA.** Representative cells from each bin sorted from the experiment in Figure 3.18. Alexa647 signal is imaged with a Cy5 filter set.

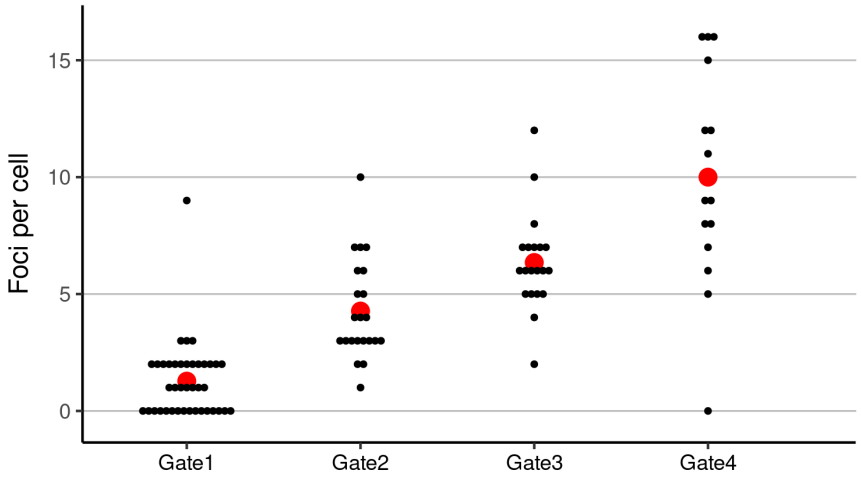

Figure 3.20: **Quantification of microscopy of cells sorted by *GAP1* mRNA.** Cells sorted from Figure 3.18 were manually scored in z-stacks for Alexa647 foci. Each black dot represents the total for a single cell. The mean number of foci per cell in each bin is displayed as a red point.

Previous SortSeq studies of the yeast deletion collection have used outgrowth to generate sufficient material for Barseq (Sliva et al. 2016). However, formaldehyde fixation precludes outgrowth. We found that below approximately 10^6 templates, the Barseq reaction produces primer dimers that outcompete the intended PCR product (Design of

Barseq after FACS after FISH experiment). Therefore, we re-designed the PCR reaction (Robinson et al. 2014; Smith et al. 2009) to be robust for very low sample inputs (Design of Barseq after FACS after FISH experiment). Our protocol incorporates a 6-bp unique molecular identifier (UMI) into the first round of extension to identify PCR duplicates, and uses 3'-phosphorylated oligonucleotides and a strand-displacing polymerase (Vent exo-) to block primer dimer formation and off-target amplification. Because strain barcodes are of variable lengths, we developed a bioinformatic pipeline to extract barcodes and UMIs using pairwise alignment to invariant flanking sequences. Based on *in silico* benchmarks, this approach was robust to systematic and simulated random errors that can confound analysis of the yeast deletion barcodes (Availability of data and analysis scripts, Design of Barseq after FACS after FISH experiment).

We refer to this experimental approach as BFF (Barseq after FACS after FISH). We used BFF to estimate *GAP1* mRNA abundance for every mutant in the haploid prototrophic deletion collection (VanderSluis et al. 2014) in nitrogen-limiting conditions and 10 minutes following the upshift. This approach facilitates identification of mutants with defects in mRNA regulation at both the transcriptional and post-transcriptional level without altering *GAP1* mRNA *cis*-elements that may affect its regulation. Moreover, this design enables identification of factors that regulate both the steady-state abundance of *GAP1* mRNA and its transcriptional repression following an upshift. We analyzed the deletion pool in biological triplicate (Figure 3.23). We found that UMIs approached saturation at a slower rate than expected for random sampling, consistent with PCR amplification bias (Figure 3.35), and therefore we adopted the correction of Fu et al. 2011 (dicussed in depth later). After filtering, we calculated a pseudo-events metric that approximates the number of each mutant sorted into each bin. Principal components analysis shows that the samples are separated primarily by FACS bin within each condition and biological replicates are clustered indicating that our approach re-

producibly captures the variation of *GAP1* mRNA flow cytometry signal across the library (Figure 3.21).

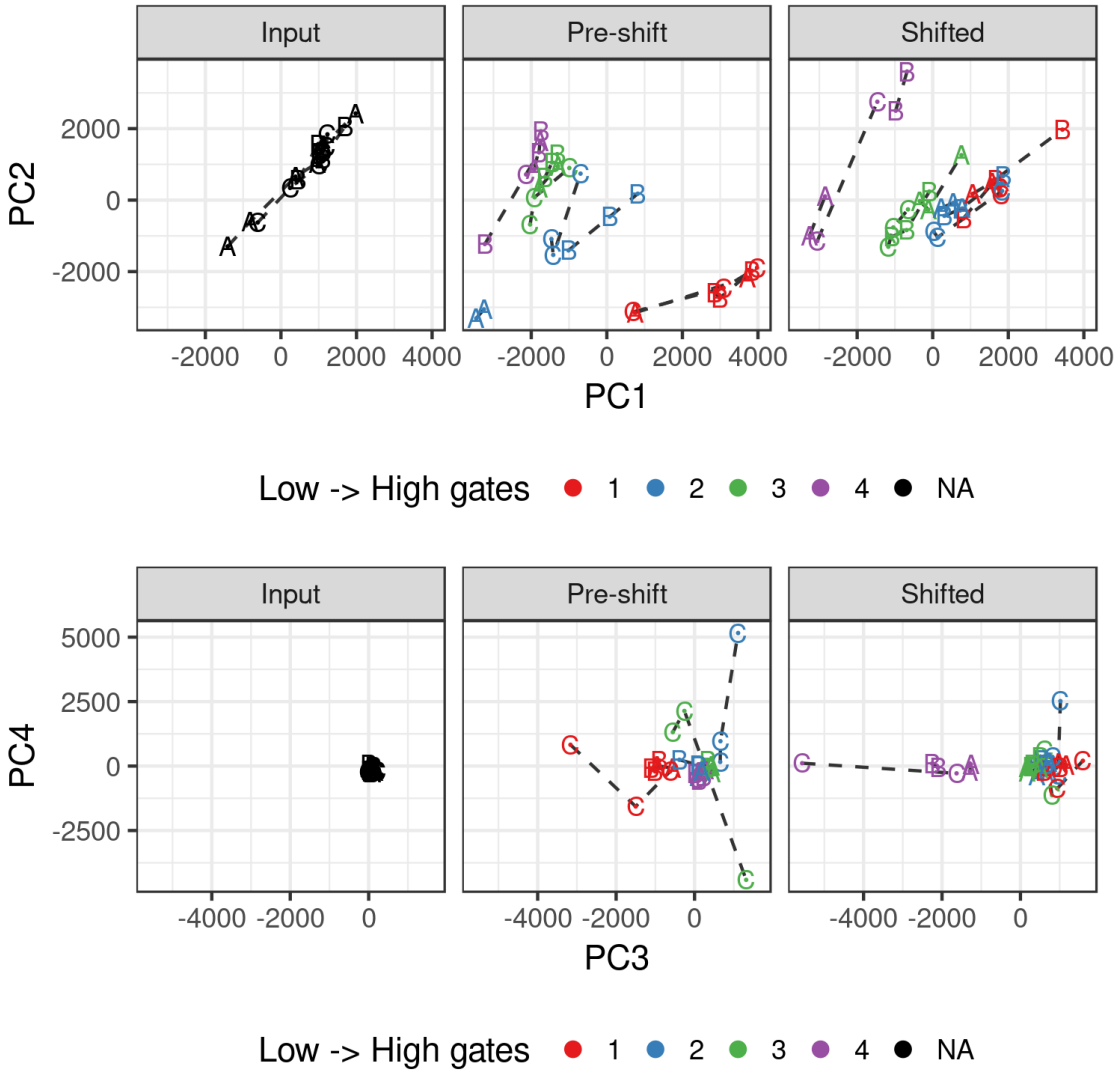

Figure 3.21: **Principal components analysis of the abundance estimates for samples captures variation along *GAP1* abundance.** Each letter is the point, with the letter denoting the biological replicate and dashed lines connecting the technical replicates of each sample. Each color is a type of sample, from low to high gates (with black denoting the input samples before sort). **(Top)** The first two prinicpal components show the separation of gates by signal intensity, and reflects that the lower gates on the upshifted samples were both sampling from the same negative population (blue and red samples on far right panel, lowest two bins post-upshift in Figure 3.23). **(Bottom)** A similar pattern in principal components 3 and 4, although this highlights that bin 1 is the most distinct before the shift and bin 4 is most distinct after the shift.

3.4.2 Estimating *GAP1* mRNA abundance for individual mutants

We estimated the distribution of *GAP1* mRNA for each mutant by modeling pseudo-events in each quartile as a log-normal distribution using likelihood maximization (Figure 3.22). From model fits we estimated the mean *GAP1* abundance for each mutant and found that the distribution of means estimated for 3,230 strains (Supplementary tables, Figure 3.23) recapitulates the overall distribution of flow cytometry signal (Figure 3.23). To validate our approach we first examined strains for which we expected to have a specific phenotype and compared their mean *GAP1* abundance to the distribution of *GAP1* abundances for the entire population (Figure 3.24).

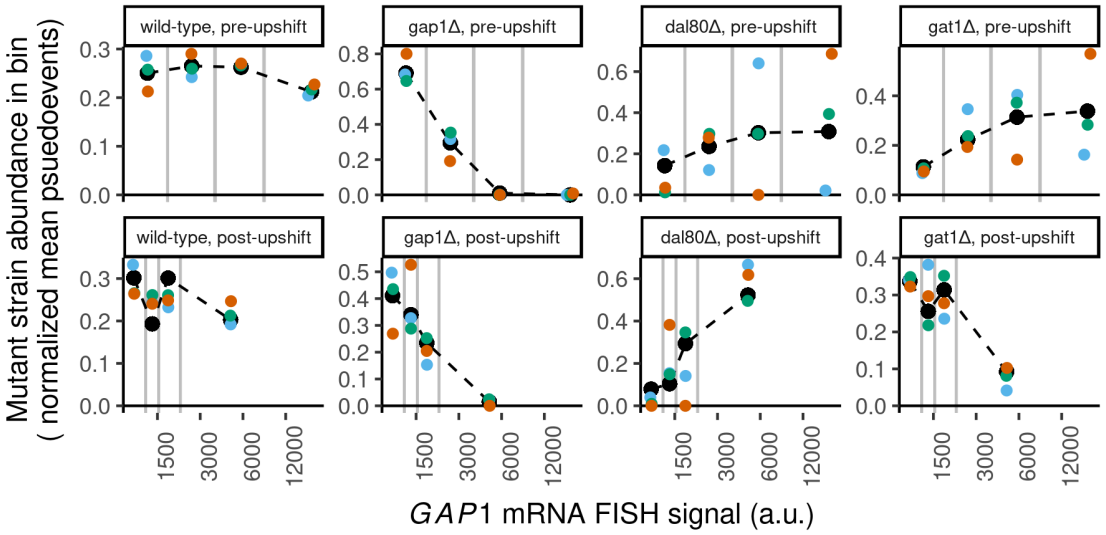

Figure 3.22: **Data and models for several individual sample genes from the BFF modeling.** Measurements for individual genes before and after the upshift. Black dashed lines indicate maximum-likelihood fits of a log-normal to pseudo-events for each mutant. Each color is a biological replicate.

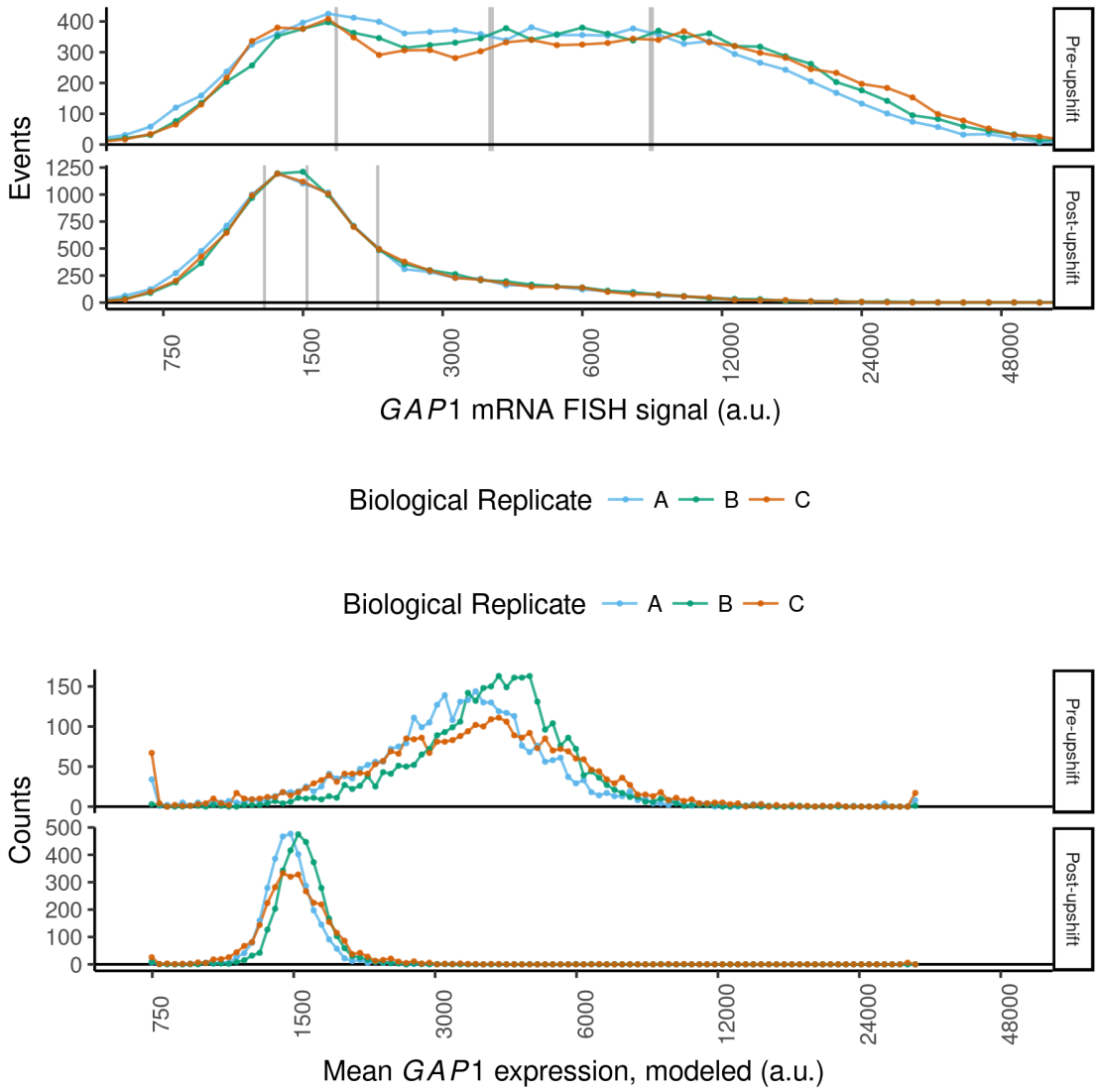

Figure 3.23: **Flow cytometry of the *GAP1* mRNA distribution across all mutants, and global distribution of *GAP1* mRNA abundance estimates. (Top)** Flow cytometry analysis of *GAP1* mRNA abundance in the prototrophic deletion collection before and after the upshift. The vertical gray lines denote FACS gates used. Biological replicates are indicated by color. **(Bottom)** Distribution of mean modeled *GAP1* mRNA levels for each mutant. The broad trends of changes in *GAP1* abundance are captured, as well as some of the differences between replicates (replicate A is slightly lower than B in both timepoints, replicate C had half as many sorted events and is thus noiser in estimates).

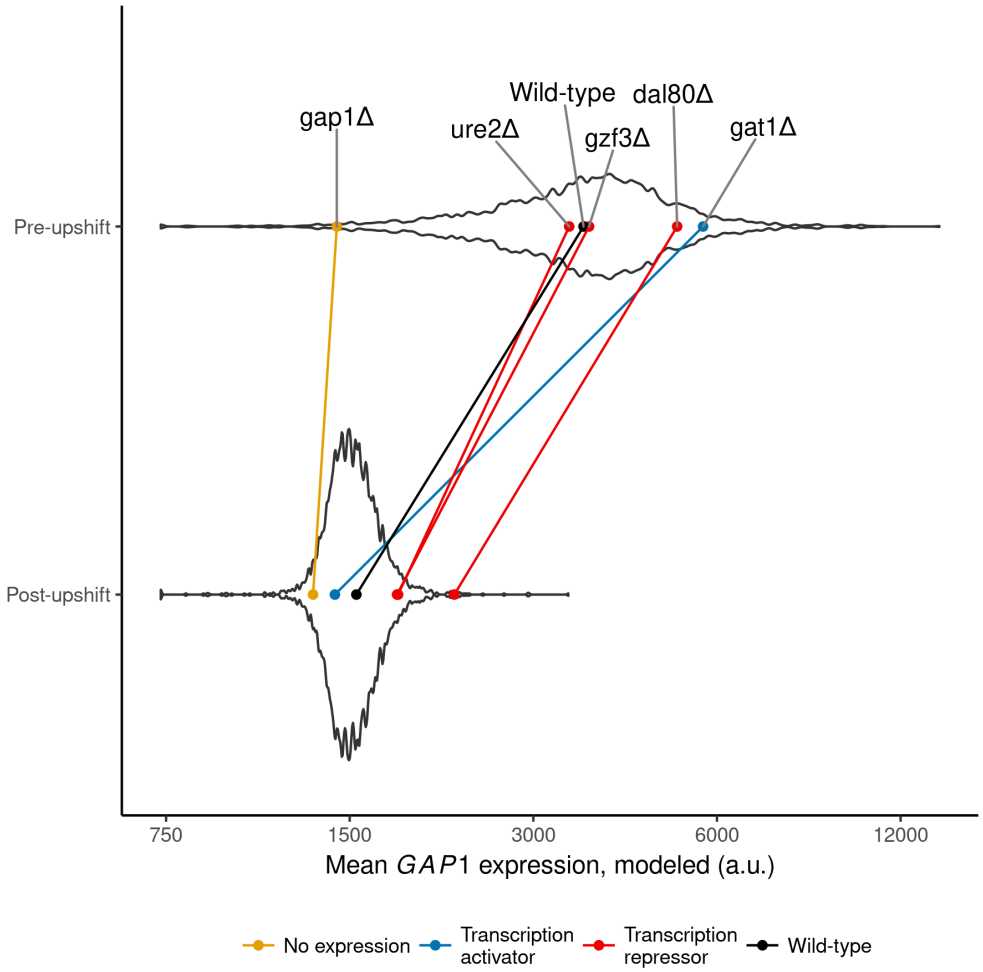

Figure 3.24: **Individual BFF estimates of *GAP1* mRNA abundance for mutants known to play a role in *GAP1* regulation.** The mean *GAP1* mRNA abundance estimated for individual mutants before and after the upshift are shown as points connected by a line, colored according to the type of gene. For reference, the background violin plot shows the distribution of all 3,230 mutants fit.

We found that the wildtype genotype (*his3*Δ, complemented by a *S. pombe HIS5* gene in library construction) has a *GAP1* abundance estimate that is centrally located in the distribution both before and following the upshift. The *gap1*Δ genotype is a negative control and we estimate that it is at the extreme low end of the distribution before and following the upshift. *dal80*Δ is a direct transcriptional repressor of NCR transcripts and we found that this strain is defective in repression of *GAP1* before and after the upshift. Counter-intuitively, deletion of *GAT1*, a transcriptional activator of *GAP1*, appears to

have higher steady-state abundance of *GAP1* mRNA. However, increased abundance of *GAP1* mRNA in a *gat1*Δ background has previously been reported (Scherens et al. 2006) and is thought to result from the complex interplay of NCR transcription factors on their own expression levels. Data and models for each mutant strain can be visualized in browser using a Shiny application (see `http://shiny.bio.nyu.edu/users/dhm267/` or Availability of data and analysis scripts).

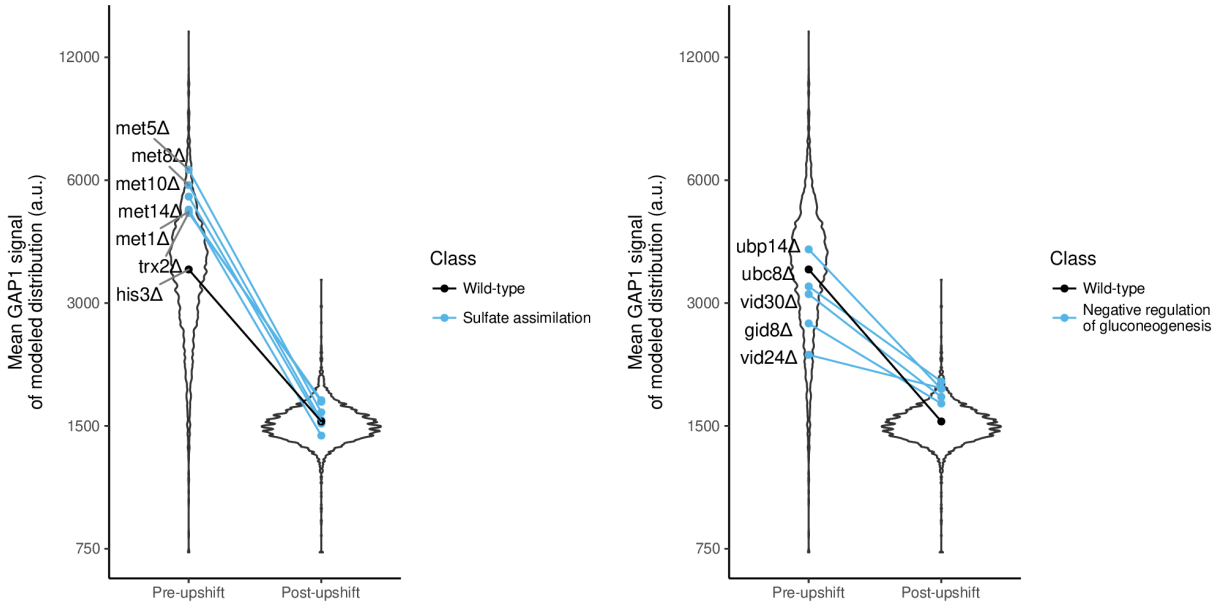

Figure 3.25: **Mutants of negative regulators of gluconeogenesis or sulfate assimilation are associated with defects in *GAP1* expression.** Mutants deleted for genes involved in sulfate assimilation **(left)** or negative regulation of gluconeogenesis **(right)** are associated with higher *GAP1* expresion before **(left)** or after **(right)** the upshift, by GSEA analysis of GO-terms (p-value < 0.05).

To identify new cellular processes that regulate *GAP1* mRNA abundance, we used gene-set enrichment analysis (Supplementary tables). Following the upshift we found that mutants with high *GAP1* abundance before the upshift are enriched for mutants in sulfate assimilation, and mutants that maintain high *GAP1* mRNA abundance are enriched for negative regulation of gluconeogenesis (Figure 3.25). However, the strongest enrichment for high *GAP1* abundance was components of the Lsm1-7p/Pat1p complex (Figure 3.28). Mutants in the TORC1 signalling pathway were not enriched, but, I did

find that a *tco89*△ mutant has greatly increased *GAP1* mRNA abundance before and after the upshift (Figure 3.26), consistent with the repressive role of TORC1 on the NCR regulon. To compare *GAP1* abundance before and after the upshift for each mutant, we regressed the post-upshift mean *GAP1* abundance against the pre-upshift mean *GAP1* abundance for each genotype (Figure 3.27).

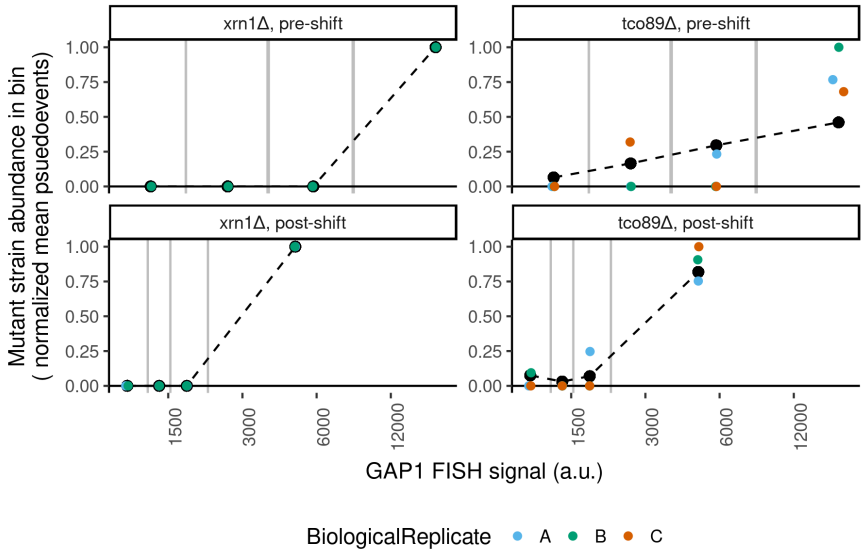

Figure 3.26: ***tco89*△ and *xrn1*△ show defects in *GAP1* mRNA regulation in the BFF assay.** Data and fits for several mutants. *xrn1*△ mutant (left) is lowly abundant in the library and is only observed in the highest bin of *GAP1* signal, consistent with the role of Xrn1p as a global exonuclease. *tco89*△ is the only detected member that would abrogate TORC1 activity. This mutant (right) has elevated *GAP1* mRNA before and after the upshift, consistent with the role of TORC1 in repressing the NCR regulon.

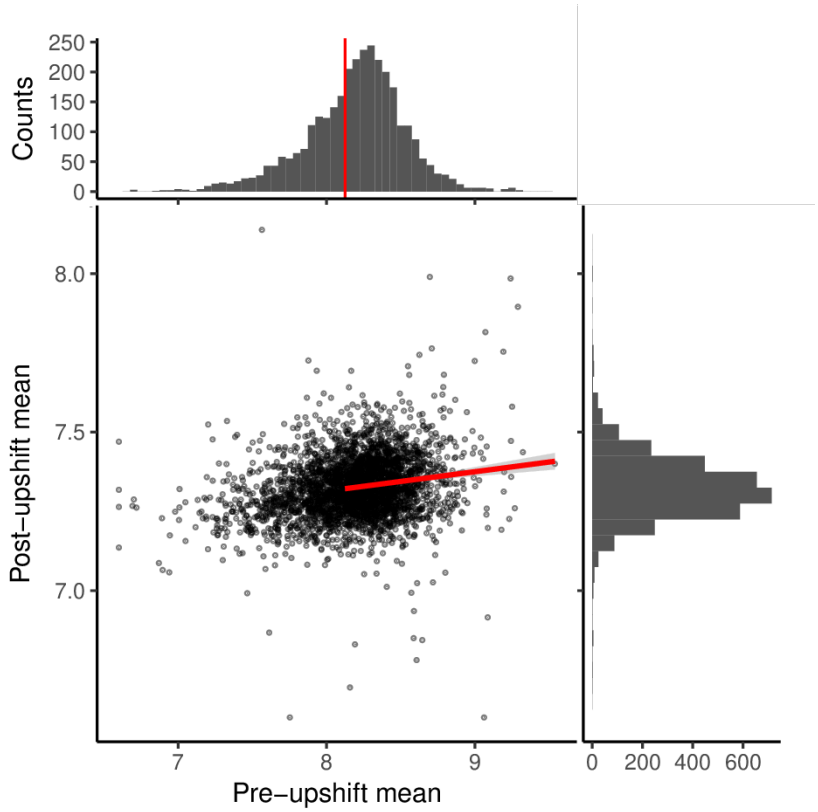

Figure 3.27: **The pre-upshift mean has a significant but slight relationship in predicting the post-upshift mean.** Scatter plot of the estimated *GAP1* abundances, with marginal histograms along top and right. Blue vertical line on top histogram is a cut-off of *GAP1* mRNA induction for this analysis, and is one standard deviation below the mean of the wild-type strain. The red linear regression line is fit to all points above this threshold, in which expression was detected before the upshift.

We used the residuals for each strain to identify mutants that clear *GAP1* mRNA with kinetics slower than expected by this model. We found that the Lsm1-7p/Pat1p complex is again strongly enriched for slower than expected *GAP1* mRNA clearance (Supplementary tables). Specifically the *lsm1*Δ, *lsm6*Δ, and *pat1*Δ strains are highly elevated in *GAP1* abundance before the upshift and strongly impaired in the repression of *GAP1* mRNA after the upshift (Figure 3.28).

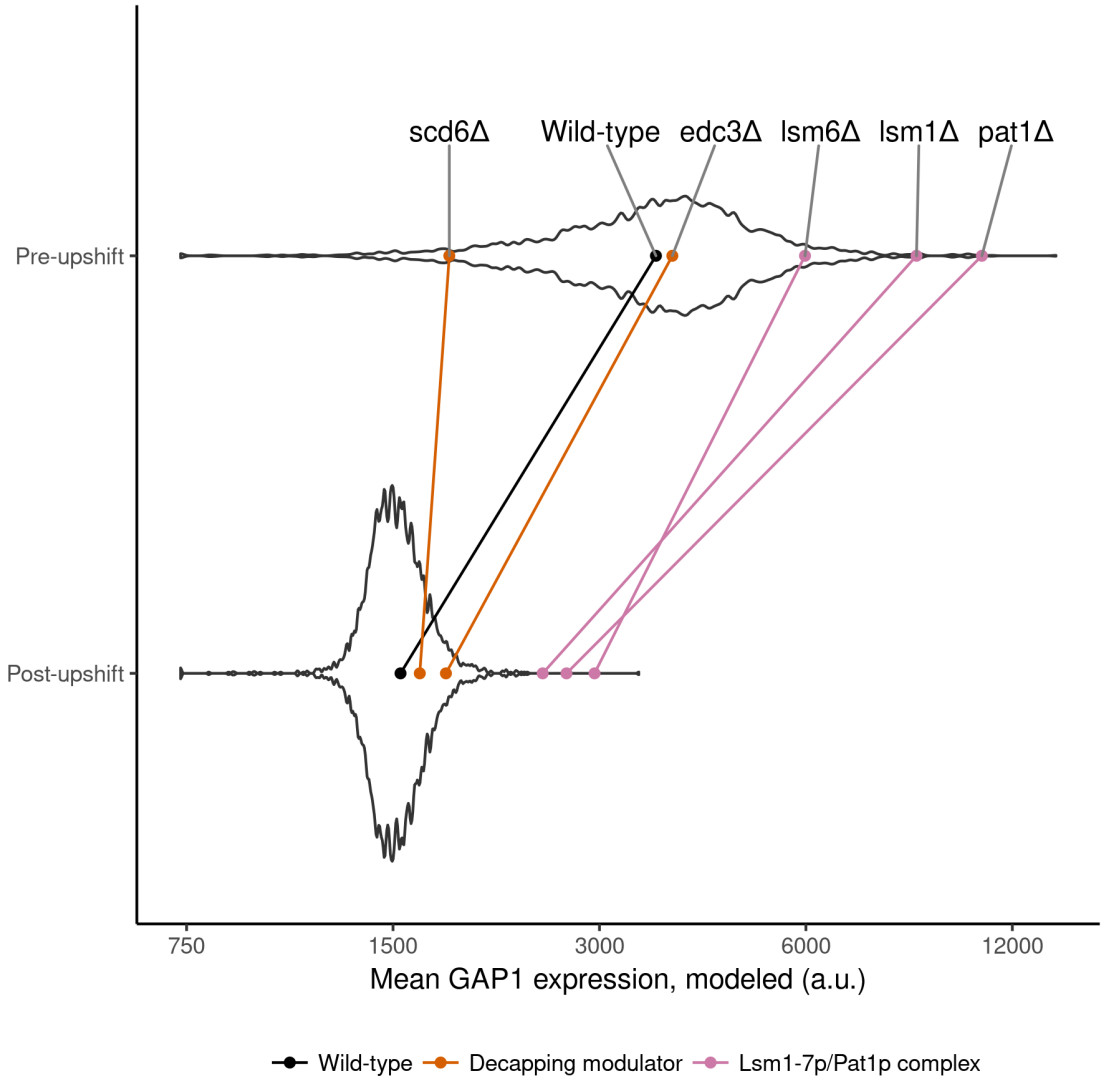

Figure 3.28: **Disrupting the Lsm1-7p/Pat1p complex impairs clearance of *GAP1* mRNA.** In the background is the distribution of fit *GAP1* mRNA mean abundance levels for all mutants in the pool. Indicated by colored points and lines are the means for individual knockout strains, as labeled.

3.4.3 Testing the roles of decapping modulators and associated components

As these factors are associated with processing-body dynamics, we tested if microscopically-observable processing-bodies form or disassociate during the upshift, using microscopy

of Dcp2-GFP. We did not observe qualitative changes in Dcp2-GFP distribution (Figure 3.29), and thus the upshift does not result in a microscopically visible changes in processing-body foci as seen in other stresses. This is consistent with previous investigations of amino-acid limitation stress (Hoyle et al. 2007) and suggests that the defects in *GAP1* mRNA clearance result from their roles in decapping or associated processes.

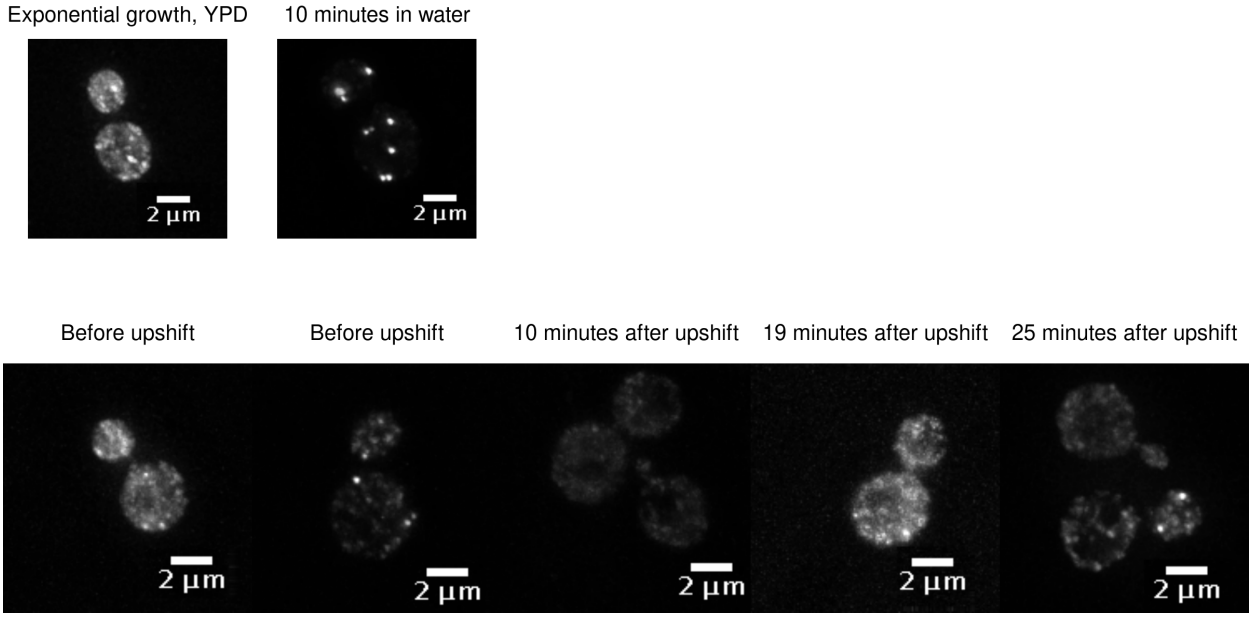

Figure 3.29: **Processing-body dynamics are not associated with the nitrogen upshift, by Dcp2p-GFP microscopy.** A strain harboring a copy of Dcp2p-GFP expressed from a plasmid was grown in conditions of exponential phase in YPD or 10 minutes of starvation in water (first row). Starvation in water is a common condition known to result in the strong formation of processing-body foci of Dcp2-GFP, and is thus a positive control. The bottom row shows microscopy during the upshift. We do not see either formation or dissolution of Dcp2-GFP foci resembling p-bodies during the nitrogen upshift.

To confirm the role of the Lsm1-7p/Pat1p complex in clearing *GAP1* mRNA during the nitrogen upshift we measured *GAP1* mRNA repression using qPCR normalized to *HTA1*, which is not subject to destabilization upon the upshift (Figure 3.4). We also tested mutants that were not detected using BFF, or were only detected in the highest *GAP1* bin and therefore not suitable for modeling (e.g. *xrn1*Δ Figure 3.26). Using this assay we found that the main 5'-3' exonuclease *xrn1*Δ and mRNA deadenylase complex (*ccr4*Δ

and *pop2*Δ) are impaired in *GAP1* repression (Figure 3.30). We found that qPCR confirms results from BFF. We confirmed that the accelerated degradation of *GAP1* mRNA is impaired in *lsm1*Δ and *lsm6*Δ (Figure 3.30). We also tested *scd6*Δ and *edc3*Δ, two modifiers of the decapping or processing-body assembly functions associated with this complex, and found two distinct phenotypes (Figure 3.30). *edc3*Δ has similar abundance as wild-type before the upshift, but is cleared much more slowly. *scd6*Δ has a greatly reduced *GAP1* abundance before the upshift but is impaired in *GAP1* clearance. *tif4632*Δ, a deletion of the eIF4G2 known to interact with Scd6p (Rajyaguru et al. 2012), has a similar phenotype.

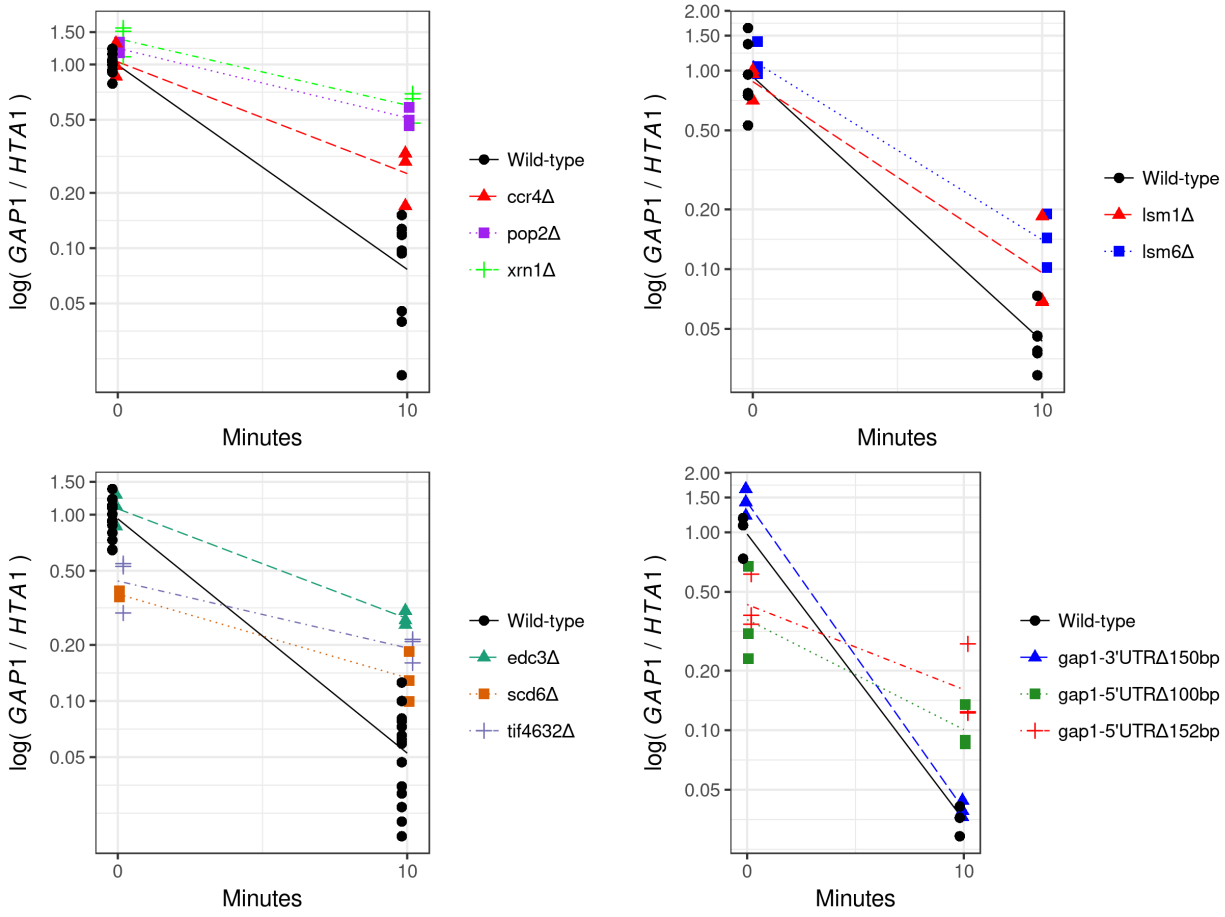

Figure 3.30: **Disrupting core pathways of mRNA degradation, decapping modulators, or the 5' UTR impairs the clearance of *GAP1* mRNA, by qPCR** Points are the ratio of *GAP1* mRNA to *HTA1* mRNA before and 10 minutes after a glutamine upshift, in biological triplicates. Lines are a log-linear regression fit. Points are dodged horizontally for clarity, but this is not used for modeling. Wild-type is FY4. **(Top Left)** *xrn1*Δ, *ccr4*Δ, *pop2*Δ are all slowed in clearance (p-values < 0.004). **(Top Right)** *lsm1*Δ and *lsm6*Δ are slowed in clearance (p-values < 0.0132 and 0.0299, respectively). **(To Left)** *edc3*Δ is slowed in clearance (p-value < 10^{-4}). *scd6*Δ and *tif4632*Δ are slowed in clearance (p-values < 10^{-5}) and have lower mRNA abundance before the upshift (p-values < 0.003). **(Top Right)** A deletion of 150bp immediately downstream of *GAP1* stop codon has no significant effect, but a deletion of 100bp immediately upstream of the start codon has slower clearance (p-value < 10^{-4}) and lower level of *GAP1*/*HTA1* before the upshift (p-value < 0.0015). During strain construction, a deletion of 152bp 5' of the start codon was also generated, and expresses a similar phenotype (p-value < 10^{-5} clearance defect, p-value < 0.0061).

Identification of an initiation factor subunit with defects in *GAP1* mRNA clearance suggests that translation control may impact stability changes. Therefore we deleted

sequence of the 5’ UTR and 3’ UTR of *GAP1*, specifically 100bp and 152bp upstream of the start codon (approximate 5’ UTR) or the 100bp downstream of the stop codon (approximate 3’ UTR). Whereas the 3’ UTR deletion does not have an effect, the 5’ UTR deletion exhibits the phenotype of reduced *GAP1* mRNA before the upshift and a reduced rate of transcript clearance following the upshift (Figure 3.30). We observed a similar phenotype with a different deletion of 152bp upstream of the *GAP1* start codon (Figure 3.30). This indicates that *cis*-elements responsible for the rapid clearance of *GAP1* are unlikely to be located in the 3’ UTR, and instead may be exerting an effect at the 5’ end of the mRNA.

3.4.4 Methods and materials

3.4.4.1 Strains

Strains with deletions 5’ of the start codon and 3’ of the stop codon were generated by the "delitto-perfeto" method (Storici and Resnick 2006), by inserting the pCORE-Kp53 casette at either the 5’ or 3’ end of the coding sequence, then transforming with a short oligo product spanning the deletion junction and counter-selecting against the casette with Gal induction of p53 from within the cassette. These strains were generated and confirmed by Sanger sequencing, and traces are available in directory `data/qPCRfollowup/` within the data zip archive (Availability of data and analysis scripts).

3.4.4.2 qPCR

Each strain was grown from single colonies. Samples were collected before, during the first ten minutes of the nitrogen upshift (Figure 3.16), or at ten minutes after the upshift (Figure 3.30). For the experiments described in Figure 3.30, all work was done in biological replicates. Each 10mL sample was collected by vacuum filtration, and RNA

extracted using the hot-acid phenol technique. For Figure 3.16 only, at the beginning of this extraction incubation I added 10μL of a 0.1ng/μL in-vitro synthesized spike-in mRNA BAC1200 (as generated for the label-chase RNAseq (Synthetic RNA spike-in generation, but without 4-thiouridine). RNA was treated with DNAse RQ1 (Promega) according to manufacturer instructions, cleaned and precipitated. All samples were reverse transcribed. For Figure 3.16 2μg RNA was primed with 2.08ng/μL random hexamers (Invitrogen) and 2.5mM total dNTPs (Promega), while for Figure 3.30 1μg RNA was primed with 5.6mM Oligo(dT)18 primers (Fermentas) and 0.56mM total dNTPs (Promega). These mixtures were reverse transcribed with M-MulvRT (NEB) according to manufacturer's instructions, then diluted 1/8 with hyclone water and used as direct template in 10μL reactions with SybrGreen I Roche qPCR master-mix (Roche). These were measured on a Roche Lightcycler 480. For Figure 3.16, I used primers DGO230,DGO232 to quantify *GAP1* and DGO605,DGO606 to quantify the synthetic spike-in BAC1200. For Figure 3.30, Nathan Brandt used primers DGO229, DGO231 to quantify *GAP1* and DGO233, DGO236 to quantify *HTA1*. See Table 3.3 for sequences. These were run on a Roche480 Lightcycler, with a max-second derivative estimate of the cycles-threshold (the C_p value output by analysis) used for analysis by scripts included in the git repo (Availability of data and analysis scripts). Linear regression of the log-transformed values was used to quantify the dynamics and assess significance of changes in mRNA abundance levels or rates of change.

3.4.4.3 Microscopy of Dcp2-GFP

To look for processing-body dynamics in response to a nitrogen upshift, I used strain DGY525, which is FY3 containing plasmid pRP1315 (gift from Roy Parker). Samples were collected before and following a nitrogen upshift (4, 10, 12, 19, or 25 minutes later), from exponential growth in YPD, or 10 minutes after resuspending YPD-grown cells in DI water. All samples were collected by brief centrifugation (1 minute) then resuspension in

PBS buffered 4% PFA for aspirating most supernatant, then centrifugation for 20 seconds and aspirating all media. Each pellet was immediately resuspended in 4% PFA (diluted from EMS 16% PFA ampule RT15710) with 1x PBS for 15 minutes on bench, then spun at 10,000g for 1 minute, aspirated, then washed once and resuspended with 1x PBS. Samples were kept on ice, then put onto a coverslip for imaging on a DeltaVision scope. Raw images available in the microscopy zip archive (Availability of data and analysis scripts).

3.4.5 Methods and materials of Barseq after FACS after FISH experiment

3.4.5.1 Culturing and sampling

An aliquot of the prototrophic deletion collection (VanderSluis et al. 2014) was thawed and diluted, with approximately 78 million cells added to 500mL of proline-limited media in a 1L baffled flask. This was shaken at 30°C overnight, then split into three flasks (A, B, and C). After three hours (at mid-exponential) we collected samples of 30mL culture by filtration and flash-freezing. The collection times for each sample were A: 10 minutes and 38 seconds, B: 10 minutes and 12 seconds C: 10 minutes and 17 seconds.

3.4.5.2 Fixation and permeabilization

Frozen samples of the pool were fixed with formaldehyde (4% PFA diluted in PBS, 2 hours room-temperature) and digested with lyticase (in BufferB with VRC 37C 1 hour). Microscopy monitoring of the reaction showed the classic greying of the cells under phase contrast microscopy to a dark grey, but did not digest to ghosts and fragments. Critically, 1/5th volume 2.5M glycine was added to quench the fixation before pelleting and washing the cells with centrifugation at 1200g room temperature. An experiment where quenching did not take place resulted in smaller fixed cells that were less accessible to the FISH hybridization. After washing three times with Buffer B (Pringle et al.

1991) these were permeabilized with ethanol at 4C overnight.

3.4.5.3 Hybridization

The samples were processed with a Quantigene Flow RNA kit purchased in March of 2015 (product code 15710), and designed for GAP1 mRNA in *Saccharomyces cerevisiae*. The probe sequences are proprietary. This procedure is largely as described by the manufacturer, with some critical modifications. The incubator used was calibrated to 40°C using a Traceable 4004 Type-K thermometer, with the probe inserted into an eppendorf tube through a hole and sealed with parafilm, and inserted into the aluminum heatblock in the air incubator as used for incubating samples. The ethanol-permeabilized samples were pelleted by centrifuging 1200g for 5 minutes room temperature, then washed with "Solution D" from the kit before proceeding with the kit instructions, with the exception that all reactions were conducted with 1/4 volume. For each wash, the complete supernatant was discarded, and cells resuspended in wash buffer to 25μL (to replicate the "about 100μL residual" in the instructions). Upon final wash, these were incubated for 5 minutes with DAPI to counter-stain.

3.4.5.4 Flow cytometry and FACS

Samples were sonicated, then run through a BD FACSAria II by a NYU GenCore technician. Cells were gated for singlets and DAPI content (estimated 1N or more), then sorted based on emission area from a 660/20nm filter with a 633nm laser activation into four gates within each timepoint, across replicates. Importantly, the sorting gates were set with a GUI interface until they approximated splitting the libraries into quartiles for the six samples. These were sorted using PBS sheath fluid at room-temperature, into poly-propylene FACS tubes, then stored at -20°C.

Note that we later in analysis add a fixed number to all observations and gates in linear scale in order to get into positive values.

3.4.5.5 Cell collection and DNA extraction

For each gate, cells were collected in eppendorfs via laborious repeated gentle centrifugation steps and genomic DNA extracted by NaCl reverse-crosslinking at 65° for 16 hours, inspired by Klemm et al. 2014, with subsequent proteinase K and RNase A digestions. DNA was extracted from each sample with a very careful phenol:chloroform extraction, with back-extraction, estimated to yield 1/3rd the theoretical input (by qubit and estimation), twice as good as by either Zymo columns or Ampure beads. This may be a result of trying to obtain genomic DNA.

3.4.5.6 Construction of amplicon sequencing libraries for barcode counting

gDNA was amplified in technical triplicates in a heavily modified BarSeq protocol.

A master mix of buffer, BSA, dNTPs, $MgSO_4$, and Vent (exo-) polymerase (NEB) is made containing three oligos DGO1562, DGO1588, and DGO1589. This is combined with about 1/3rd of the genomic DNA extracted from the sample, and the reaction is loaded into individual PCR tubes (the optimization was in individual PCR tubes and 96 well plates did not work, likely due to particularities of the sealing mechanism). 30 reactions were run in each batch of preparation. All 30 reactions were put into a BioRad T100 thermocycler set for a 30μL reaction.

This was cycled through 4 minutes at 95C to denature, then a single annealing and extension step. This was then cooled to 37C and immediately ExoI (Thermo) was added and incubated (with periodic mixing) for twenty minutes. This exonuclease proceeds from un-annealed 3' ends.

The exonuclease was then inactivated with a 80C incubation, 5 minutes, then DGO1576, DGO1567, and DGO1519 were added in a master mix containing glycerol to bring the whole reaction to about 5% glycerol content. This became essential for keeping the forward primer effective at lower primer concentrations, presumably due to the com-

putationally predicted hairpin in the 3' end.

This reaction was cycled 40 times to anneal and extend the product. I do not expect all the cycles to be productive. Rather, the lower concentrations used (10nM forward DGO1567) limit the product generation.

To this generated intermediate product, I then added more primers, more buffer, and indexed forward primers. These incorporate a 5bp sample index. This is of insufficient complexity for error-correction bioinformatically, but should be sufficient to demultiplex most samples. This was cycled 12 times to extend the product.

All reactions were then frozen, then thawed on ice and pooled into four pools. These were purified, then one last reaction used the same polymerase to do three rounds of extension to add on the final Illumina P5 adapter onto the molecule. This was resolved on a 3% agarose gel, then the only visible bands were purified, quantified using qPCR, and submitted for sequencing on an Illumina NextSeq.

Based on previous runs, the Genomics Core spiked-in 5% PhiX onto the run, to help maintain diversity. However, during the run there was a massive failure in Illumina software to discern clusters given low base-diversity. This run only yielded approximately 127 million reads (out of 400 million listed yield). Thus, 5% PhiX is too low, and I would recommend trying $\sim$25% in future runs.

3.4.6 Design and analysis of Barseq after FACS after FISH experiment

3.4.6.1 Design of Barseq after FACS after FISH experiment

First, we motivate this development, as it departs from previous procedures in a few ways. The main impetus for this was the generation of primer dimers that form when the forward universal primer primes off the reverse universal primer. For example, Figure 3.31 shows a failed experiment that shows dimer formation in the sample lanes (on right).

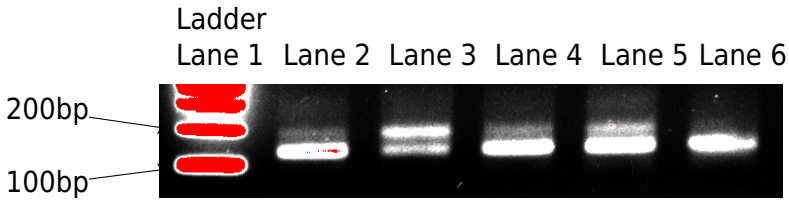

Figure 3.31: **An example of a dimer.** Here, I show an example of the primer-dimer formed by indexed versions of the universal deletion-collection barcode primers. Products after presumable addition of Illumina P5 and P7 adapter sequences were run on a 3% TAE agarose gel and stained with Sybr Safe dye. The left-most lane is a NEB 100bp ladder, with the bottom two bands as 100bp and 200bp. The red is due to overexposure. The right five bands are from samples prepared with an earlier version of this protocol. The band approximately 190bp is throught to be the library product, and the band approximately 160bp is thought to be the inhibitory and unwanted barcode-less dimer. Lane 3 clearly shows both bands, while lane 6 is all dimer.

Below a critical threshold, this dimer greatly out-competes the desired product and can result in a loss of amplicon before the amplicon is amplified enough to gel extract (above figure, lane 6). The dimer is also sequenced via Illumina chemistry (not desired). By Sanger sequencing we found that it appears to result from a three base truncation of the forward primer priming perfectly for about 6 bases off the reverse primer. This was not solved by switching to a polymerase without 3' exonuclease activity, or by using HPLC purified primers. Using different reverse primers lead to off-target products.

We saw these dimers before incorporating a UMI step into the protocol. We used a UMI because we wanted the protocol to be as quantitative as possible, despite the multiple amplification steps that would introduce randomly sampled noise at each cycle. The design of this was 6 bp degenerate sequence spaced with fixed bases, in the design of `NCNCNCNTNCN` because we estimated this would best block annealing to any 3' ends of the primers used. In future work, we would strongly recommend using more degenerate bases for such a low-complexity library (Fu et al. 2011).

In order to digest the excess un-incorporated UMI primers, addition of a exonuclease is required. ExoI is characterized to be maximally effective at 37°C, and although it can have activity at 42°C for some time (Fei et al. 2015), it will be inactivated. This low temperature requirement likely exacerbates dimer and off-target product forma-

tion. The common, but incorrect, one-UMI-one-molecule assumption is based on the belief that each UMI and each genomic template is used once in the first round. The exonuclease step must therefore digest all un-extended UMI-containing primers for this to be true. One control for this is to monitor the primer concentrations using a technology like HPLC to measure abundance, but a small number is, again, not necessarily negligible. The proper control is to not use the polymerase to extend the first round, and instead immediately digest the UMI-containing primers. This is a crucial control, and on the basis of experiments I did using this setup using dilutions of template, I estimate that the effect of the exonuclease, in the absence of the first round of extension, reduced product formation by about 20 fold. However, it was not absent. Thus, I suspect that the exonuclease digestion only ensures that ≈20/21 UMIs are from the first round of incorporation. While small, this is not negligible, especially in conditions where template number changes dramatically (as here it does not, given similar inputs to extractions). Optimization of this step did not improve upon this efficacy, and in the lack of commercially available thermostable (and active) exonucleases (Fei et al. 2015), this background noise must be understood and accepted.

To address this, we optimized the reactions on a dilution series of gDNA from a different experiment with the same knockout library. By balancing $MgSO_4$ and glycerol concentrations, we got better amplification and then tried to use a "booster" (Ruano et al. 1989) PCR approach. This gave some improvements in how low we could detect before saturating the reaction with dimers, but we could not go lower in primer concentration and attributed this to the predicted secondary structure in the 3' end of the primer amplifying from the outside of the UPTAG barcodes. Adding DMSO helped with this, but we still had to leave the reaction with plenty of primer as intra-molecular interference from this process would out-compete inter-molecular productive annealing. We still could not get reliable amplification from < 10^5 templates (estimated by qubit

assuming 12.5 picograms gDNA per genome).

The major solution to this problem was the addition of 3' phosphorylated blocker oligos. These are not extended by DNA polymerases but are displaced by a strand-displacing polymerase like Vent exo-. By using this polymerase and blocker combination, we prevent new 3' ends from annealing but allow properly annealed primers to extend through this region. This, in combination with the exonuclease digestion of most of the reverse primer, prevented dimer formation. This revealed that these universal priming sequences will amplify from two loci near *CIA1* and *RDN37*. This was identified by Sanger sequencing gel-extracted bands, so we designed more 20-mers that again block off-target annealing and found they worked wonderfully. In test experiments, we believe we got amplicons of the correct size from as low as $\sim$ 300 targets but have not sequence verified this.

To simplify the addition of the last 5' Illumina P5 adpater, we kept this as a separate reaction. To minimize chimera formation between different samples in this reaction, this is a 2-step polymerase extension reaction which partially forms the sequencing product (1/3 of results, theoretically). This is sufficient for qPCR quantification of the library and Illumina sequencing. Given our gel-extraction clean up and small product size, we do not expect formation of chimeras on the flow cell.

Figure 3.32 shows a cartoon of the amplicon library-making procedure, up to the generation of the product before the Illumina P5 addition Figure 3.33. Given the simplicity of this last reaction (simply adding sequence on the 5' end), it is omitted.

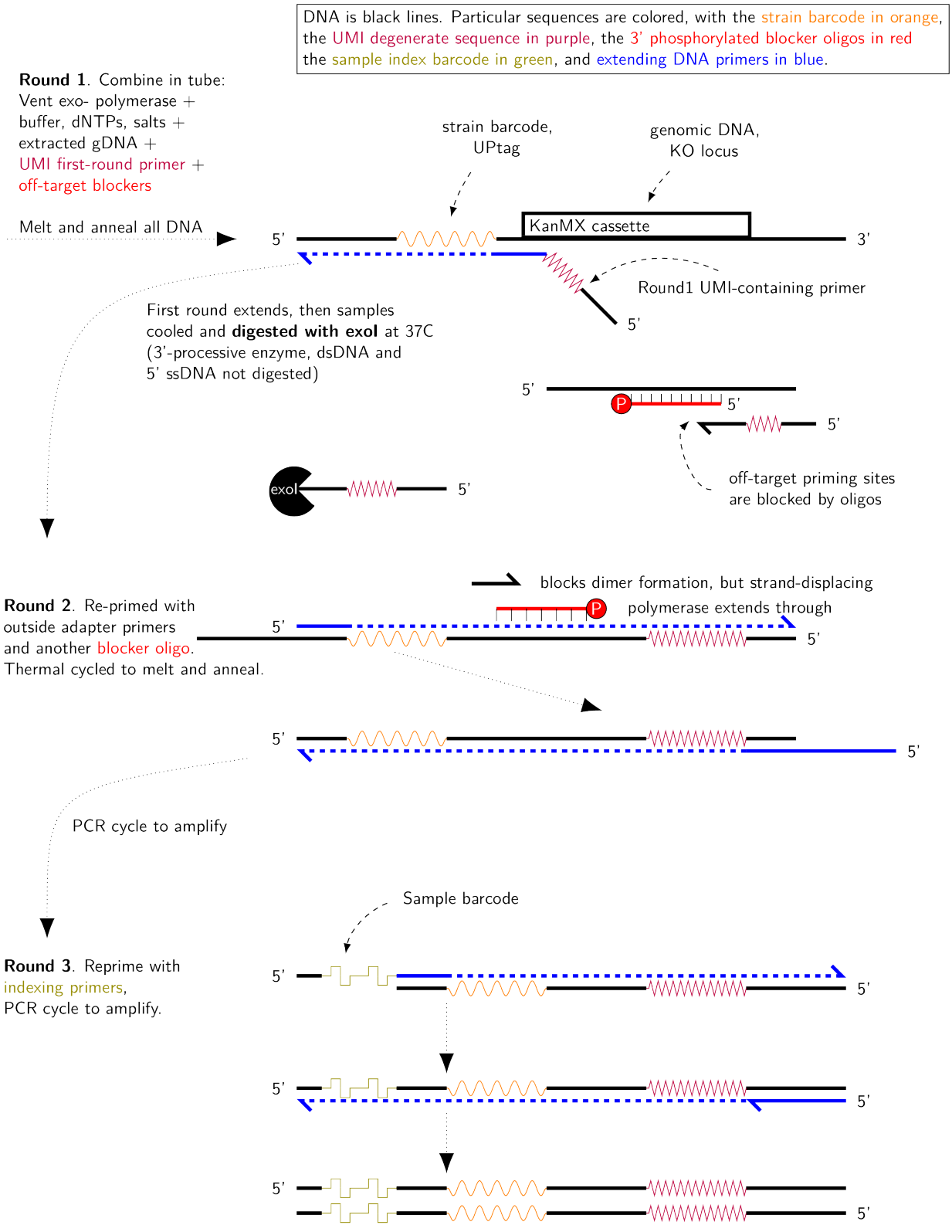

Figure 3.32: **A schematic of the barcode sequencing strategy.**

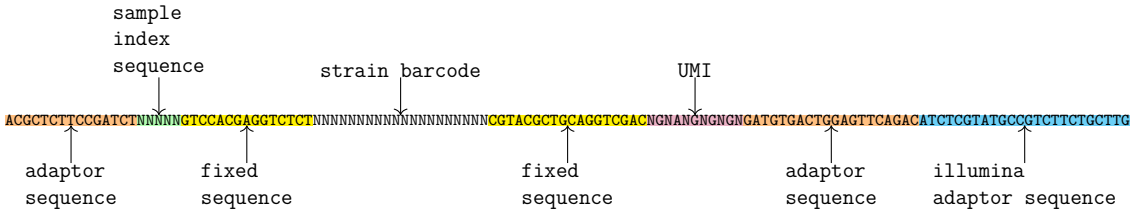

Figure 3.33: **The expected amplicon, before adding P5 sequences at the 5’ end.**

These were checked with sanger sequencing, for pools 1 and 3, using primers DGO 276 or DGO 1519, with Genewiz sequencing. Representative Sanger sequencing image of library pool 1, sequenced forward (with DGO 216) is shown in figure 3.34.

Trace colors: red is T, green is A, blue is C, black is G.

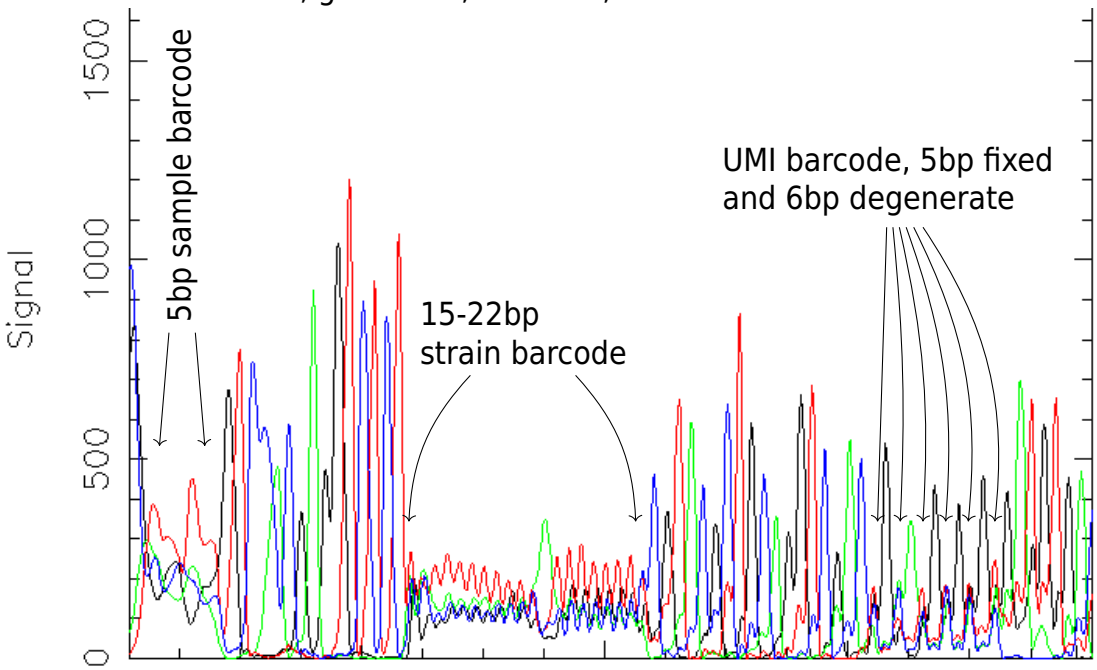

Figure 3.34: **Sanger sequencing of the produced library shows the expected degenerate positions.**

3.4.6.2 Designing an analysis pipeline to filter dimers and extract UMIs from indeterminate locations

We previously used the one-program solution of BarNone (`http://varianceexplained.org/BarNone/`) to rapidly and easily quantify barcode counts from yeast barcode sequencing experiments. However, our new amplicon design makes use of UMIs to help account for the amplicon noise inherent in the BarSeq method, and BarNone does not account for these. We also wanted to devise a pipeline that would be modular, consisting of multiple well-designed tools that could be modified independently and would maintain read information along the pipeline to assist in debugging and benchmarking.

1. FASTQ files of the reads are fed into a custom python script called `SLAPCHOP.py`. This is named because it Simply Looks At Pair-wise Comparisons to Help Optimize Parsing (`https://github.com/darachm/slapchop`). This parallelized script takes each read, aligns the expected fixed sequences that bracket the informative barcodes (using BioPython Cock et al. 2009), decides if the read matches the expected structure based on a specified criteria, then extracts out the sample index, strain barcode, and UMI degenerate sequence into appropriate positions in a FASTQ format. This keeps the filtering and strain barcode identification separate from the fixed sequences.

2. A simple perl script (`pickyDemuxer.pl`) demultiplexes the processed FASTQ file on perfect matches of the 5bp index sequence and generates a demultiplexing report.

3. The strain barcode regions, padded with flanking sequence to a uniform length of 26bp, from the demultiplexed FASTQ files are aligned using `bwa mem` (Li 2013) to the expected barcodes as re-annotated by Smith et al. 2009.

4. From the resulting `bam` alignment files, we extract the strain identification and UMI. Using the UMI-collision / label-saturation concept and equation of Fu et. al. 2011 (PNAS), we adjust the saturated pool to estimate the input of strain genomes into the library preparation.

This allowed us to recognize and extract barcodes from indeterminate positions in the amplicon and filter the reads for real, intact amplicons in one step. This extraction improved our accuracy, for example eliminating spurious alignments of the forward priming sequence against the barcode of *ymr258c*Δ, a barcode re-annotated with striking similarity to the fixed priming sequence (Smith et al. 2009).

There are several different ways to use the UMI information to estimate unique input molecules from a sequencing assay. The naive approach is to assume that every combination of strain barcode with a certain UMI sequence in a sample is a unique event, and any repetitions of this are only PCR duplicates. The molecular biology caveats for this assumption are addressed earlier. However, we only have $4^6 = 4096$ possible UMIs for ~ 4500 possible strain barcodes, with approximately a million reads per sample. Thus, due to a short length of UMI we cannot make this assumption, and instead are confronted with a space of UMIs with a fairly high chance of two UMI-strain combinations being generated by random chance alone.

We refer to this as a UMI-collision (similar concept to a hash collision) or the phenomenon of label saturation. There are multiple ways to deal with this. The simplest is to simple take each unique UMI, but errors in library amplification could diversify spuriously duplicated UMIs. Error-correcting algorithms exist that use graph information to improve accuracy of this method, but these require that the space of all usable UMIs is sparse. Another solution is the label saturation correction of Fu et al. 2011. This depends on treating the chance that any UMI-collisions are a random and rare event, thus modeled as a Poisson distribution, similar to the classic Luria-Delbruck method of mu-

tation rate estimation. If we have 4096 possible UMIs, and for one strain in one sample we observe x different UMIs associated, then we estimate that there were z different original molecules in the sample, where $z = 4096(1 - e^{-\frac{x}{4096}})$.

Figure 3.35 plots this function, and compares it to actual sequencing data from the experiment, with and without the error-correcting approach of UMI-tools (Smith et al. 2017). Figure 3.36 plots the distribution of counts per UMI for one mutant (the most abundant one in the library).

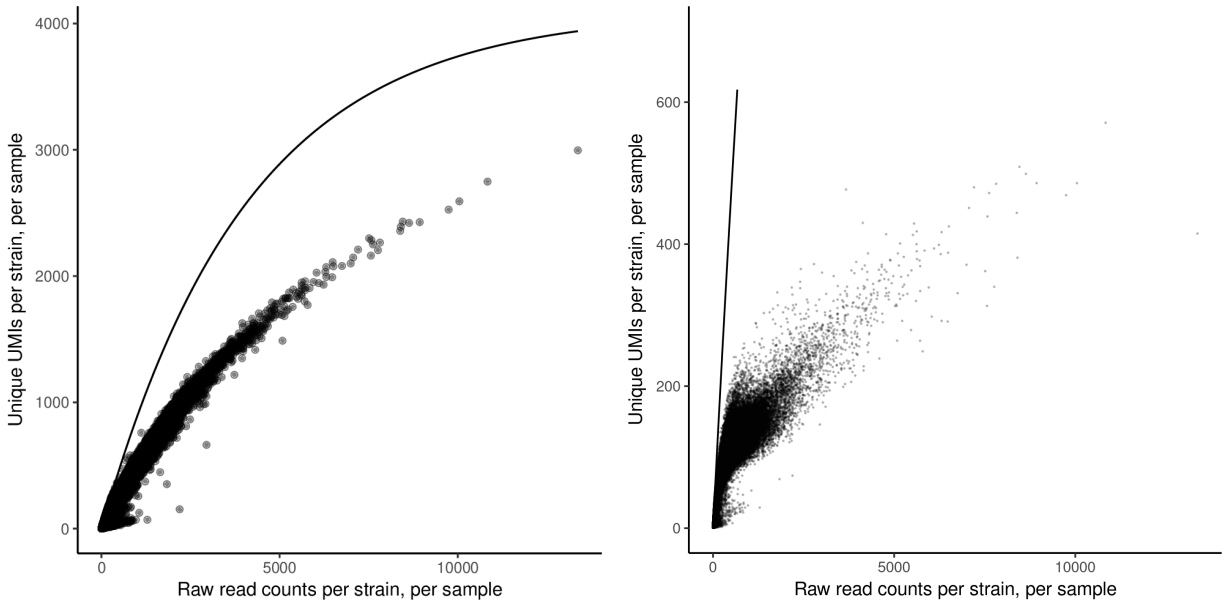

Figure 3.35: **A comparison of the unique UMIs versus input UMIs for uncorrected and error-corrected UMIs.** For each sample, each combination of UMIs and strain barcodes was collected. For each point, the y-axis denotes the unique UMIs observed for that combination of strain and sample. On the x-axis is the raw counts of observing that strain barcode in that sample, without error-correction **(Left)** and with `umi-tools` error-correction algorithim on the right **(Right)**. The line denotes the curve expected just from label saturation with increased re-sampling of a limited pool as it approaches 4096.

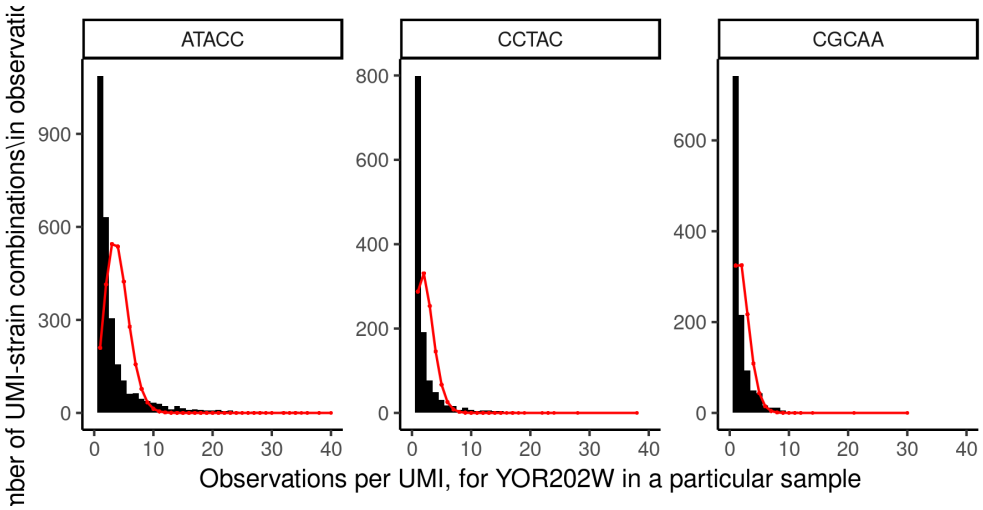

Figure 3.36: **Histograms of UMI observations associated with the YOR202W barcode in three samples.** In black is the observed data, in red is the expected distribution if Poisson. We see that there is a long-tail of UMIs with more reads than observed for that combination of strain and sample.

Comparing these, we see that the unique UMIs detected decreases as a function of input-reads, as expected. We see that the error-correction algorithim greatly reduces the reads used, and falls well below this expectation. As shown in Figure 3.36, we see that for some UMI-strain barcode combinations, we see much more counts per UMI label than expected by a Poisson distribution. Both label saturation and PCR duplication are at play to distort the mapping between either raw counts or unique labels and the actual underlying estimate of input genome targets per strain in each sample. However, since UMI-tools uses abundance of counts per UMI-cluster to aggregate neighboring UMIs into the cluster, I believe that the PCR-duplicate UMIs that are overdispersed on the high-counts-side are scavenging the lower end of the poisson distribution into a small number of real clusters. This is not surprising given that we are using this tool in a labeling regime that is wholy inappropriate for what it is trying to do. Thus, I do not use this tool and instead used the more conservative correction of Fu et al. 2011, Figure 3.35 left. An appropriately complex UMI design would allow a future user to make use of error-correcting algorithims in this method.

3.4.6.3 Benchmarking this pipeline

We benchmarked this pipeline against an *in silico* dataset to determine performance across a range of mutation rates and read depths similar to what we would expect for this experiment. We also compared the two UMI correction approaches described in the previous section, the "UMI-collision correction" and the "number unique" method. We used a python script `makingFakeReads.py` to generate several datasets with the following parameters:

- 16 million reads per FASTQ, split amongst 32 samples
- each strain barcode is sampled from an emipirically observed distribution averaged from the first timepoints of an unpublished dataset, quantified by BarNone
- each amplicon has a poisson number of random single nucleotide mutations to a different base, based on a given parameter of `0`, `1`, `2`, or `3` lambda of mutations per amplicon.
- each generated amplicon is added to the file x number of times, where x is an exponential distribution with mean 5
- 3 "biological" replicate datasets are generated per set of parameters

After quantification, we calculate pearson correlation, spearman correlation, and the number of mistaken strain identifications. Tolerated mismatches is a parameter set in BarNone or by the score requirements for alignment in `bwa`.

As seen in Figure 3.37, it would appear that by pearson correlation, the filtration step of the `bwa` alignment allows us to make more robust assignment of strain barcodes. The spearman correlation tells us that as mutation rate increases, high mismatch tolerance on the `bwa` tool is very dangerous for misaligning and can cause large rank changes.

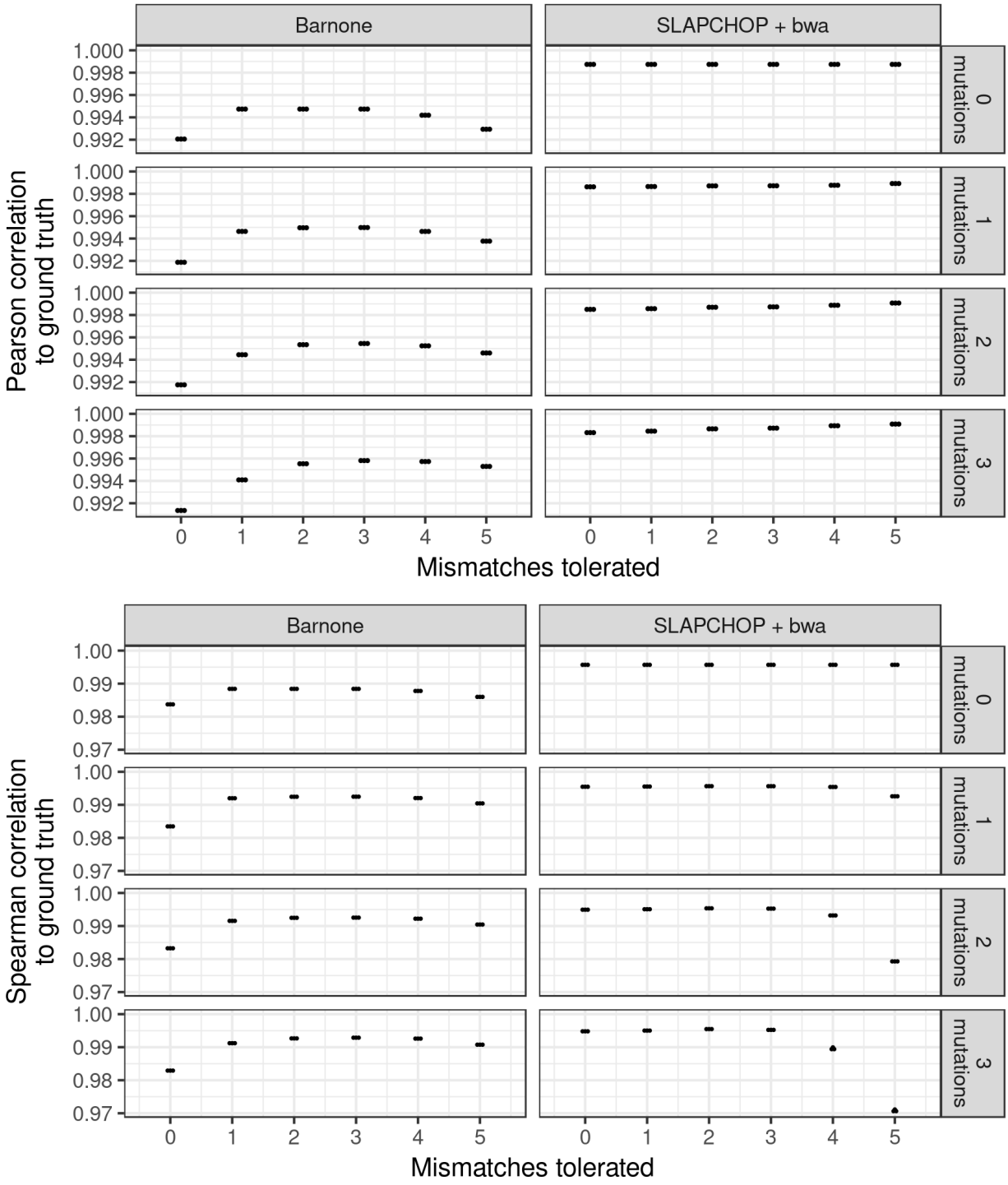

Figure 3.37: **Optimization of mutant quantification methods, looking at simulated data on a whole-lane comparison.** Tool quantification was compared to the *in silico* ground truth using correlations of Pearson **(top)** or Spearman **(bottom)**.

How does the UMI-collision correction perform? We see that on the whole, un-

demultiplexed datasets (16 million reads across ~4000 strains and 4096 possible UMIs) that the performance is best with the UMI-collision correction Figure 3.38. We see that just using unique UMI counts in this regime leads to a good reconstruction of the rank order (Spearman), but inaccurate of the magnitude (Pearson) against ground truth. Does this change with lower read density? Each point is one of 32 demultiplexed samples of three whole-library replicates, and we see that in this lower read regime, we get similar performance from both methods Figure 3.39. To avoid biases arising from differences in abundance between strains, I keep the UMI-collision correction.

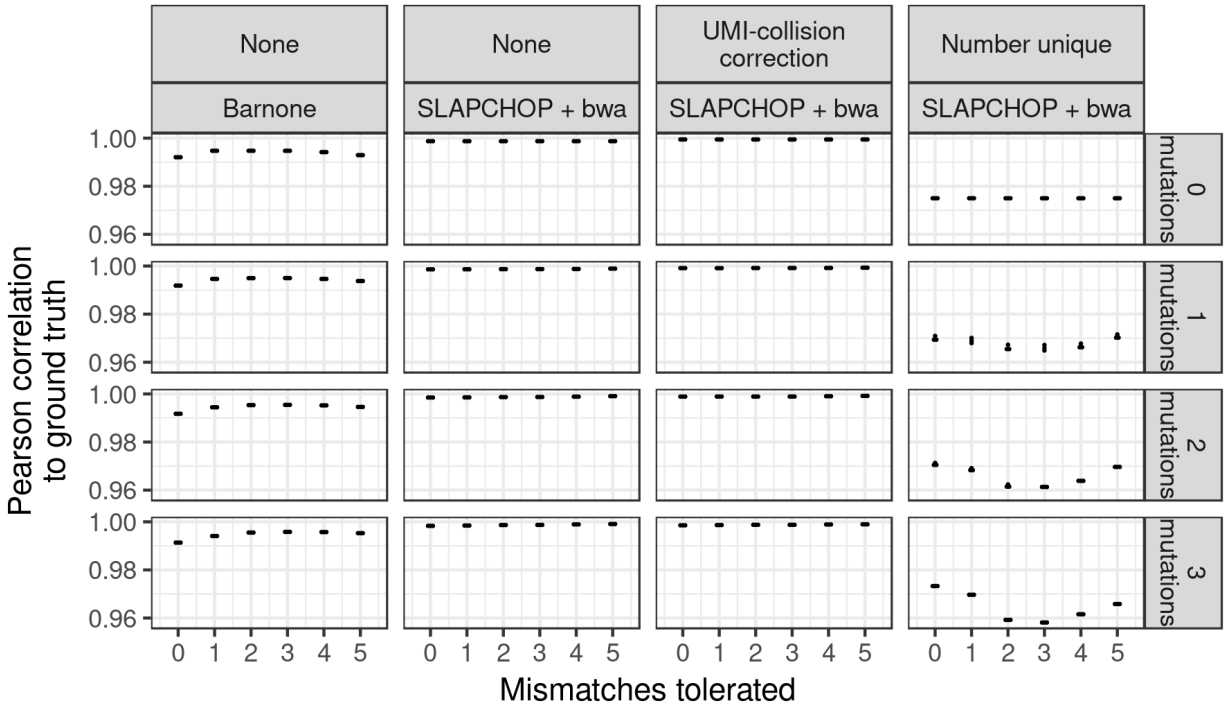

Figure 3.38: **Optimization of mutant quantification methods, looking at deduplicating methods on whole comparisons.** On a whole-sample basis, the error of the "number unique" quantifier of UMIs is evident, in this saturated regime.

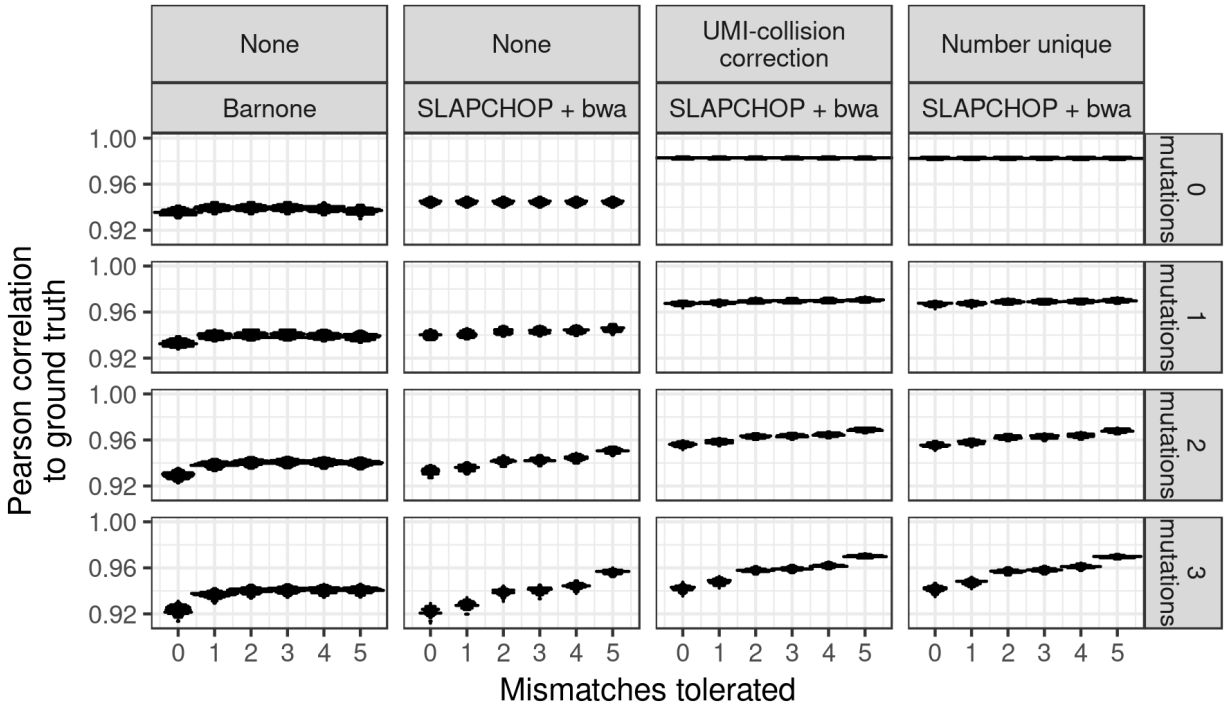

Figure 3.39: **Optimization of mutant quantification methods, looking at deduplicating methods on per-sample comparisons.** On a per-multiplexed-sample basis with less total counts, the error of the "number unique" quantifier of UMIs is less evident.

BarNone appears to be more robust to mutations, in that it maintains a flatter profile in the higher regimes of mutations. However, `bwa` starts out higher. Accounting for duplication, as generated by the exponential distribution described above, greatly improves performance. At an average coverage here of a half-million reads, the difference between the UMI-collision and unique counts is less than with large coverage. In conclusion, our pipline for analysis is able to use an early filtration step (SLAPCHOP) to improve strain barcode identification and to extract UMIs that are useful for de-duplicating PCR duplicates for better estimates of the ground truth.

3.4.6.4 Modeling *GAP1* FISH signal per strain in the pool

In order to use the counts of each mutant in each sample to estimate *GAP1* mRNA abundance per strain, we used a maximum-likelihood modeling approach.

We are interested in the number of cells of a certain strain that went into each bin. We estimate this as a metric we define as "pseudocounts", or u_{ik} where i is the strain index, and k is the FACS bin. We call the sequencing counts c_{ijk}, where j is the particular PCR replicate out of J PCR replicates that were successfully sequenced. We assume the sequencing counts are linearly amplified from the "events" of actual cells being sorted into each collection tube, and we assume that all of these "events" have equal chance to be amplified and detected by this sequencing assay. Then we scale this estimate by the total number of "events" we observed during the FACS procedure going into each bin e_k. We assume that all "events" had equal chances in all bins to get sequenced. Then we have

$$u_{ik} = \frac{\sum_j \frac{c_{ijk}}{\sum_i c_{ijk}}}{J} \quad \frac{e_k}{\sum_k e_k}$$

This is intuitively more simple than the notation used here to describe it precisely. Since we split the library into quartiles for the sequencing, $\frac{e_k}{\sum_k e_k}$ is about one quarter for each bin. $\frac{c_{ijk}}{\sum_i c_{ijk}}$ is just the proportion of counts in that sample that are that mutant i. $\frac{\sum_j \frac{c_{ijk}}{\sum_i c_{ijk}}}{J}$ is simply the average of the proportion of counts, across the PCR replicates.

Thus, u_{ik} is essentially the proportion of the original library that is the mutant in that bin, and $\sum_k u_{ik}$ is the total proportion of the library that is that mutant. So then if we divide $\frac{u_{ik}}{\sum_k u_{ik}}$, we have an estimate of the proportion of that mutant that went into each bin, out of all the mutant that was in the experiment.

Once we have this normalized pseudocounts metric within each biological replicate, then we fit a log-normal model. We explored a logistic model and several mixture models (similar to DNA content flow cytometry with two log-normals and a middle quasi-uniform

distribution), and found that the log-normal robustly fit well. The log-normal and logistic largely agreed on ranking of estimated means, but the likelihood was slightly higher for the log-normal fits on the whole library, so we used that model.

From this model (fit using `mle()` in R), we used the fit mean as the estimate for the GAP1 abundance for that strain in that sample.

3.5 Discussion

Regulated changes in mRNA stability allow cells to rapidly reprogram gene expression, clearing extant transcripts that are no longer required and potentially reallocating translational capacity. Pioneering work in budding yeast has shown that mRNA stability changes facilitate transcriptome reprogramming in response to changes in nutrient availability including changes in carbon sources (Scheffler et al. 1998) and iron starvation (Puig et al. 2005). Here, we characterized genome-wide changes in mRNA stability in response to changes in nitrogen availability and identified factors that mediate the rapid repression of the destabilized mRNA, *GAP1*. Our study extends our previous work characterizing the dynamics of transcriptome changes using chemostat cultures (Airoldi et al. 2016) and shows that accelerated mRNA degradation targets a specific subset of the transcriptome in response to changes in nitrogen availability. We developed a novel approach to identify regulators of mRNA abundance using pooled mutant screens and find that modulators of decapping activity, and core degradation factors, are required for accelerated degradation of *GAP1* mRNA.

Measuring the stability of the transcriptome requires the ability to separate pre-existing and newly synthesized transcripts. We modified existing methods to measure post-transcriptional regulation of the yeast transcriptome in a nitrogen upshift using 4-thiouracil labeling (Miller et al. 2011; Munchel et al. 2011; Neymotin et al. 2014). These modifications included improved normalization and quantification of extant tran-

scripts and explicit modeling of labelling dynamics to account for some of the inherent limitations of metabolic labeling approaches (Pérez-Ortín et al. 2013). Continued development of fractionation biochemistry (Duffy et al. 2015) and incorporation of explicit per-transcript efficiency terms will improve these methods further (Chan et al. 2017).

Our experiments show that the process of physiological and transcriptome reprogramming occur on very different timescales in response to a nitrogen upshift. Cellular physiology is remodeled over the course of two hours to achieve a new growth rate. By contrast, transcriptome remodeling occurs rapidly and through states that are distinct from increases in steady-state growth rates. Previous studies have shown that transcriptional activation of the NCR regulon is rapidly repressed upon a nitrogen upshift (Airoldi et al. 2016). Our results indicate that accelerated degradation of many NCR transcripts (Godard et al. 2007) contributes to this repression. A three-fold increase in the degradation rate of *GAP1* mRNA provides an additional layer of repressive control. Importantly, our results show that accelerated degradation is not limited to NCR transcripts but also targets transcripts enriched in carbon metabolism pathways, particularly pyruvate metabolism. Conversely, we also detect an apparent reduction in the degradation rate for some transcripts including *MAE1*. *MAE1* encodes an enzyme responsible for the conversion of malate to pyruvate, and combined with the accelerated degradation of *PYK2* mRNA may reflect an adaptive shunt of carbon skeletons from glutamine to alanine via the TCA cycle (Boles et al. 1998). Recently, Tesnière et al. 2017 described destabilization of carbon metabolism mRNAs after repletion of nitrogen following 16 hours of starvation. We do not detect destabilization of *PGK1* mRNA and note that the basal half-life of 6.2 minutes estimated in our study is similar to the accelerated rate reported by Tesnière et al. 2017.

Destabilized transcripts are enriched for a binding motif of Hrp1p in the 5’ UTR. This essential component of mRNA cleavage for poly-adenylation in the nucleus has been

shown to shuttle to the cytoplasm and bind to amino-acid metabolism mRNAs (Guisbert et al. 2005) and been shown to interact genetically to mediate nonsense-mediated decay (NMD) of a *PGK1* mRNA harboring a premature stop-codon (González et al. 2000) or a *cis*-element spanning the 5' UTR and first 92 coding bp of *PPR1* mRNA (Kebaara et al. 2003). A potential role for these Hrp1p sites warrants further investigation.

BFF identified mutants in the Lsm1-7p/Pat1p complex as having elevated *GAP1* mRNA levels both before and after the upshift. This is expected given their central role in mRNA metabolism, and experiments using *GAP1* normalized to *HTA1* demonstrate that the effect before the upshift is likely a global effect (Figure 3.30). However, these mutants still have a significant defect in clearance of *GAP1*, and the assay demonstrates that associated decapping factors *EDC* and *SCD6* have specific effects (Figure 3.30). Given that the *GAP1* mRNA is destabilized during this transition we suspect that these mRNA degradation factors are directly involved. While we found that the *edc3*Δ mutant has defects in clearance of *GAP1*, we also found that *scd6*Δ, *tif4632*Δ, and deletion of the 5' UTR of *GAP1* impairs clearance (Figure 3.30). This deletion does not include the TATA box (ending at -179) or GATAA sites (nearest at -237) responsible for NCR GATA-factor regulation of *GAP1* (Stanbrough and Magasanik 1996). This suggests that interactions of these factors with *cis*-elements in the 5' UTR might be responsible for stabilizing *GAP1* mRNA during limitation, although the truncation of the 5' sequence may be enough to inhibit translation initiation by virtue of the shorter length (Arribere and Gilbert 2013). Elements in the 5' UTR have also been demonstrated to modulate *GAL1* mRNA stability (Baumgartner et al. 2011) and destabilize *SDH2* mRNA upon glucose addition, perhaps due to the competition between translation initiation and decapping mechanisms (Cruz et al. 2002). Interestingly, both *GAP1* and *SDH2* share the feature of a second start codon downstream of the canonical start (Neymotin et al. 2016) and we have previously found that mutation of the start codon of *GAP1* results in lower steady-state

mRNA abundances (Neymotin et al. 2016). This suggests a mechanism of degradation through dynamic changes in translation initiation that triggers decapping of *GAP1* and other mRNA. Future work interrogating this possible interaction of translational status and mRNA stability during dynamic conditions could also expand our understanding of the relationship between these two processes.

To our knowledge, this is the first time mRNA abundance has been directly estimated using a SortSeq approach, although using mRNA FISH and FACS to enrich subpopulations of cells has been previously reported (Hanley et al. 2013; Klemm et al. 2014; Sliva et al. 2016). This approach could be used with other barcoding mutagenesis technologies, like transposon-sequencing or Cas9 mediated perturbations, to systematically test the genetic basis of transcript dynamics. The use of branched-DNA mRNA FISH, or other methods (Rouhanifard et al. 2017), allows for mRNA abundance estimation without requiring genetic manipulation which makes it suitable for a variety of applications such as extreme QTL mapping. Furthermore, our methods for library construction should permit accurate quantification of pooled barcode libraries with small inputs, expanding the possibilities for flow cytometry markers to fixed-cell assays.

Why is *GAP1* subject to multiple layers of gene product repression upon a nitrogen upshift, at the level of transcript synthesis, degradation, protein maturation, and post-translational inactivation? Given the strong fitness cost of inappropriate activity (Risinger et al. 2006), this overlap could ensure mechanistic redundancy for robust repression in the face of phenotypic or genotypic variation. Alternatively, it could reflect a systematic need to free ribonucleotides or translational capacity, or result from some as yet uncharacterized process. Future work aimed at determining the adaptive basis of accelerated mRNA degradation will serve to illuminate the functional role of post-transcriptional mRNA abundance regulation.

3.6 General methods and materials

3.6.0.1 Availability of data and analysis scripts

Computer scripts used for all analyses are available as a git repository on GitHub (`https://github.com/darachm/millerBrandtGresham2018`) and data is available as zip archives on the Open Science Framework (`https://osf.io/7ybsh/`).

To reproduce the entire analysis, or to access a particular analysis, clone the git repo. Download the `zip` data archives from the above OSF link, and put them inside this git repo folder (here, `millerBrandtGresham2018`). At minimum, you should have the `data.zip` archive in that directory, although records of all R analyses are in `html_reports.zip` and intermediate files are in `tmp.zip`. Consult the `README.md` file in the repository for more instructions and options, including how to unzip intermediate files and HTML reports generated for every R script which detail the results.

A Shiny application is also available to explore the two main datasets in this paper more easily, at `http://shiny.bio.nyu.edu/users/dhm267/`. It is also included in the OSF as a separate zipped archive for local installation and long-term archiving. To use the Shiny applications from the zipped archive, download, unzip the archive, and direct R to run the `runApp` command to use the directory as a Shiny app. It can thus be used as an interactive tool for visualization.

3.6.0.2 Supplementary tables

These are available on the Open Science Framework archive `https://osf.io/9ct3m/` .

- Gene set enrichment analysis of loadings on principal components one and two. `Figure1_Table_GSEofGOtermsAgainstPCcorrelation.csv`
- Raw counts of labeled mRNA quantified by RNAseq in label-chase experiment. `Figure2_Table_RawCountsTableForPulseChase.csv`
- Filtered label-chase RNAseq data for modeling, normalized directly within sample.

`Figure2_Table_PulseChaseDataNormalizedDirectAndFiltered.csv`

- Filtered label-chase RNAseq data for modeling, normalized by modeling across samples.
  `Figure2_Table_PulseChaseDataNormalizedByModel.csv`
- Degradation rate modeling results, from data normalized within samples.
  `Figure2_Table_PulseChaseModelingResultTable_DirectNormalization.csv`
- Degradation rate modeling results, from data normalized across samples.
  `Figure2_Table_PulseChaseModelingResultTable_ModelNormalization.csv`
- Enriched GO and KEGG terms within the set of mRNA destabilized upon a nitrogen upshift, across sample normalization.
  `Figure2_Table_AcceleratedDegradationTranscripts_EnrichedGOandKEGGterms.csv`

- Raw counts of strain barcode quantification within each bin in the BFF experiment, and gate settings for the observations.
  `Figure4_Table_BFFcountsAndGateSettingsFACS.csv`
- BFF data filtered for modeling.
  `Figure4_Table_BFFmodelingData.csv`
- The parameters of all models fit to the BFF data.
  `Figure4_Table_BFFallFitModels.csv`
- All 3230 models used for identifying strains with defective *GAP1* dynamics.
  `Figure4_Table_BFFfilteredPooledModels.csv`
- Gene-set enrichment analysis results using *GAP1* estimates.
  `Figure4_Table_GSEanalysisOfBFFresults.csv`

3.6.0.3 Media and upshifts of media

Nitrogen-limited media (abbreviated as "Nlim") is a minimal media supplemented with various salts, metals, minerals, vitamins, and 2% glucose, as previously described (Airoldi et al. 2016; Brauer et al. 2008). For proline limitation, Nlim base media was made with 800μM L-proline as the sole nitrogen source (NLim-Pro). YPD media was made using standard recipes (Amberg et al. 2005). All growth was at 30°C, in an air-incubated

200rpm shaker using baffled flasks with foil caps, or roller drums for overnight cultures in test tubes. For glutamine upshift experiments, 400μM L-glutamine was added from a 100mM stock solution dissolved in MilliQ double-deionized water and filter sterilized. All upshift experiments were performed at a cell density between 1 and 5 million cells per mL, in media where saturation is approximately 30 million cells per mL. For all experiments, a colony was picked from a YPD plate and grown in a 5mL NLimPro pre-culture overnight at 30°C, then innoculated into the experimental culture from mid-exponential phase.

3.6.0.4 Strains

See Table 3.2 for details. The wild-type strain used is FY4, a S288C derivative. The pooled deletion collection is as published in VanderSluis et al. 2014. For all experiments with single strains, colonies were struck from a -80°C frozen stock onto YPD (or YPD+G418 for deletion strains) to isolate single colonies. For pooled experiments we inoculated directly into NLim media from aliquots of frozen glycerol stocks.

All primers were synthesized by Integrated DNA Technologies (IDT). `N` refers to a standard degenerate position. Barseq multiplexing barcode sequences and index numbers available in the file `data/dme209/sampleBarcodesRobinson2014.txt` within the data zip archive (Availability of data and analysis scripts).

Table 3.2: Yeast strains used in this study

Strain ID	Short description	Details
DGY1	FY4	Isogenic to S288C, prototrophic, MATa
-	Deletion collection pool	Haploid (MATa) prototrophic deletion collection as described in the publication of VanderSluis et al. 2014
DGY410	xrn1Δ::KanMX	ygl173cΔ::KanMX from the prototrophic deletion collection
DGY564	ccr4Δ::KanMX	yal021cΔ::KanMX from the prototrophic deletion collection
DGY565	pop2Δ::KanMX	ynr052cΔ::KanMX from the prototrophic deletion collection
DGY547	lsm1Δ::KanMX	yjl124cΔ::KanMX from the prototrophic deletion collection
DGY571	lsm6Δ::KanMX	ydr378cΔ::KanMX from the prototrophic deletion collection
DGY545	pat1Δ::KanMX	ycr077cΔ::KanMX from the prototrophic deletion collection
DGY554	edc3Δ::KanMX	yel015wΔ::KanMX from the prototrophic deletion collection
DGY552	scd6Δ::KanMX	ypr129wΔ::KanMX from the prototrophic deletion collection
DGY611	tif4632Δ::KanMX	ygl049cΔ::KanMX from the prototrophic deletion collection
DGY539	*GAP1* 5' UTR delete	confirmed by Sanger sequencing to have 152bp deleted 5' of the start codon
DGY576	*GAP1* 5' UTR delete	confirmed by Sanger sequencing to have 100bp deleted 5' of the start codon
DGY577	*GAP1* 3' UTR delete	confirmed by Sanger sequencing to have 150bp deleted 3' of the stop codon
DGY525	FY3 + pRP1315	FY3, a ura- auxotroph (ura3-52), transformed with pRP1315 (URA3 marker, expressing a Dcp2-GFP fusion)

Table 3.3: Primers used in this study

ID	Sequence	Description
DGO230	ACGGTATCAAGGGTTTGCCAAG	Figure 3 qPCR *GAP1* reverse
DGO232	GCATAAATGGCAGAGTTAC	Figure 3 qPCR *GAP1* forward
DGO229	CTCTACGGATTCACTGGCAGCA	Figure 5 qPCR *GAP1* reverse
DGO231	TTTGTTCTGTCTTCGTCAC	Figure 5 qPCR *GAP1* forward
DGO236	TTACCCAATAGCTTGTTCAATT	qPCR HTA1 forward
DGO233	GCTGGTAATGCTGCTAGGGATA	qPCR HTA1 reverse
DGO605	CTGGACGACTTCGACTACGG	qPCR 1200 spike-in forward
DGO606	ATCAGCCTTTCCTTTCGTCA	qPCR 1200 spike-in reverse
DGO1562	GTCTGAACTCCAGTCACATCNCNCNCNTNCNGTCGACCTGCAGCGTA	Degenerate first round primer
DGO1588	CCATTGGTGAGCAGCGAAGGATTTGGTGGA/3Phos/	First round blocker oligo
DGO1589	AGAAAAAGCAGCGTAGATGTAGAAGCAAGA/3Phos/	First round blocker oligo
DGO1567	GATGTCCACGAGGTCTCT	Second round outside primer
DGO1576	CGTACGCTGCAGGTCGAC/3Phos/	Second round blocker oligo
DGO1519	CAAGCAGAAGACGGCATACGAGATGTCTGAACTCCAGTCAC	Second and third round inside primer and P7 adapter
Forward index primer	ACGCTCTTCCGATCTXXXXXGTCCACGAGGTCTCT	Multiplexing primer, where XXXXX is one of 120 different barcodes (see below). Table 3.6.0.4.
DGO276	AATGATACGGCGACCACCGAGATCTACACTCTTTCCCTACACGACGCTCTTCCGATCT	Illumina P5 adapter incorporation primer
DGO366	AATGATACGGCGACCACCGAGATCTACAC	RNAseq Illumina library amplification, forward
DGO367	CAAGCAGAAGACGGCATACGAGAT	RNAseq Illumina library amplifcation, reverse

— 4 —

Investigations of physiological remodeling upon a nitrogen upshift

This chapter describes lines of investigation that were not pursued deeply, but may inform future investigations of the physiological remodeling that occurs as yeast resumes rapid growth.

The study of microbial physiology is a long standing area of investigation, and with modern systems biology approaches this question of how the physiological composition of microbes change in order to accomplish the essential project of growth is still the subject of advances both quantitative and conceptual (Carter et al. 1978; Erickson et al. 2017; Henrici 1928; Kafri et al. 2016; Kief and Warner 1981; Kjeldgaard et al. 1958; Metzl-Raz et al. 2017; Schaechter et al. 1958; Scott et al. 2010; Slator 1918; Waldron 1977; Waldron and Lacroute 1975; Wehr and Parks 1969). In recent years, the study of changes in abundance of specific mRNA factors in the budding yeast has characterized a phenomenon in which approximately one quarter of the yeast transcriptome scales with growth rate (Airoldi et al. 2009; Brauer et al. 2008). This phenomenon is characterized at the level of molecular species, and thus can be compared to changes that occur in response to stressors, summarized as the Environmental Stress Response (Gasch et al. 2000). In addition, a shared signature of knockout mutants, commonly used to probe gene function, is that associated with changes in cell-cycle progression distribution due to growth rate changes (O'Duibhir et al. 2014). Thus the appreciation of the systematic physiological changes that occur in response to genetic perturbations holds light to

many biological problems, even if only to identify the domineering and confounding factor of growth-associated physiological changes.

4.1 Changes in poly-adenylated transcript content per cell upon changes in growth rates

This section describes work that contributed to a submitted article titled: "*Growth Rate-Dependent Global Amplification of Gene Expression.*" Authorship of this article is: Niki Athanasiadou, Benjamin Neymotin, Nathan Brandt, **Darach Miller**, Daniel Tranchina, and David Gresham. The *biorxiv* draft is at `doi.org/10.1101/044735`

The writing and figures of this chapter are original to this document.

4.1.1 Introduction

We know that the total RNA content of a cell changes upon changes in growth rates (Waldron and Lacroute 1975). We know that specific mRNA, each a small component of the cell's total RNA also change in relative abundance. A less-characterized question is if the whole mRNA transcriptome changes and if this has a significant effect on the regulatory role of absolute or relative changes in mRNA abundance. Transcriptomic measurements are usually normalized to relative measures, and is thus based (sometimes explicitly (Love et al. 2014)) on the assumption that the total transcriptome does not change in abundance. However, we now know of cases of where this assumption is violated (Nie et al. 2012).

Spike-in normalized RNA sequencing can estimate absolute mRNA abundance per cell, but has been criticized before for being "too noisy" and instead computational methods of "removing unwanted variation" were used (Risso et al. 2014). Led by Rodoniki Athanasiadou, our group pursued a more thorough approach to this design by normalizing RNA sequencing data using the ERCC spike-in set (Jiang et al. 2011), using pre-

liminary sequencing runs to first determine the appropriate amount of spike-ins necessary for accurate sequencing. Then, yeast were grown in systematically varied nutrient limitations of growth, then RNA sequencing using a known quantity of the exogenous spike-ins was used to normalize the measurements to absolute mRNA per cell.

I sought to complement this work by orthogonally estimating the size of the whole yeast transcriptome. To do this, I adapted the screening strategy of Amberg et al. 1992 to flow cytometry. Essentially, this utilized a poly-deoxythymidine oligo singly labeled with a fluorophore. This was hybridized in with the fixed and permeabilized yeast cell, and the resulting fluorescence after washing is taken to be a proxy for the number of hybridized poly-dT probes, presumably hybridized to a poly-adenosine sequence, and thus mRNA.

Another motivation of this was to serve as a fixation-digestion control for methods involving single-gene mRNA FISH. We had patterns of mRNA FISH hybridization signal that appeared bimodal (Figure 3.17). This could be a technical issue of incomplete permeabilization due to over-fixing, or a biological phenomenon. To distinguish the two would take two-color FISH, with a positive control (Andersen et al. 2014). Since nitrogen-limitation causes a severe restriction of the total transcriptome content, we don't have an obvious pick for a uniformly expressed positive control. However, most of the mRNA should be poly-adenylated, so FISH against that sequence should be present in all cells, and in high-copy. While I did not integrate this into the single gene mRNA FISH as an internal control, I did use it to optimize fixation/permeabilization conditions.

4.1.2 The assay design

The assay uses a similar fixation permeabilization method as the single-gene mRNA FISH assay, then an overnight hybridization against a poly-dT probe, then flow cytometry.

The yeast cells are sampled via vacuum filtration onto nylon filters, then the filters

are quickly flash-frozen in liquid nitrogen. These are resuspended in 0.75x PBS buffered 4% PFA (from ampules from EMS), the cells vortexed off the filter, then the filter discarded. The cell suspension in the fixative is incubated for hours at RT to complete fixation, with the assumption that rapid fixation halts RNA metabolism in the cell and long-term fixation stabilizes the fixed components into a configuration that can survive digestion and permeabilization. The fix is critically quenched using 2.5M glycine, then collected by centrifugation and washed with PBS. The cells are digested for one hour at 37C using lyticase and beta-mercaptoethanol in 1.2M sorbitol buffered by potassium phosphate at about 7.4 pH, with 20mM vanadyl ribonucleoside complex to inhibit RNAses. This is washed and further permeabilized with 70% ethanol overnight, then is resuspened using hybridization buffer (10% dextran sulfate w/v, 2x SSC final, 100ug/ml ecoli tRNA, 250mg/ml salmon sperm DNA) plus 100nM of a (dT)50+V oligo 5'-labeled with with Alexa 488, as ordered from IDT. This is incubated for 14+ hours on a 37C roller drum, then washed with 2x SSC several times before resuspending in PBS and flowing through an Accurri flow cytometer. Poly(A) content signal was determined by the signal area on the 514/20nm detector.

To test this procedure, I used RNAseA treated cells as a negative control. Figure 4.1 shows the RNAseA-treated controls for two samples, where the treatment abrogates the signal for the vast majority of the cells in the sample.

To optimize this design, I varied formamide from 0% to 50%, and probe concentrations from 10nM to 1μM. I found that 100nM and 0% formamide saturated the signal of YPD-grown cells without largely increasing the signal on the RNAseA-treated cells. This assay takes approximately 4 hours of work spread over 3 days. More detailed protocol is maintained by the Gresham laboratory.

4.1.3 Nutrient limitation and transcriptome size

Yeast growing in YPD complete a division approximately every 1.5 hours (0.45 specific growth rate), while proline-limited media (NLimPro) only supports division approximately every 4.5 hours (.15 specific growth rate). Using this poly-dT FISH method, we see differences in the total poly-adenylated mRNA signal between the different media conditions (Figure 4.1). The distributions are significantly different (KS test and Wilcoxon, p-value < 2.2×10^{-16}). We know that fast growing cells (YPD) have more RNA per cell, so it appears that part of this difference is contributed by a global scaling of the mRNA content as well. The fold-changes in the mean and median of the YPD-grown cells versus the proline-limited cells were 3.34 and 3.68, respectively.

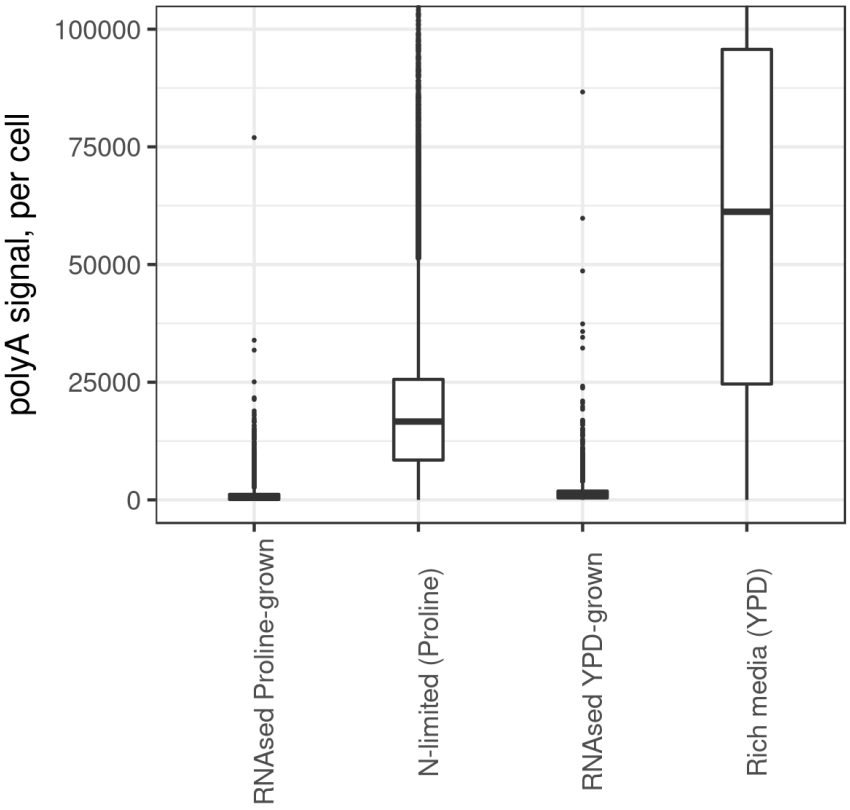

Figure 4.1: **Changes in whole cell polyA content in YPD or nitrogen-limitation.** Wild-type yeast grown in proline-limited media (left) or YPD rich media (right) were assayed in exponential growth for poly-A content. Included are RNAsed controls treated with RNAseA, to show negative samples. The plot is cropped from 0 to 10^5 arbitrary units of polyA signal to show the center of the distributions. The distributions from different media have different means by KS or Wilcoxon tests, with unreasonably small p-values.

To investigate the dynamics of changes in poly-A abundance between different growth conditions, I grew cells in proline-limited media overnight to reach a steady-state of growth, then collected samples during a nitrogen-upshift. I assayed the poly-A content of the cells using the above assay (Figure 4.2). I found that the total poly-A content took about two hours to increase to the new steady-state of a larger transcriptome, a similar timescale as the changes in cell size and lag in population growth rate (Figure 3.1). The final steady-state differences were of a fold-change of 2.16 and 1.93 for the mean and

median poly-A content, consistent with the change between specific growth rates of 0.15 and 0.35 being lower than the difference with YPD (0.45 specific growth rate).

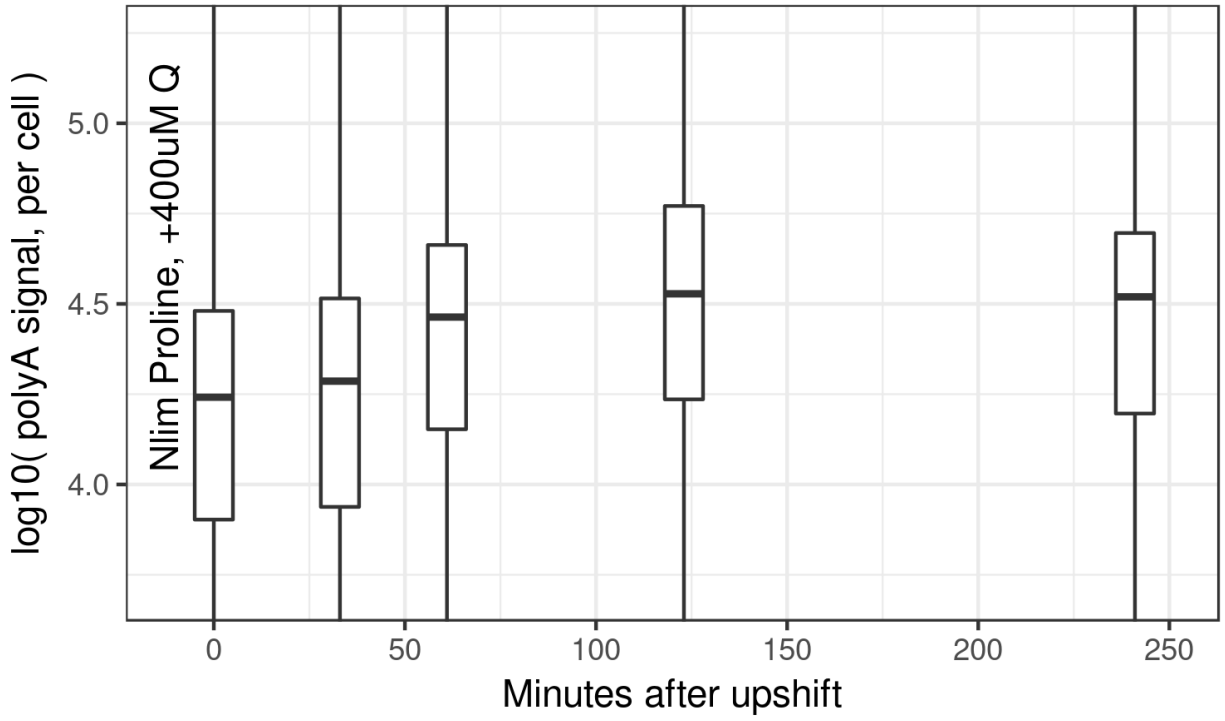

Figure 4.2: **Changes in polyA content upon a nitrogen upshift.** Wild-type yeast were grown in proline-limited media, then glutamine was added at time 0 minutes. Samples were assayed for polyA content using the poly-dT assay.

Previously, others in the lab (as described at the beginning of this section) had used ERCC-normalized RNA sequencing to assay the absolute abundance of mRNA in yeast grown at systematically varied growth rates (0.12, 0.2, 0.3 specific growth rate) in chemostats. In a repeat experiment of this, I took samples from chemostats limited by nitrogen or carbon at these growth rates, and processed them to assay the distribution of poly-A content of the cells. Figure 4.3 shows the distributions and the relationship between the distribution means and the estimates from SPARQ (the spike-in normalized RNAseq method). We see that the poly-dT method also captures the scaling of the whole yeast transcriptome across different growth rates, and correlates well with the spike-in normalized method.

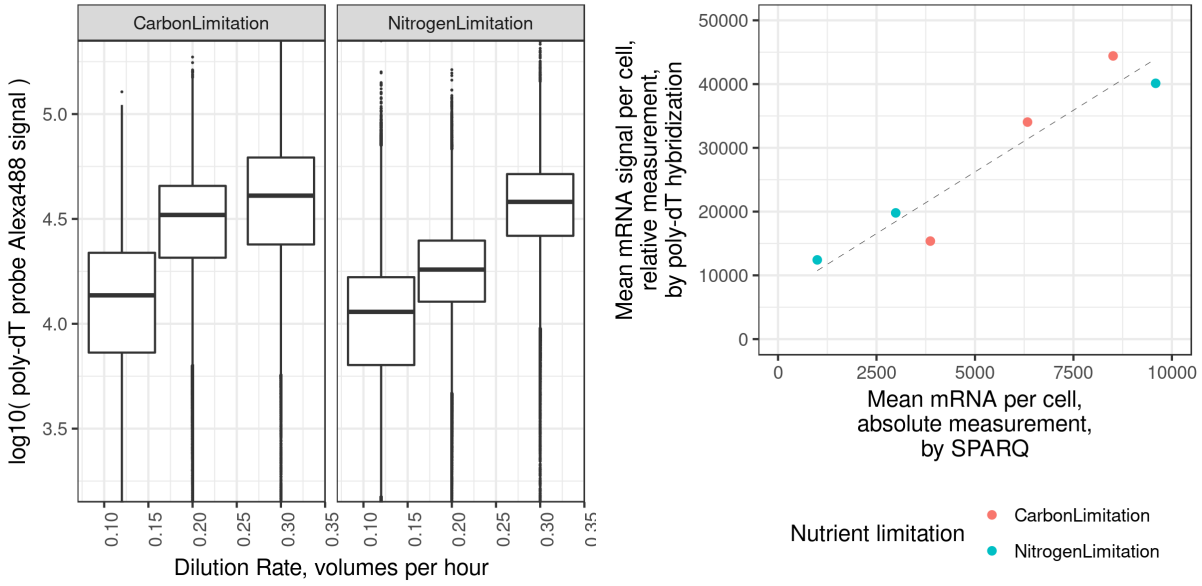

Figure 4.3: **Measuring polyA content across systematically varied growth rates in chemostats, and comparison to a spike-in normalized RNA sequencing method.** (Left) PolyA content was estimated for cultures grown in two nutrient limitations at three different dilution (growth) rates. (Right) Comparing these measurements to SPARQ (the spike-in normalized RNAseq method) shows that two methods are well correlated (Pearson's r=0.95, `cor.test` p-value = 0.003684, dashed-line shows linear regression through all points), although the poly-dT method remains uncalibrated.

4.1.4 Conclusion and future directions

This assay appears to detect changes in the scaling of the yeast mRNA content between different growth rates. It is consistent with spike-in normalized RNAseq (random hexamer-primed) estimates of the total mRNA content. As a flow cytometry assay this has the potential to be used as a marker for high-throughput investigations of the genetics of transcriptome size changes (or regulation), using methods as described in Design of Barseq after FACS after FISH experiment. This method offers a conveniently high-throughput assay for total transcriptome size, and as such is one more tool that microbial physiologists can use to probe the functional changes that occur as organisms systemically adapt to their environments and growth programs.

However, more work remains to use the assay to reliably inform on these changes

without incorporating an orthogonal measure. Changes in polyA tail length could hypothetically affect hybridization, and a distribution shifting such that more of the functional mRNA have a tail length less than minimum tail length requisite for hybridization would produce a similar graded effect. Hybridization of this probe to synthetic mRNA cross-linked to a nylon substrate would allow quantitative testing of this in similar conditions as the hybridization occurs, provided a method for manufacturing accurately generated poly-A tail lengths exists.

Future investigations of mRNA content per cell will illuminate the role or significance of total mRNA abundance versus relative mRNA abundance in gene regulation and physiological adjustments to changing environments. Adjustment is apparent during a nitrogen upshift: what causes it, and is it adaptive?

4.2 Screening for genes important for remodeling physiology for growth

4.2.1 Introduction

With changing physiology in response to growth rate changes, many molecular and functional phenotypes change. One of these is the resistance to stress. It has been long known that slow growing cells are more resistant to stressors (Elliott and Futcher 1993; Lu et al. 2009; Sherman and Albus 1923). Yeast appears to have adapted to its ecological niche by adopting a boom/bust, feast or famine approach to quickly growing during favorable conditions at the expense of stress resistance. Resistance to stress seems to offer "cross-protection", and the anti-correlation of growth rate and stress resistance suggests that the two processes might be opposed in mechanisms to achieve these objectives. The dimension of coordinated cellular growth may be a simple axis that explains much of the variation in gene expression and phenotypic differences in budding yeast (Brauer et al. 2008; Lu et al. 2009).

One approach to identify the characteristics required for yeast to achieve a faster growth rate is to monitor the regulated changes that occur upon the upshift. We could infer that since the most logical response to a stress is to express this adaptation, then the gene expression increasing upon a stress must be adaptive (Gould and Lewontin 1979). This has been demonstrated to be a false assumption, at least for the case of heatshocks, as the genes whose expression increases do not overlap well with the genes important for resistance (Gibney et al. 2013). The later functional genetic measurement is possible to do in high-throughput, as the yeast community has access to a yeast deletion collection and high-throughput means of assaying genetic effects on the quantitative phenotype of continued existence. Thus, an assay of the functional consequences is a more direct approach to understand these processes.

The nitrogen upshift enriches for differences in growth rate, by growth. Subtle effects can be magnified over time, for example a 1% growth rate defect over 7 hours would be magnified to an abundance change of at least 20%. However, the phenotype I am interested in is in the completion of remodeling for rapid growth, so I am most interested in the duration of the lag between nitrogen addition and increased growth. Thus, the compounding of growth rate effect does not apply. One approach would be to repeat the upshift many times on the same batch of cells, but this greatly confounds the fitness between various growth stages and does not offer the reproducibility of cells being in a particular physiological status — nitrogen-limitation can take hours to reach a steady-state of signalling (Tate and Cooper 2013), and the life history of an individual cell could have physiological consequences.

After practicing the Feynmen method with a scientific advisor in California (Acknowledgements), and given the opportunity to work with a talented young scientist named Stephen Nyarko, we decided to pursue this question by using the correlated phenotypes of growth and susceptibility to stress. The logic is that if we are interested in isolating

mutants that are defective in increasing their growth rate upon a nitrogen upshift, and an increase in growth is associated with a susceptibility to stress, then a somewhat-lethal stress should enrich for mutants defective in susceptibility to the stress — ie defective in rapidly increasing growth rate. Upon further reading, we found that the group of Johan Theiveilen had used a similar approach to isolate mutants defective for increasing growth upon repletion of glucose, and had identified new critical components of the PKA pathway, *CYR1* and *GPR1* (Van Dijck et al. 2000). Thus encouraged, we intended to use the anti-correlation of growth and stress resistance to isolate mutants defective in resuming growth rapidly.

4.2.2 Results

We first determined if the heatshock resistance of the wild-type FY4 yeast changed during a nitrogen upshift. I grew cells in proline-limited media (approximately 4.5 hour doubling time), then added glutamine to induce the nitrogen upshift. For each sample, cells were subject to a 52C heatshock for 30 minutes by the addition of pre-warmed media, or for negative control were simply kept at room temperature. The processed samples were arrayed in a 96 well plate, then pinned onto YPD, grown at 30C for approximately 40 hours, and imaged (Figure 4.4).

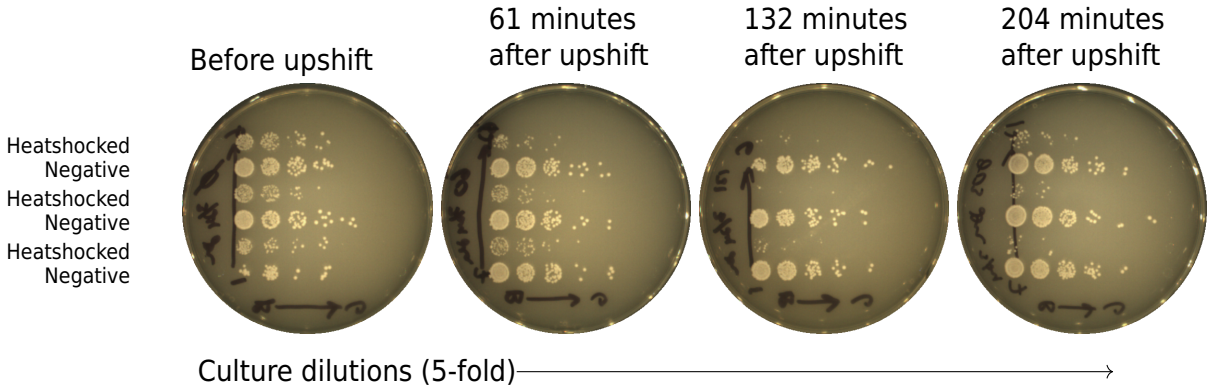

Figure 4.4: **Glutamine upshift causes a lost in heatshock-resistance.** Wild-type (FY4) cells were subject to nitrogen-limitation, then a nitrogen upshift with 400μM glutamine. Cultures were heatshocked at 52C for 30 minutes, or at roomtemperature (negative). 5-fold serial dilutions were plated on YPD plates.

Thus, the glutamine upshift triggers a loss in resistance to the heatshock. We then devised a screen, wherein a barcoded and pooled yeast deletion collection is grown in conditions of nitrogen-limitation then upshifted. Samples were taking before or after 120 minutes after the glutamine upshift, heatshocked or not (negatives), then outgrown to enrich for living mutants. These libraries were sequenced using an amplicon-sequencing procedure to quantify the mutants in the resulting library.

Direct measurement of mutant abundance is preferred, but we used outgrowth of the heatshocked population, counting on the severe selection of a heatshock to appropriately select. We did this in six biological replicates in order to generate robust signal. These were extracted with standard Hoffman-Winston DNA preparations, then amplified using the same primers and protocol as described in (Robinson et al. 2014). These were sequenced along with other samples on an Illumina MiSeq run.

Barcode sequencing, like other molecule-counting applications of sequencing like RNAseq, is presented to the researcher as a relative measurement in integer quantities. One of the first steps in reading this data in is to look at the distribution of counts per strain barcode identified Figure 4.5. We see that our heatshock and outgrowth has a

much more profound distribution of effects. For which genes is this significant?

Numerous statistical approaches exist to normalize the data for accurate detection of differential abundance. One flexible and robust method is using the `voom` statistical pre-processing step with `limma`. This calculates the expected noise contributed by low integer count observation, but has the advantage of converting the measurement to a "counts per million" relative metric for normalization. It also has useful visualizations for characterizing the distribution of signal across complex experimental designs.

One other observation in Figure 4.5 is that the histograms show a log-normal distribution of high counts, then a long tail downwards. Then, there appears to be a low distribution of single digit counts which enter the distribution from around zero Figure 4.6. These are believed to occur from spurious amplicon products or software misalignment counting barcodes that do not exist. To characterize this further, I used `limma/voom` to generate plots of variance against abundance for different thresholds of cutoffs based on total counts across the entire library Figure 4.7. I found that a threshold of 30 counts in total across the library was sufficient to remove these effects.

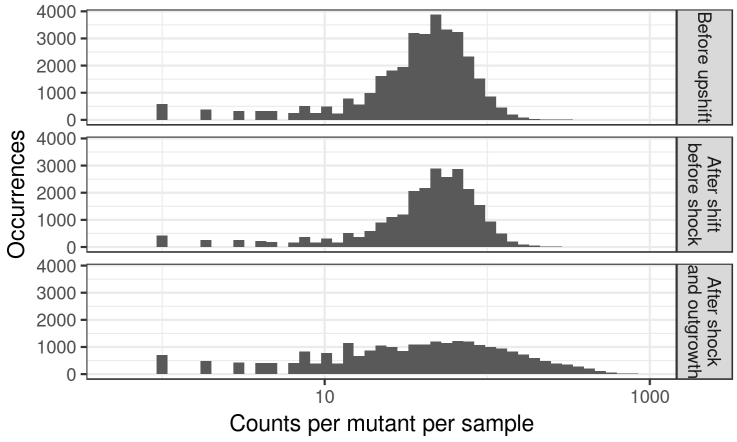

Figure 4.5: **Histogram of mutant counts, within each sample.** Histograms of counts, for each mutant in each sample. Three histograms show the occurrences of these observations for the library before the upshift (top), 2 hours after adding glutamine (middle), and after the heatshock and outgrowth (bottom). The wider spreading is a good indication of complex selection of large effects occurring in the library.

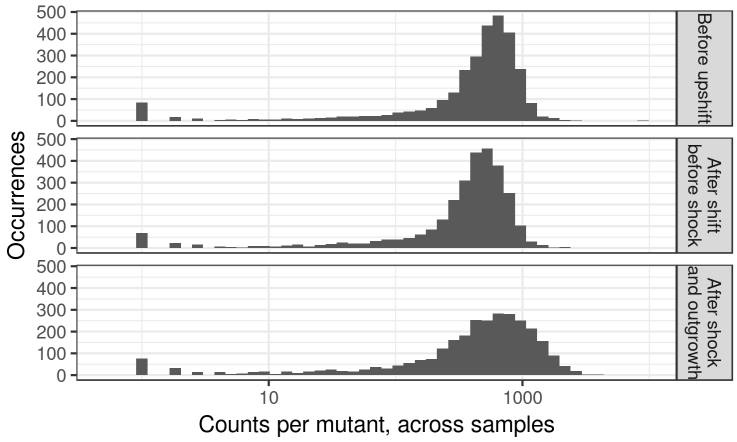

Figure 4.6: **Histogram of mutant counts, summed across samples.** Histograms of counts, for each mutant, summed across all samples in the three treatments: before the upshift (top), 2 hours after adding glutamine (middle), and after the heatshock and outgrowth (bottom). We see that most features are log normally distributed, but some appear to be noisy counts near zero, due to unknown factors.

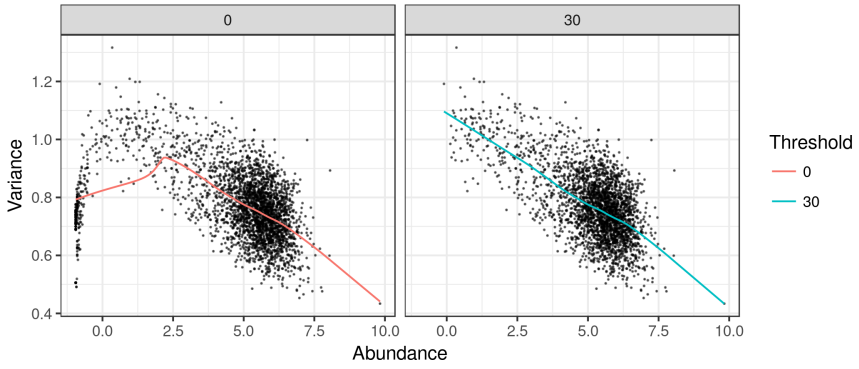

Figure 4.7: **Diagnostic `limma/voom` plots show the effects of low-count barcodes in confounding the noise model.** Each plot shows each gene average abundance (x-axis) against its residual variation (y-axis), with a line smoothing the relationship as expected by `limma` modeling. The threshold of minimum total counts per feature is shown for each plot in the grey bar. We see that thresholding above 30 counts **(right)** gives us the expected relationship, while not thresholding **(left)** demonstrates how lowly abundance counts behave aberrantly with artificially reduced variance that may confound statistical analyses of barcode sequencing data (`limma` uses the model fit as the line).

I used this tool's flexible general linear modeling interface to ask how our treatment enriched for particular mutants. We saw no significant effects from a glutamine upshift, confirming the intuition that this is such a subtle effect of momentary fitness that it becomes hard to detect without amplification. Testing for the effect of changes in

abundance based on a glutamine treatment before the heatshock, we find that four deletion strains significantly (multiple-hypothesis adjusted p-values < 0.05) increase in abundance specifically after glutamine treatment, and 41 are decreased in abundance.

Of the four genes increased in abundance (suggesting a failure to resume rapid growth), *SLA1* and *CAP2* are involved in actin binding and dynamics. *SLA1* is involved in assembly of the cortical actin cytoskeleton (Holtzman et al. 1993), while *CAP2* is an actin barbed-end capping protein that localizes to cortical actin patches (Amatruda et al. 1990). This suggests that these mutants specifically are involved in remodeling the cortical exoskeleton in a way that makes cells more susceptible to heatshock, or that these mutants are defective in increases in stress-resistance associated with slow growth rates. *SXM1* over-expression rescues mutants defective in mRNA export from the nucleus (Seedorf and Silver 1997), suggesting that it may play a role in mRNA export itself and that mRNA export may regulate some important downstream factor associated with increasing growth. *MAE1* encodes a malate dehydrogenase. This reaction takes malate, a citric-acid cycle metabolite, and converts it to pyruvate (Boles et al. 1998). Pyruvate is an essential substrate for the biogenesis of the carbon structures of alanine, valine, and other amino-acids. Carbon-skeletons of glutamine can enter the citric-acid cycle from a point between the entry of pyruvate, and shunt from malate to pyruvate via *MAE1*. Considering the enrichment of pyruvate metabolism mRNA identified as destabilized in the 4tU label-chase work in subsection 3.3.2, and that the same experiment showed either a stabilization or dramatic synthesis up-regulation of *MAE1* mRNA upon the nitrogen upshift, one prediction might be that Mae1p provides a shunt by which yeast re-directs the excess of carbon skeletons from glutamine deamination through the citric-acid cycle to provide substrates for alanine biosynthesis. This may be adaptive.

To explore this, I regenerated a *mae1*$\triangle$ mutant using a KanMX knockout cassette am-

plified from the yeast deletion collection, confirming incorporation by PCR. I subjected this mutant to a glutamine upshift, and saw an increase in the lag-phase duration (Figure 4.8) compared to wild-type (Figure 3.1). I sought to test if this was specifically due to disruption of the malate to pyruvate shunt for the effect of alanine metabolism, and so repeated the experiment but added 200μM alanine, 200μM pyruvate, or water (mock) to the cell culture at the same time as glutamine. I did not see a significant effect on the growth rate increase (Figure 4.8). Thus, disruption of this gene may not result in slower upshift in growth by virtue of blocking this metabolic pathway, but instead the metabolic state of the cell before the upshift may not be well prepared to resume rapid growth.

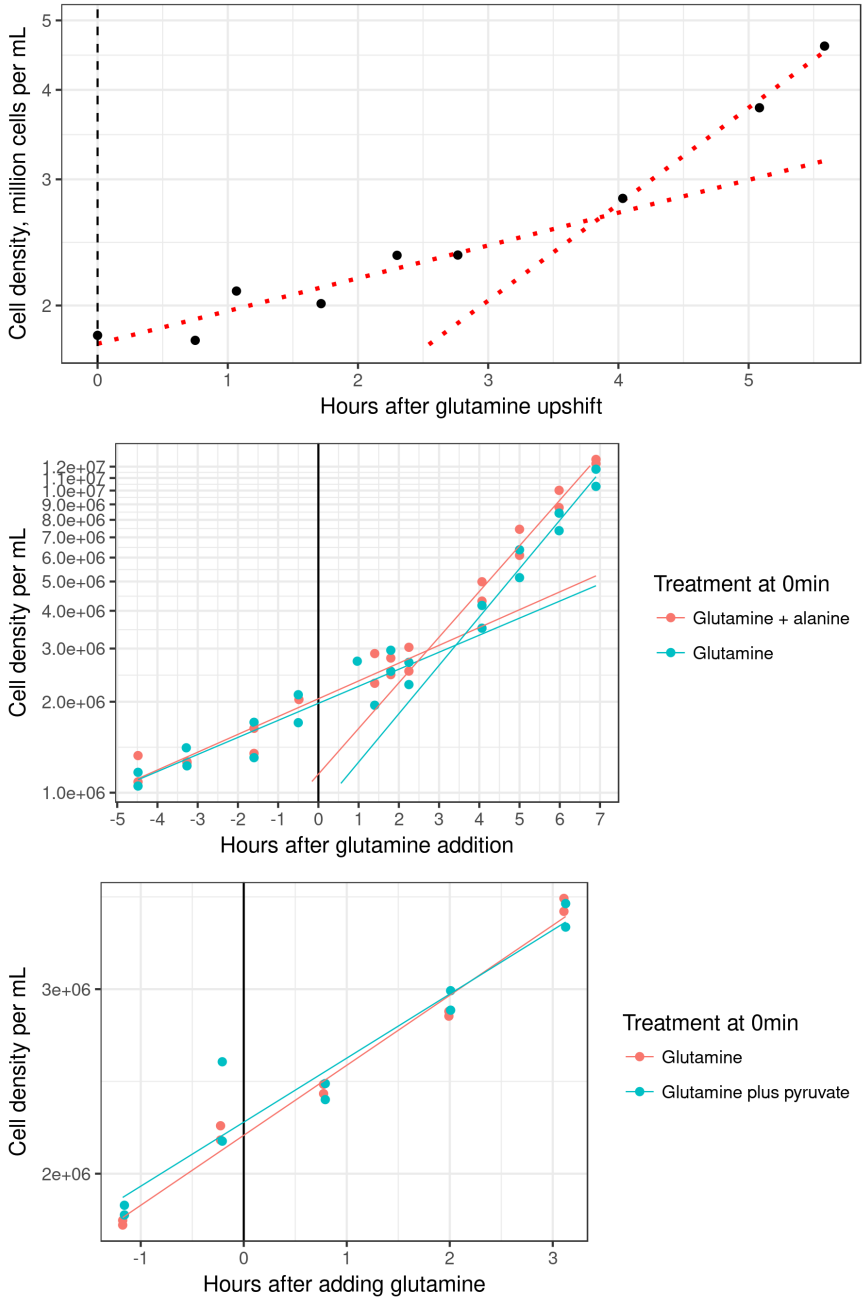

Figure 4.8: **A *mae1*Δ mutant is slower in a glutamine upshift, but this is not rescued by supplementation with alanine or pyruvate.** A *mae1*Δ strain was subject to a glutamine upshift. **(Top)** The mutant alone appears to show a slight defect in the lag phase (approximately 3 hours compared to approximately 2 hours Figure 3.1). **(Middle and bottom)** The mutant had glutamine or glutamine and either alanine (middle) or pyruvate (bottom) added, with two cultures per treatment. Neither showed a significant effect in reducing lag phase or increasing growth rate.

4.2.3 Conclusion

We found mutants knocked out for several non-essential genes changed their relative susceptibility upon heatshock treatment, suggesting that their resistance does not decrease as much as wild-type upon the re-addition of a nitrogen source with adding glutamine. These mutants could be involved in either the increase in stress resistance upon slow growth conditions, or the decrease in stress resistance upon increase in growth. For the factors of the actin cytoskeleton, this points towards a hypothesis that the increase in stress resistance results from specifically the cortical actin network, and would be testable by determining when these mutants are more or less resistant to stress than the wild-type. For *MAE1*, I found that there appears to be a longer lag phase, but this is not rescued by addition of pyruvate or alanine. This suggests that the deletion of this gene puts the cell in a metabolic configuration less capable of rapidly increasing growth rate upon glutamine addition.

— 5 —

Conclusion

Upon repletion of nitrogen, *Saccharomyces cerevisiae* resumes rapid growth. This involves physiological remodeling as discussed in chapter 4. Rapid transcriptional reprogramming also occurs to repress mRNA of genes newly unneeded in the replete nitrogen condition, especially NCR-regulated transporters as seen in chapter 2 and chapter 3. In efforts to determine the genetic basis of the rapid clearance of *GAP1* mRNA in particular, I found that decapping modulators play a role in these dynamics, as discussed in chapter 3.

5.1 Summary

Here, I summarize these findings and speculate on future directions that this work could contribute to.

5.1.1 mRNA destabilization hastens functional reprogramming

The five fastest decreasing mRNA in the transcriptome upon the nitrogen upshift are NCR transporter mRNAs (Figure 2.1). Using principal components analysis, we find that the changes in mRNA abundances across the transcriptome during the upshift are in some ways distinct from simply a switch from a slow-growing gene expression state to a fast-growing gene expression state (Figure 3.3). Instead, there is an enrichment in promotion of RNA production and processing, and a repression of cytoskeleton and membrane organization (Figure 3.3.1).

mRNA degradation rate control is known to play a role in other environmental tran-

sitions, so I used a 4-thiouracil label-chase experiment with RNAseq to characterize the stability and changes of stability of individual mRNA in the yeast transcriptome (Figure 3.4). To avoid problems of nitrogen-regulation of the uracil transporter necessary for labeling changes, I used an interrupted chase design. To smooth technical noise inherent in the normalization of sequencing data to low amounts of spike-ins, I used a normalization that models the change of the whole yeast transcriptome. This prevents particularly noisy measurements of spike-ins from being interpreted as changes in mRNA dynamics (subsubsection 3.3.4.2). To address the potential confounding of synthesis rate changes with measures of destabilization, I used modeling to characterize the expected error and threshold our calls of significance on the effect size (subsubsection 3.3.4.2). These methods may assist the future application of the 4tU label-chase approach to studying extant mRNA stability across dynamic conditions.

Using these methods, I estimated mRNA degradation rates for the yeast transcriptome and found a median half-life of 6.92 minutes (Table 3.1). This is less than previous estimates in rich media, suggesting that mRNA may be less stable during these conditions of limitation of nitrogen-quality in batch growth conditions. This may reflect an evolved preference for flexibility in nitrogen allocation over the energy costs of turning over mRNA frequently. Upon the upshift, I found that degradation rates and changes in mRNA abundance are, as expected, anti-correlated but not entirely co-directional in their effect (Figure 3.6,Figure 3.8).

I found that 78 mRNA are destabilized upon the upshift, with enrichment for NCR mRNA as well as mRNA encoding factors of carbon metabolism and vacuole components (Figure 3.3.2). Amongst these, *GAP1* is subject to an approximately three-fold increase in degradation rates. Thus, mRNA destabilization plays a role in the regulation of this canonical NCR-regulated mRNA, in addition to the previously known regulation at layers of mRNA synthesis and post-translational control.

5.1.2 Decapping is important for *GAP1* clearance

I aimed to determine the genetic factors of this swift clearance, and so combined mRNA FISH with FACS and sequencing to estimate *GAP1* mRNA for mutants in a barcoded pool. Development of this method required several technical advances in optimizing *in situ* hybridization methods, developing a robust method for barcode sequencing in the face of seemingly inescapable dimer formation (subsubsection 3.4.6.1), and implementing a modeling analysis to estimate mutants distributions across bins of *GAP1* abundance (Figure 3.22).

Using this method, I determined that factors of the Lsm1-7p/Pat1p complex were important for wild-type *GAP1* expression dynamics (Figure 3.28). Importantly, the modulators *EDC3* and *SCD6* had defects that did not appear to generally affect the whole transcriptome, unlike with defects in *LSM1* and *LSM6* (Figure 3.30). Fortunately, more analyses of related genes had been completed by Nathan Brandt, and a re-analysis of this data revealed that the Scd6p-interacting eIF4G2/Tif4632p had a similar defect. Nathan Brandt had also characterized the effects of truncations of sequence upstream of the *GAP1* start codon or downstream of the *GAP1* stop codon, and re-analysis showed that the 5' UTR truncations had a very similar phenotype as deletions of *SCD6* or *TIF4632*. These similarities suggest a connection between translation initiation and mRNA stability during steady-state and dynamic conditions that may inform our general understanding of the competition of these processes.

5.1.3 Physiological changes that occur during nitrogen upshift

Combining a fluorescent poly-dT probe assay (Amberg et al. 1992) with flow cytometry, I was able to orthogonally confirm the phenomenon of mRNA transcriptome scaling in different nutrient environments (Figure 4.3) and measure the dynamics of this transition (Figure 4.2). Given the compatibility of this assay with the SortSeq approach described

in chapter 3, this could be used to efficiently probe the genetic factors of transcriptome scaling dynamics in response to changing environments. Understanding this process in yeast may inform the study of how c-Myc signalling affects (or effects) this process (Nie et al. 2012).

It is well known that stress-resistance decreases with an increasing growth rate, and we demonstrated this is true for a nitrogen-upshift as well (Figure 4.4). We used this property to enrich a mutant library for defects in increased susceptibility upon a nitrogen upshift, and found an enrichment of two components that regulate the cortical actin cytoskeleton. Future studies of these, and the two other identified mutants, may reveal growth-rate regulation of the cortical actin cytoskeleton involvement in yeast stress-resistance, and a potential of Mae1p to connect nitrogen and carbon metabolism.

5.2 Suggested future directions

I would like to expand on these findings to suggest future directions of inquiry.

5.2.1 An efficient method for estimating mRNA abundance in barcoded mutant pools

Much of what we know about mRNA degradation has relied on genetics, but perturbing an exquisitely homeostatic system, like a living cell, can result in indirect effects as systems of regulatory feedback percolates the signal through the network. Thus in this work, the use of knockout mutants is the use of an indeterminately perturbed system. Additionally, the laborious individual creation and maintenance of a collection of mutants can introduce potential artifacts of suppressor and passenger mutations (Kwan et al. 2016; Markowitz et al. 2017). The development of new methods for making mutant pools with high internal replication and minimal strain-handling selection offers a new paradigm of yeast genetics that avoids or minimizes some of these drawbacks (Smith

et al. 2016). The methods described here for doing SortSeq can be adapted to any DNA-barcode-based sequencing assay of pooled mutants.

With the integration of single-cell RNA sequencing with RNA-guided Cas9 genetic-editing (Dixit et al. 2016; Hill et al. 2018), this approach of mRNA SortSeq may no longer be absolutely necessary for doing high-throughput genetics for mRNA markers. However, this method works now with common lab reagents and equipment, and only requires quantifying the mutants across bins— not quantifying all mRNA for all mutants. For questions regarding a small number of transcripts, the depth of replicates and timepoints possible with a SortSeq design may be advantageous. Additionally, the recalcitrance of budding yeast for single-cell molecular analysis is still technically challenging (Gasch et al. 2017). Scaling this BFF assay up to more cells input and a greater investment in FACS sorting (Boer et al. 2017) has the potential to estimate mRNA dynamics across multiple timepoints for all barcoded mutants in a library. However, single-cell RNA sequencing is advantaged in its global perspective and will presumably scale with methodological developments to increase cell throughput (thus replicating measures per genotype) and sequencing throughput. The efficiency of the pooled SortSeq approach could also be used to limit the search space of more precise but resource-intensive automated assays (Worley et al. 2016), and thus a hybrid approach could be used to efficiently increase throughput of measured transcript dynamics. SortSeq for estimating mRNA abundance, or other steps of gene expression, may be a useful orthogonal tool complementing other approaches with its potential for scaling measurements across timepoints, conditions, variants, and replicates.

5.2.2 All metabolism is connected

We often reduce phenomena to simple models in order to create a more powerful generality, but sometimes a powerful categorization can be too far (Lazebnik 2002). In the label-chase experiment, I found that mRNA encoding factors of carbon metabolism

(namely pyruvate metabolism, and the isoenzymes *PYK2* and *HXK1*) were destabilized. In the genetic screen (BFF), we found that mutants in negative regulation of gluconeogenesis were enriched in mutants with high *GAP1* mRNA estimated after the shift (Figure 3.25), suggesting defects in repression. The core of nitrogen metabolism (glutamate and glutamine) are intimately connected with the citric acid cycle via alpha-ketoglutarate, and the roles of these metabolites or their rates of inter-conversion have been proposed to play roles in signalling changes in growth (Fayyad-Kazan et al. 2016). Thus, continued study of the metabolic networks during perturbations (like a glutamine upshift) may reveal an unappreciated cross-talk amongst sub-networks that are currently considered as distinct. This may reveal contingent or adaptive regulation of diverse signalling pathways from secondary metabolite read-outs that are distal from the experimenter's intended input. Here, glutamine is considered as a nitrogen-source but delivers to the cell two nitrogen atoms and a carbon skeleton that can be delivered into the citric-acid cycle. Thus, a systematic view of metabolism during this transitions may reveal that the effects of a glutamine upshift may be more broad than just nitrogen metabolism and regulation, and may inform our more specific interpretation of these perturbation experiments.

5.2.3 pH as a possible cause of mRNA destabilization

Addition of a preferred nitrogen source triggers a destabilization for several mRNA. A similar phenomenon of mRNA destabilization is observed during the re-addition of glucose to cultures limited for growth by carbon availability (Braun et al. 2016). The mechanisms by which this occurs appear to be diverse, although they tend to occur via the canonical 5'-decapping mechanism. How might these two transitions be similar?

Yeast acidify their media via the action of the ATP-dependent proton export pump *PMA1*, regulating their cytoplasmic pH at approximately pH 7 (or $\sim$3000 protons in total Orij et al. 2011). The General Amino-Acid Permease 1 (*GAP1*) and other transporters

use this proton-gradient to symport amino-acids into the cell (Grenson 1992). The re-addition of amino acids is expected to depolarize this gradient, and *GAP1* mutants who are defective in the inactivation of Gap1p upon refeeding have a growth defect (Risinger et al. 2006), suggesting that the process of active transport is what contributes to the defect in cellular metabolism and growth. Glucose upshifts result in a rapid but transient reduction in pH (Kresnowati et al. 2008), thought to result from a sudden increase in proton-release during the early steps of glycolysis (Orij et al. 2011). Similarly, the catabolism of glutamine into alpha-ketoglutarate and free ammonium ions should produce one proton per glutamine (Magasanik and Kaiser 2002), in addition to the proton from symport of one glutamine.

Both of these upshifts are likely to decrease cytoplasmic pH. This could affect mRNA stability via effects through signalling pathways like Ras/PKA, which is known to affect the signalling of this pathway through cAMP (Orij et al. 2011). Recently it has been shown that the proton-influx from nutrient uptake via symport mechanisms is implicated in directly causing the spike in TORC1 activity normally attributed to the nutrient source (Saliba et al. 2018). The GAAC pathway via the Gcn2p kinase has been shown to respond and be important for responding to acidification (Hueso et al. 2012). Single or combinations of these pathways may signal to alter mRNA degradation rates.

Alternatively, changing pH can have strong biophysical effects on protein-protein interactions and folding that may perturb mRNA degradation metabolism. Pab1 has been recently shown to have a pH-dependent tendency to condense in response to stressors, a process that affects its function likely through Ccr4-dependent deadenylation (Riback et al. 2017; Yao et al. 2007). Additionally, the condensation of mRNA processing-bodies is correlated with impacts on the pace of mRNA degradation metabolism in the yeast cytoplasm (Huch and Nissan 2017; Rao and Parker 2017). Thus large changes in the pH may directly perturb the molecular interactions that effect the processes of mRNA

degradation.

pH changes as directly impacting the molecular processes that are sensitive to changes in post-translational modifications and localization would be a mechanism to explain the general phenomenon of mRNA stability changes during environmental changes (Canadell et al. 2015; Pérez-Ortín et al. 2013). The role of metabolism or proton-symporters in causing this would explain some of the generality of the phenomenon that has been described as "transceptors" in the work of Theiveilen.

Future work to define the extent and impact of this phenomenon would make a significant impact on our understanding of cytoplasmic processes and the determinants of mRNA degradation metabolism. Precisely defining the changes in cytoplasmic pH on the seconds timescale during these environmental changes would define the timescales of interest. Metabolic label-chase experiments with mutants allow a genome-wide assay of functional impact. Live-cell microscopy in micro (or milli) fludics devices would allow the integration of these datasets to test if molecular-condensation events may play a role, a hypothesis that could be explored mechanistically with biochemical *in vitro* work.

5.2.4 Possible mechanisms of *GAP1* clearance

GAP1 mRNA is now an example of mRNA destabilized upon a nutrient upshift. What effects this regulation? I identified several candidate factors, here I speculate on the implications of one group of factors.

Scd6p interaction with eIF4G1 has been primarily studied, but here we see a similar phenotype with eIF4G2 (eIF4G1 was not tested). These are homologs with very similar functionality (Clarkson et al. 2010), although eIF4G1 is expressed higher during normal laboratory growth conditions, ie rich media. eIF4G2 has been shown to be more highly expressed and localized to processing-bodies during conditions of nutrient limitations, and this is suggested to specify the storage of mRNA in anticipation of resuming rapid growth (Brengues and Parker 2007). This initiation factor may help to globally (or specif-

ically) reduce the initiation frequency, thus reducing the fraction of ribosomes consuming tRNA under conditions of low amino-acid, and thus low charged-tRNA, availability (Figure 5.1) This would help ensure an adequate supply of charged-tRNAs for elongation of engaged ribosomes. Differential regulation of translation initiation could explain the observation of sub-maximal usage of extant ribosomes in initiation-limited regimes of cellular growth (Kafri et al. 2016; Metzl-Raz et al. 2017). Continued studies of the role of Scd6p in specifying ribosome loading in diverse environmental conditions could reveal a mechanism to effect these adaptive changes in translation. Additionally, a systematic study of the *GAP1* 5' UTR could reveal *cis*-elements necessary for this regulation. In particular, the study of the rapid changes that occur during the nitrogen upshift may shed light on their role during steady-state growth.

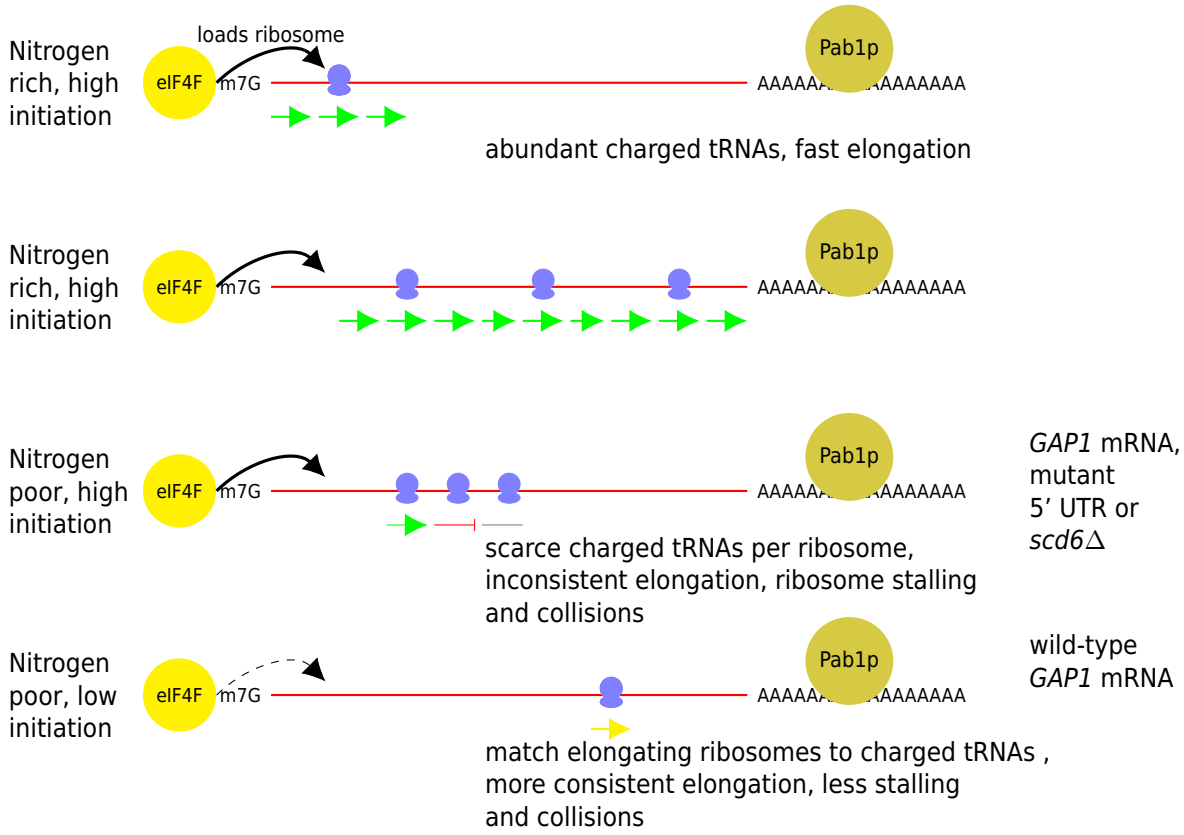

Figure 5.1: **Hypothetical adaptive role for slowed translation under low amino-acid conditions** Low tRNA charging could limit translation elongation rates, and this could result in ribosome collisions that have been proposed to trigger quality control mechanisms. Limiting translation initiation in an elongation-limited regime would prevent such collisions and conserve the tRNA pool to allow engaged ribosomes to finish elongation.

The translation and degradation of mRNA are intimately coupled processes which compete for the same substrate, the mRNA. Very recently, imaging studies have challenged the 5'-3' closed loop model of mRNA (Adivarahan et al. 2017), and demonstrated a strong effect of the translational status of ribosomal loading in separating the 5' and 3' ends of a single mRNA. Degradation is mediated by connections between 3' and 5' ends, with the Lsm1-7p/Pat1p complex strongly promoting the decapping of mRNA requisite for degradation in the main pathway of mRNA degradation. One explanation of the interaction between the degradation and translation initiation machinery has been proposed as the competition for the 5' m7G cap. The interaction of translation initia-

tion factor eIFG2 and decapping modulator Scd6p in affecting the degradation of *GAP1* suggests and interaction with ribosome loading status. One explanation that connects these processes could be that the presence of elongating ribosomes separates the 5' and 3' ends of the mRNA, similar to the cohesin-dependent loop extrusion model currently used by some to explain chromatin-organization (Figure 5.2). This would directly explain the connection between translation status and degradation for individual mRNA as a simple function of 3'-associated decapping factors stochastically interacting with the 5' end of the mRNA tether.

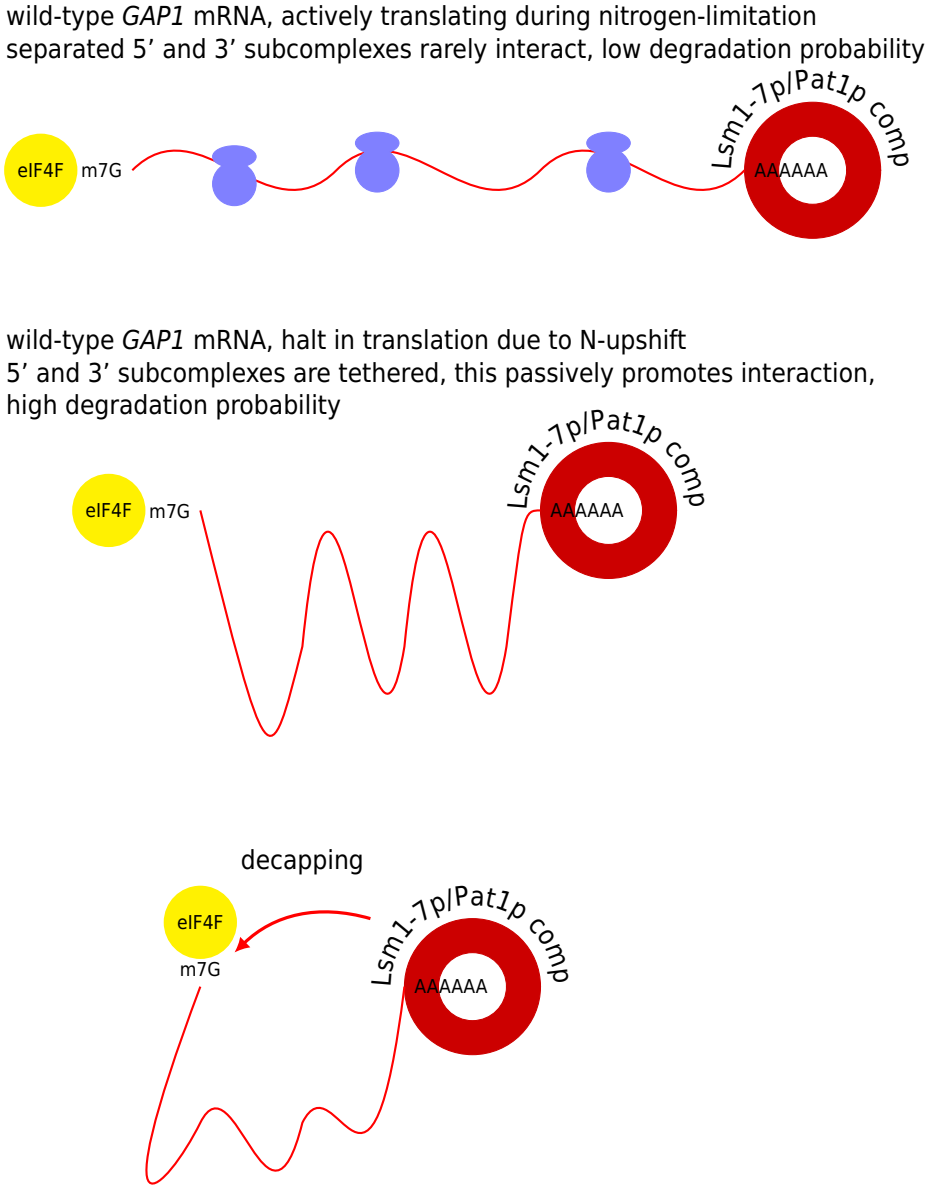

Figure 5.2: **Hypothetical mechanism by which translation initiation and elongation inhibit mRNA degradation — ribosome extrusion.** In the crowded cytoplasm, mRNA are not likely to resemble straight lines. The tethering of the 5’ to the 3’ end by the mRNA molecule would be expected to drive interaction of the two RNP subcomplexes. Some evidence points toward ribosomal elongation as a process by which the two halves are separated, and would be a simple explanation for the observation that inhibiting either elongation or initiation appears to affect mRNA degradation rates, given that the assembly of the decapping complex with the assistance of the 3’ Lsm1-7p/Pat1p complex appears to important for decapping.

References

Adams, CHRISTOPHER C and DAVID S Gross (1991). “The yeast heat shock response is induced by conversion of cells to spheroplasts and by potent transcriptional inhibitors.” In: *Journal of bacteriology* 173.23, pp. 7429–7435 (cit. on p. 24).

Adivarahan, Srivathsan, Samir Rahman, and Daniel Zenklusen (2017). “Spatial organization of single mRNPs at different stages of the gene expression pathway”. In: *bioRxiv*, p. 237008 (cit. on p. 150).

Aghib, DF et al. (1990). “A 3’truncation of MYC caused by chromosomal translocation in a human T-cell leukemia increases mRNA stability.” In: *Oncogene* 5.5, pp. 707–711 (cit. on p. 44).

Airoldi, Edoardo M et al. (2009). “Predicting cellular growth from gene expression signatures”. In: *PLoS Computational Biology* 5.1, e1000257 (cit. on pp. 3, 7, 34, 123).

Airoldi, Edoardo M et al. (2016). “Steady-state and dynamic gene expression programs in Saccharomyces cerevisiae in response to variation in environmental nitrogen”. In: *Molecular biology of the cell* 27.8, pp. 1383–1396 (cit. on pp. 8, 45, 46, 48, 50, 51, 53, 56, 57, 59, 60, 65, 114, 115, 119).

Albig, Allan R and Carolyn J Decker (2001). “The target of rapamycin signaling pathway regulates mRNA turnover in the yeast Saccharomyces cerevisiae”. In: *Molecular biology of the cell* 12.11, pp. 3428–3438 (cit. on pp. 21, 39).

Alonso, Claudio R (2012). “A complex mRNA degradation codecontrols gene expression during animal development”. In: *Trends in Genetics* 28.2, pp. 78–88 (cit. on p. 44).

Amatruda, James F et al. (1990). “Disruption of the actin cytoskeleton in yeast capping protein mutants”. In: *Nature* 344.6264, p. 352 (cit. on p. 137).

Amberg, David C, Alan L Goldstein, and Charles N Cole (1992). “Isolation and characterization of RAT1: an essential gene of Saccharomyces cerevisiae required for the efficient nucleocytoplasmic trafficking of mRNA.” In: *Genes & development* 6.7, pp. 1173–1189 (cit. on pp. 125, 143).

Amberg, David C, Daniel J Burke, and Jeffrey N Strathern (2005). “Methods in Yeast Genetics: A Cold Spring Harbor Laboratory Course Manual, 2005 Edition (Cold Spring)”. In: (cit. on p. 119).

Anders, Simon, Paul Theodor Pyl, and Wolfgang Huber (2015). “HTSeqa Python framework to work with high-throughput sequencing data”. In: *Bioinformatics* 31.2, pp. 166–169 (cit. on p. 69).

Andersen, Kaj Scherz et al. (2014). “Genetic basis for Saccharomyces cerevisiae biofilm in liquid medium”. In: *G3: Genes, Genomes, Genetics* 4.9, pp. 1671–1680 (cit. on p. 125).

Andrade, Raquel P et al. (2005). “Multiple transcripts regulate glucose-triggered mRNA decay of the lactate transporter JEN1 from Saccharomyces cerevisiae”. In: *Biochemical and biophysical research communications* 332.1, pp. 254–262 (cit. on p. 22).

Arribere, Joshua A and Wendy V Gilbert (2013). “Roles for transcript leaders in translation and mRNA decay revealed by transcript leader sequencing”. In: *Genome research* 23.6, pp. 977–987 (cit. on p. 116).

Aviv, Tzvi et al. (2003). “The RNA-binding SAM domain of Smaug defines a new family of post-transcriptional regulators”. In: *Nature Structural and Molecular Biology* 10.8, p. 614 (cit. on pp. 9, 17).

Baumgartner, Bridget L et al. (2011). “Antagonistic gene transcripts regulate adaptation to new growth environments”. In: *Proceedings of the National Academy of Sciences* 108.52, pp. 21087–21092 (cit. on pp. 22, 39, 116).

Beck, Thomas and Michael N Hall (1999). “The TOR signalling pathway controls nuclear localization of nutrient-regulated transcription factors”. In: *Nature* 402.6762, pp. 689–692 (cit. on pp. 5, 33, 46).

Bennett, Matthew R et al. (2008). “Metabolic gene regulation in a dynamically changing environment”. In: *Nature* 454.7208, p. 1119 (cit. on pp. 22, 39).

Boehlke, KW and JD Friesen (1975). “Cellular content of ribonucleic acid and protein in Saccharomyces cerevisiae as a function of exponential growth rate: calculation of the apparent peptide chain elongation rate.” In: *Journal of bacteriology* 121.2, pp. 429–433 (cit. on p. 7).

Boer, Carl de et al. (2017). “Deciphering cis-regulatory logic with 100 million synthetic promoters”. In: *bioRxiv*, p. 224907 (cit. on pp. 29, 145).

Boer, Viktor M et al. (2010). “Growth-limiting intracellular metabolites in yeast growing under diverse nutrient limitations”. In: *Molecular biology of the cell* 21.1, pp. 198–211 (cit. on p. 40).

Boles, Eckhard, Patricia de Jong-Gubbels, and Jack T Pronk (1998). “Identification and Characterization ofMAE1, the Saccharomyces cerevisiae Structural Gene Encoding

Mitochondrial Malic Enzyme". In: *Journal of bacteriology* 180.11, pp. 2875–2882 (cit. on pp. 115, 137).

Brauer, Matthew J et al. (2008). "Coordination of growth rate, cell cycle, stress response, and metabolic activity in yeast". In: *Molecular biology of the cell* 19.1, pp. 352–367 (cit. on pp. 2, 3, 7, 34, 40, 59, 119, 123, 131).

Braun, Katherine A et al. (2014). "Phosphoproteomic analysis identifies proteins involved in transcription-coupled mRNA decay as targets of Snf1 signaling". In: *Sci. Signal.* 7.333, ra64–ra64 (cit. on pp. 22, 47).

Braun, Katherine A, Kenneth M Dombek, and Elton T Young (2016). "Snf1-dependent transcription confers glucose-induced decay upon the mRNA product". In: *Molecular and cellular biology* 36.4, pp. 628–644 (cit. on pp. 18, 47, 146).

Brengues, Muriel and Roy Parker (2007). "Accumulation of polyadenylated mRNA, Pab1p, eIF4E, and eIF4G with P-bodies in Saccharomyces cerevisiae". In: *Molecular biology of the cell* 18.7, pp. 2592–2602 (cit. on p. 148).

Broach, James R (2012). "Nutritional control of growth and development in yeast". In: *Genetics* 192.1, pp. 73–105 (cit. on p. 2).

Burger, Kaspar et al. (2013). "4-thiouridine inhibits rRNA synthesis and causes a nucleolar stress response". In: *RNA biology* 10.10, pp. 1623–1630 (cit. on p. 24).

Canadell, David et al. (2015). "Impact of high pH stress on yeast gene expression: A comprehensive analysis of mRNA turnover during stress responses". In: *Biochimica et Biophysica Acta (BBA)-Gene Regulatory Mechanisms* 1849.6, pp. 653–664 (cit. on pp. 21, 44, 45, 56, 62, 148).

Caponigro, Giordano and Roy Parker (1996). "Mechanisms and control of mRNA turnover in Saccharomyces cerevisiae." In: *Microbiological reviews* 60.1, p. 233 (cit. on pp. 12, 16).

Carter, BLA, A Lorincz, and GC Johnston (1978). "Protein synthesis, cell division and the cell cycle in Saccharomyces cerevisiae following a shift to a richer medium". In: *Microbiology* 106.2, pp. 221–225 (cit. on pp. 2, 123).

Castells-Roca, Laia et al. (2011). "Heat shock response in yeast involves changes in both transcription rates and mRNA stabilities". In: *PloS one* 6.2, e17272 (cit. on pp. 21, 44).

Celik, Alper et al. (2017). "High-resolution profiling of NMD targets in yeast reveals translational fidelity as a basis for substrate selection". In: *RNA* 23.5, pp. 735–748 (cit. on p. 15).

Chan, Leon Y et al. (2017). “Non-invasive measurement of mRNA decay reveals translation initiation as the major determinant of mRNA stability”. In: *bioRxiv*, p. 214775 (cit. on pp. 16, 19, 74, 115).

Chen, Shaoxiong and Linda E Hyman (1998). “A specific RNA-protein interaction at yeast polyadenylation efficiency elements”. In: *Nucleic acids research* 26.21, pp. 4965–4974 (cit. on pp. 9, 62, 77).

Cheng, Jun et al. (2017). “Cis-regulatory elements explain most of the mRNA stability variation across genes in yeast”. In: *RNA*, rna–062224 (cit. on pp. 16, 23).

Cheng, Zhe et al. (2016). “Differential dynamics of the mammalian mRNA and protein expression response to misfolding stress”. In: *Molecular systems biology* 12.1, p. 855 (cit. on p. 27).

Chowdhury, Ashis and Sundaresan Tharun (2009). “Activation of decapping involves binding of the mRNA and facilitation of the post-binding steps by the Lsm1-7–Pat1 complex”. In: *Rna* 15.10, pp. 1837–1848 (cit. on p. 11).

Chowdhury, Ashis, Swathi Kalurupalle, and Sundaresan Tharun (2014). “Pat1 contributes to the RNA binding activity of the Lsm1-7–Pat1 complex”. In: *RNA* 20.9, pp. 1465–1475 (cit. on p. 11).

— (2016). “Mutagenic Analysis of the C-Terminal Extension of Lsm1”. In: *PloS one* 11.7, e0158876 (cit. on p. 11).

Christiano, Romain et al. (2014). “Global proteome turnover analyses of the yeasts S. cerevisiae and S. pombe”. In: *Cell reports* 9.5, pp. 1959–1965 (cit. on p. 7).

Chu, Dominique et al. (2014). “Translation elongation can control translation initiation on eukaryotic mRNAs”. In: *The EMBO journal* 33.1, pp. 21–34 (cit. on p. 17).

Clarkson, Bryan K, Wendy V Gilbert, and Jennifer A Doudna (2010). “Functional overlap between eIF4G isoforms in Saccharomyces cerevisiae”. In: *PLoS One* 5.2, e9114 (cit. on p. 148).

Cock, Peter JA et al. (2009). “Biopython: freely available Python tools for computational molecular biology and bioinformatics”. In: *Bioinformatics* 25.11, pp. 1422–1423 (cit. on p. 105).

Coller, Jeff and Roy Parker (2004). “Eukaryotic mRNA decapping”. In: *Annual review of biochemistry* 73.1, pp. 861–890 (cit. on pp. 11, 12, 23, 46).

Conibear, Elizabeth and Tom H Stevens (2002). “Studying yeast vacuoles”. In: *Methods in enzymology*. Vol. 351. Elsevier, pp. 408–432 (cit. on p. 29).

Conrad, Michaela et al. (2014). “Nutrient sensing and signaling in the yeast Saccharomyces cerevisiae”. In: *FEMS microbiology reviews* 38.2, pp. 254–299 (cit. on p. 2).

Conway, Michael K, Douglas Grunwald, and Warren Heideman (2012). “Glucose, nitrogen, and phosphate repletion in Saccharomyces cerevisiae: common transcriptional responses to different nutrient signals”. In: *G3: Genes, Genomes, Genetics* 2.9, pp. 1003–1017 (cit. on pp. 2, 3, 44).

Cooper, Terrance G (1982). “Nitrogen metabolism in Saccharomyces cerevisiae”. In: *The molecular biology of the yeast Saccharomyces: metabolism and gene expression* 2, pp. 39–99 (cit. on pp. 2, 4, 32, 33).

— (2002). “Transmitting the signal of excess nitrogen in Saccharomyces cerevisiae from the Tor proteins to the GATA factors: connecting the dots”. In: *FEMS microbiology reviews* 26.3, pp. 223–238 (cit. on p. 4).

Cooper, TG and R Ao Sumrada (1983). “What is the function of nitrogen catabolite repression in Saccharomyces cerevisiae?” In: *Journal of bacteriology* 155.2, pp. 623–627 (cit. on pp. 6, 46).

Cox, Kathleen H et al. (2000). “Saccharomyces cerevisiae GATA sequences function as TATA elements during nitrogen catabolite repression and when Gln3p is excluded from the nucleus by overproduction of Ure2p”. In: *Journal of Biological Chemistry* 275.23, pp. 17611–17618 (cit. on p. 5).

Crespo, José L et al. (2002). “The TOR-controlled transcription activators GLN3, RTG1, and RTG3 are regulated in response to intracellular levels of glutamine”. In: *Proceedings of the National Academy of Sciences* 99.10, pp. 6784–6789 (cit. on p. 4).

Cruz, Bernard J de la, Susana Prieto, and Immo E Scheffler (2002). “The role of the 5 untranslated region (UTR) in glucose-dependent mRNA decay”. In: *Yeast* 19.10, pp. 887–902 (cit. on pp. 22, 45, 116).

Csárdi, Gábor et al. (2015). “Accounting for experimental noise reveals that mRNA levels, amplified by post-transcriptional processes, largely determine steady-state protein levels in yeast”. In: *PLoS genetics* 11.5, e1005206 (cit. on p. 27).

Cunningham, Thomas S, Roopa Andhare, and Terrance G Cooper (2000). “Nitrogen Catabolite Repression of DAL80Expression Depends on the Relative Levels of Gat1p and Ure2p Production in Saccharomyces cerevisiae”. In: *Journal of Biological Chemistry* 275.19, pp. 14408–14414 (cit. on p. 5).

Curran, James F and Michael Yarus (1989). “Rates of aminoacyl-tRNA selection at 29 sense codons in vivo”. In: *Journal of molecular biology* 209.1, pp. 65–77 (cit. on p. 15).

Daugherty, JR et al. (1993). “Regulatory circuit for responses of nitrogen catabolic gene expression to the GLN3 and DAL80 proteins and nitrogen catabolite repression in Saccharomyces cerevisiae.” In: *Journal of bacteriology* 175.1, pp. 64–73 (cit. on p. 5).

Decker, Carolyn J and Roy Parker (1993). “A turnover pathway for both stable and unstable mRNAs in yeast: evidence for a requirement for deadenylation.” In: *Genes & development* 7.8, pp. 1632–1643 (cit. on p. 11).

Decker, Carolyn J, Daniela Teixeira, and Roy Parker (2007). “Edc3p and a glutamine/asparagine-rich domain of Lsm4p function in processing body assembly in Saccharomyces cerevisiae”. In: *The Journal of cell biology* 179.3, pp. 437–449 (cit. on p. 13).

Deneke, Carlus, Reinhard Lipowsky, and Angelo Valleriani (2013). “Complex degradation processes lead to non-exponential decay patterns and age-dependent decay rates of messenger RNA”. In: *PloS one* 8.2, e55442 (cit. on p. 25).

Dever, Thomas E et al. (1992). “Phosphorylation of initiation factor 2α by protein kinase GCN2 mediates gene-specific translational control of GCN4 in yeast”. In: *Cell* 68.3, pp. 585–596 (cit. on p. 18).

Dever, Thomas E, Terri Goss Kinzy, and Graham D Pavitt (2016). “Mechanism and regulation of protein synthesis in Saccharomyces cerevisiae”. In: *Genetics* 203.1, pp. 65–107 (cit. on pp. 2, 11, 12, 18).

Dixit, Atray et al. (2016). “Perturb-Seq: dissecting molecular circuits with scalable single-cell RNA profiling of pooled genetic screens”. In: *Cell* 167.7, pp. 1853–1866 (cit. on p. 145).

Dölken, Lars et al. (2008). “High-resolution gene expression profiling for simultaneous kinetic parameter analysis of RNA synthesis and decay”. In: *Rna* 14.9, pp. 1959–1972 (cit. on p. 24).

Doma, Meenakshi K and Roy Parker (2006). “Endonucleolytic cleavage of eukaryotic mRNAs with stalls in translation elongation”. In: *Nature* 440.7083, p. 561 (cit. on p. 14).

Donaton, Monica CV et al. (2003). “The Gap1 general amino acid permease acts as an amino acid sensor for activation of protein kinase A targets in the yeast Saccharomyces cerevisiae”. In: *Molecular microbiology* 50.3, pp. 911–929 (cit. on p. 6).

Duffy, Erin E et al. (2015). “Tracking distinct RNA populations using efficient and reversible covalent chemistry”. In: *Molecular cell* 59.5, pp. 858–866 (cit. on p. 115).

Elemento, Olivier, Noam Slonim, and Saeed Tavazoie (2007). “A universal framework for regulatory element discovery across all genomes and data types”. In: *Molecular cell* 28.2, pp. 337–350 (cit. on p. 77).

Elliott, Beth and Bruce Futcher (1993). “Stress resistance of yeast cells is largely independent of cell cycle phase”. In: *Yeast* 9.1, pp. 33–42 (cit. on pp. 2, 131).

Erickson, David W et al. (2017). “A global resource allocation strategy governs growth transition kinetics of Escherichia coli”. In: *Nature* 551.7678, p. 119 (cit. on pp. 8, 123).

Fayyad-Kazan, Mohammad et al. (2016). “Yeast nitrogen catabolite repression is sustained by signals distinct from glutamine and glutamate reservoirs”. In: *Molecular microbiology* 99.2, pp. 360–379 (cit. on pp. 4, 146).

Fei, Li et al. (2015). “Structural and Biochemical Studies of a Moderately Thermophilic Exonuclease I from Methylocaldum szegediense”. In: *PloS one* 10.2, e0117470 (cit. on pp. 100, 101).

Franks, Alexander, Edoardo Airoldi, and Nikolai Slavov (2017). “Post-transcriptional regulation across human tissues”. In: *PLoS computational biology* 13.5, e1005535 (cit. on p. 27).

Freeberg, Mallory A et al. (2013). “Pervasive and dynamic protein binding sites of the mRNA transcriptome in Saccharomyces cerevisiae”. In: *Genome biology* 14.2, R13 (cit. on p. 77).

Fu, Glenn K et al. (2011). “Counting individual DNA molecules by the stochastic attachment of diverse labels”. In: *Proceedings of the National Academy of Sciences* 108.22, pp. 9026–9031 (cit. on pp. 82, 100, 106, 108).

Gapp, Bianca V et al. (2016). “Parallel reverse genetic screening in mutant human cells using transcriptomics”. In: *Molecular Systems Biology* 12.8, p. 879 (cit. on p. 28).

Garcıa-Martınez, José, Agustın Aranda, and José E Pérez-Ortın (2004). “Genomic run-on evaluates transcription rates for all yeast genes and identifies gene regulatory mechanisms”. In: *Molecular cell* 15.2, pp. 303–313 (cit. on p. 24).

García-Martínez, José et al. (2016). “Growth rate controls mRNA turnover in steady and non-steady states”. In: *RNA biology* 13.12, pp. 1175–1181 (cit. on pp. 21, 44).

Gari, Eloi et al. (1997). “A set of vectors with a tetracycline-regulatable promoter system for modulated gene expression in Saccharomyces cerevisiae”. In: *Yeast* 13.9, pp. 837–848 (cit. on p. 23).

Garre, Elena et al. (2013). “Nonsense-mediated mRNA decay controls the changes in yeast ribosomal protein pre-mRNAs levels upon osmotic stress”. In: *PLoS One* 8.4, e61240 (cit. on pp. 15, 21).

Gasch, Audrey P et al. (2000). “Genomic expression programs in the response of yeast cells to environmental changes”. In: *Molecular biology of the cell* 11.12, pp. 4241–4257 (cit. on pp. 3, 44, 56, 59, 62, 123).

Gasch, Audrey P et al. (2017). “Single-cell RNA-seq reveals intrinsic and extrinsic regulatory heterogeneity in yeast responding to stress”. In: *bioRxiv*, p. 179093 (cit. on p. 145).

Georis, Isabelle et al. (2008). “Tor pathway control of the nitrogen-responsive DAL5 gene bifurcates at the level of Gln3 and Gat1 regulation in Saccharomyces cerevisiae”. In: *Journal of Biological Chemistry* 283.14, pp. 8919–8929 (cit. on p. 6).

Giaever, Guri and Corey Nislow (2014). “The yeast deletion collection: a decade of functional genomics”. In: *Genetics* 197.2, pp. 451–465 (cit. on p. 78).

Gibney, Patrick A et al. (2013). “Yeast metabolic and signaling genes are required for heat-shock survival and have little overlap with the heat-induced genes”. In: *Proceedings of the National Academy of Sciences* 110.46, E4393–E4402 (cit. on p. 132).

Gilbert, Wendy V et al. (2007). “Cap-independent translation is required for starvation-induced differentiation in yeast”. In: *science* 317.5842, pp. 1224–1227 (cit. on p. 11).

Gilbert, Wendy V, Tristan A Bell, and Cassandra Schaening (2016). “Messenger RNA modifications: Form, distribution, and function”. In: *Science* 352.6292, pp. 1408–1412 (cit. on p. 18).

Giordano, Nils et al. (2016). “Dynamical allocation of cellular resources as an optimal control problem: novel insights into microbial growth strategies”. In: *PLoS computational biology* 12.3, e1004802 (cit. on pp. 8, 45).

Godard, Patrice et al. (2007). “Effect of 21 different nitrogen sources on global gene expression in the yeast Saccharomyces cerevisiae”. In: *Molecular and cellular biology* 27.8, pp. 3065–3086 (cit. on pp. 33, 37, 45, 115).

González, Carlos I et al. (2000). “The yeast hnRNP-like protein Hrp1/Nab4 marks a transcript for nonsense-mediated mRNA decay”. In: *Molecular cell* 5.3, pp. 489–499 (cit. on p. 116).

Goodarzi, Hani et al. (2012). “Systematic discovery of structural elements governing stability of mammalian messenger RNAs”. In: *Nature* 485.7397, pp. 264–268 (cit. on pp. 9, 77).

Gould, Stephen Jay and Richard C Lewontin (1979). “The spandrels of San Marco and the Panglossian paradigm: a critique of the adaptationist programme”. In: *Proc. R. Soc. Lond. B*. Vol. 205. 1161. The Royal Society, pp. 581–598 (cit. on pp. 7, 20, 132).

Gray, Jesse M et al. (2014). “SnapShot-Seq: a method for extracting genome-wide, in vivo mRNA dynamics from a single total RNA sample”. In: *PloS one* 9.2, e89673 (cit. on p. 23).

Grenson, Marcelle (1983). “Inactivation-Reactivation Process and Repression of Permease Formation Regulate Several Ammonia-Sensitive Permeases in the Yeast Saccharomyces cerevisiae”. In: *The FEBS Journal* 133.1, pp. 135–139 (cit. on pp. 4, 6).

— (1992). “Amino acid transporters in yeast: structure, function and regulation”. In: *New Comprehensive Biochemistry*. Vol. 21. Elsevier, pp. 219–245 (cit. on pp. 4, 147).

Griffioen, Gerard et al. (1996). “Ribosomal protein gene transcription in Saccharomyces cerevisiae shows a biphasic response to nutritional changes”. In: *Microbiology* 142.8, pp. 2279–2287 (cit. on pp. 7, 8).

Guisbert, Karen Kim et al. (2005). “Functional specificity of shuttling hnRNPs revealed by genome-wide analysis of their RNA binding profiles”. In: *Rna* 11.4, pp. 383–393 (cit. on pp. 62, 77, 116).

Gupta, Ishaan et al. (2016). “Translational capacity of a cell is determined during transcription elongation via the Ccr4-Not complex”. In: *Cell reports* 15.8, pp. 1782–1794 (cit. on p. 18).

Haar, Tobias von der (2008). “A quantitative estimation of the global translational activity in logarithmically growing yeast cells”. In: *BMC systems biology* 2.1, p. 87 (cit. on p. 7).

Hahn, Steven and Elton T Young (2011). “Transcriptional regulation in Saccharomyces cerevisiae: transcription factor regulation and function, mechanisms of initiation, and roles of activators and coactivators”. In: *Genetics* 189.3, pp. 705–736 (cit. on pp. 1, 5).

Haimovich, Gal et al. (2013). “Gene expression is circular: factors for mRNA degradation also foster mRNA synthesis”. In: *Cell* 153.5, pp. 1000–1011 (cit. on pp. 17, 47).

Hanley, Mary Beth et al. (2013). “Detection of low abundance RNA molecules in individual cells by flow cytometry”. In: *PloS one* 8.2, e57002 (cit. on pp. 29, 79, 117).

Hargrove, James L and Frederick H Schmidt (1989). “The role of mRNA and protein stability in gene expression.” In: *The FASEB Journal* 3.12, pp. 2360–2370 (cit. on pp. 20, 44).

Harigaya, Yuriko and Roy Parker (2016). “Codon optimality and mRNA decay”. In: *Cell research* 26.12, p. 1269 (cit. on p. 16).

Hartwell, Leland H, Joseph Culotti, and Brian Reid (1970). “Genetic control of the cell-division cycle in yeast, I. Detection of mutants”. In: *Proceedings of the National Academy of Sciences* 66.2, pp. 352–359 (cit. on p. 28).

Hein, Claudine and Bruno André (1997). “A C-terminal di-leucine motif and nearby sequences are required for NH4+-induced inactivation and degradation of the general amino acid permease, Gap1p, of Saccharomyces cerevisiae”. In: *Molecular microbiology* 24.3, pp. 607–616 (cit. on p. 29).

Hein, Claudine et al. (1995). “NPI1, an essential yeast gene involved in induced degradation of Gap1 and Fur4 permeases, encodes the Rsp5 ubiquitinprotein ligase”. In: *Molecular microbiology* 18.1, pp. 77–87 (cit. on p. 53).

Henrici, AT (1928). “Morphologic Variation and the Rate of Growth of Bacteria”. In: (cit. on p. 123).

Hess, David C et al. (2006). “Ammonium toxicity and potassium limitation in yeast”. In: *PLoS biology* 4.11, e351 (cit. on p. 6).

Hill, Andrew J et al. (2018). “On the design of CRISPR-based single cell molecular screens”. In: *bioRxiv*, p. 254334 (cit. on p. 145).

Holtzman, Douglas A, Shirley Yang, and David G Drubin (1993). “Synthetic-lethal interactions identify two novel genes, SLA1 and SLA2, that control membrane cytoskeleton assembly in Saccharomyces cerevisiae”. In: *The Journal of cell biology* 122.3, pp. 635–644 (cit. on p. 137).

Hong, Jungeui and David Gresham (2017). “METHOD SUMMARY TrUMIseq adapters incorporate unique molecular identifiers (UMIs) in TruSeq adapters while maintaining the capacity to multiplex sequencing libraries using existing single-index workflows. The use of UMIs increases the accuracy of quantitative sequencing assays, including allele frequency (AF) estimation and RNA-Seq, by enabling accurate detection of PCR duplicates.” In: *BioTechniques* 63.5, pp. 221–226 (cit. on p. 67).

Hoyle, Nathaniel P et al. (2007). “Stress-dependent relocalization of translationally primed mRNPs to cytoplasmic granules that are kinetically and spatially distinct from P-bodies”. In: *J Cell Biol* 179.1, pp. 65–74 (cit. on p. 91).

Huch, Susanne and Tracy Nissan (2014). “Interrelations between translation and general mRNA degradation in yeast”. In: *Wiley Interdisciplinary Reviews: RNA* 5.6, pp. 747–763 (cit. on p. 12).

— (2017). “An mRNA decapping mutant deficient in P body assembly limits mRNA stabilization in response to osmotic stress”. In: *Scientific reports* 7, p. 44395 (cit. on pp. 13, 19, 62, 147).

Huch, Susanne et al. (2016). “The decapping activator Edc3 and the Q/N-rich domain of Lsm4 function together to enhance mRNA stability and alter mRNA decay pathway dependence in Saccharomyces cerevisiae”. In: *Biology open* 5.10, pp. 1388–1399 (cit. on pp. 13, 24).

Hueso, Guillem et al. (2012). “A novel role for protein kinase Gcn2 in yeast tolerance to intracellular acid stress”. In: *Biochemical Journal* 441.1, pp. 255–264 (cit. on p. 147).

Huggins, Peter et al. (2011). “DECOD: fast and accurate discriminative DNA motif finding”. In: *Bioinformatics* 27.17, pp. 2361–2367 (cit. on p. 77).

Ikeuchi, Ken and Toshifumi Inada (2016). “Ribosome-associated Asc1/RACK1 is required for endonucleolytic cleavage induced by stalled ribosome at the 3 end of nonstop mRNA”. In: *Scientific reports* 6, p. 28234 (cit. on p. 15).

Jiang, Lichun et al. (2011). “Synthetic spike-in standards for RNA-seq experiments”. In: *Genome research* 21.9, pp. 1543–1551 (cit. on p. 124).

Jona, Ghil, Mordechai Choder, and Opher Gileadi (2000). “Glucose starvation induces a drastic reduction in the rates of both transcription and degradation of mRNA in yeast”. In: *Biochimica et Biophysica Acta (BBA)-Gene Structure and Expression* 1491.1-3, pp. 37–48 (cit. on p. 21).

Jorgensen, Paul et al. (2004). “A dynamic transcriptional network communicates growth potential to ribosome synthesis and critical cell size”. In: *Genes & development* 18.20, pp. 2491–2505 (cit. on pp. 2, 7).

Kafri, Moshe et al. (2016). “The cost of protein production”. In: *Cell reports* 14.1, pp. 22–31 (cit. on pp. 8, 123, 149).

Kebaara, B et al. (2003). “The Upf-dependent decay of wild-type PPR1 mRNA depends on its 5-UTR and first 92 ORF nucleotides”. In: *Nucleic acids research* 31.12, pp. 3157–3165 (cit. on pp. 15, 62, 116).

Kessler, Marco M et al. (1997). “Hrp1, a sequence-specific RNA-binding protein that shuttles between the nucleus and the cytoplasm, is required for mRNA 3-end formation in yeast”. In: *Genes & development* 11.19, pp. 2545–2556 (cit. on p. 62).

Khong, Anthony et al. (2017). “The Stress Granule Transcriptome Reveals Principles of mRNA Accumulation in Stress Granules”. In: *Molecular cell* 68.4, pp. 808–820 (cit. on pp. 62, 64).

Kief, DONNA RUSSO and JR Warner (1981). “Coordinate control of syntheses of ribosomal ribonucleic acid and ribosomal proteins during nutritional shift-up in Saccharomyces cerevisiae.” In: *Molecular and cellular biology* 1.11, pp. 1007–1015 (cit. on pp. 2, 7, 8, 39, 45, 123).

Kim, Daehwan et al. (2013). “TopHat2: accurate alignment of transcriptomes in the presence of insertions, deletions and gene fusions”. In: *Genome biology* 14.4, R36 (cit. on p. 68).

Kinney, Justin B et al. (2010). “Using deep sequencing to characterize the biophysical mechanism of a transcriptional regulatory sequence”. In: *Proceedings of the National Academy of Sciences* 107.20, pp. 9158–9163 (cit. on pp. 29, 78).

Kjeldgaard, NO, O Maaløe, and Moselio Schaechter (1958). “The transition between different physiological states during balanced growth of Salmonella typhimurium”. In: *Microbiology* 19.3, pp. 607–616 (cit. on pp. 4, 123).

Klemm, Sandy et al. (2014). “Transcriptional profiling of cells sorted by RNA abundance”. In: *nature methods* 11.5, p. 549 (cit. on pp. 79, 98, 117).

Kresnowati, MTAP et al. (2006). “When transcriptome meets metabolome: fast cellular responses of yeast to sudden relief of glucose limitation”. In: *Molecular Systems Biology* 2.1, p. 49 (cit. on pp. 8, 39, 45).

Kresnowati, MTAP et al. (2008). “Quantitative physiological study of the fast dynamics in the intracellular pH of Saccharomyces cerevisiae in response to glucose and ethanol pulses”. In: *Metabolic engineering* 10.1, pp. 39–54 (cit. on p. 147).

Kussell, Edo and Stanislas Leibler (2005). “Phenotypic diversity, population growth, and information in fluctuating environments”. In: *Science* 309.5743, pp. 2075–2078 (cit. on p. 1).

Kwan, Elizabeth X et al. (2016). “rDNA Copy number variants are frequent passenger mutations in Saccharomyces cerevisiae deletion collections and de novo transformants”. In: *G3: Genes, Genomes, Genetics* 6.9, pp. 2829–2838 (cit. on p. 144).

Lawrence, Michael et al. (2013). “Software for computing and annotating genomic ranges”. In: *PLoS computational biology* 9.8, e1003118 (cit. on p. 63).

Lazebnik, Yuri (2002). “Can a biologist fix a radio?Or, what I learned while studying apoptosis”. In: *Cancer cell* 2.3, pp. 179–182 (cit. on p. 145).

Lee, Chien-Der and Benjamin P Tu (2015). “Glucose-regulated phosphorylation of the PUF protein Puf3 regulates the translational fate of its bound mRNAs and association with RNA granules”. In: *Cell reports* 11.10, pp. 1638–1650 (cit. on pp. 17, 46).

Lee, M Violet et al. (2011). “A dynamic model of proteome changes reveals new roles for transcript alteration in yeast”. In: *Molecular systems biology* 7.1, p. 514 (cit. on pp. 7, 27, 39, 45).

Li, Heng (2013). “Aligning sequence reads, clone sequences and assembly contigs with BWA-MEM”. In: *arXiv preprint arXiv:1303.3997* (cit. on p. 105).

Li, Heng et al. (2009). “The sequence alignment/map format and SAMtools”. In: *Bioinformatics* 25.16, pp. 2078–2079 (cit. on p. 69).

Li, Xiao et al. (2010). “Predicting in vivo binding sites of RNA-binding proteins using mRNA secondary structure”. In: *Rna* 16.6, pp. 1096–1107 (cit. on pp. 9, 17, 77).

Lombardo, ANGELA, GP Cereghino, and IMMO E Scheffler (1992). “Control of mRNA turnover as a mechanism of glucose repression in Saccharomyces cerevisiae.” In: *Molecular and cellular biology* 12.7, pp. 2941–2948 (cit. on p. 22).

Losson, Regine and Francois Lacroute (1979). “Interference of nonsense mutations with eukaryotic messenger RNA stability”. In: *Proceedings of the National Academy of Sciences* 76.10, pp. 5134–5137 (cit. on p. 14).

Love, Michael I, Wolfgang Huber, and Simon Anders (2014). “Moderated estimation of fold change and dispersion for RNA-seq data with DESeq2”. In: *Genome biology* 15.12, p. 550 (cit. on p. 124).

Lu, Charles, Matthew J Brauer, and David Botstein (2009). “Slow growth induces heat-shock resistance in normal and respiratory-deficient yeast”. In: *Molecular biology of the cell* 20.3, pp. 891–903 (cit. on p. 131).

Lui, Jennifer et al. (2014). “Granules harboring translationally active mRNAs provide a platform for P-body formation following stress”. In: *Cell reports* 9.3, pp. 944–954 (cit. on pp. 13, 19).

Luo, Guangzuo et al. (2011). “Nutrients and the Pkh1/2 and Pkc1 protein kinases control mRNA decay and P-body assembly in yeast”. In: *Journal of Biological Chemistry* 286.11, pp. 8759–8770 (cit. on p. 47).

Magasanik, Boris and Chris A Kaiser (2002). “Nitrogen regulation in Saccharomycescerevisiae”. In: *Gene* 290.1, pp. 1–18 (cit. on pp. 4, 5, 32, 33, 45, 147).

Markowitz, Tovah E et al. (2017). “Reduced dosage of the chromosome axis factor Red1 selectively disrupts the meiotic recombination checkpoint in Saccharomyces cerevisiae”. In: *PLoS genetics* 13.7, e1006928 (cit. on p. 144).

Martin, Marcel (2011). “Cutadapt removes adapter sequences from high-throughput sequencing reads”. In: *EMBnet. journal* 17.1, pp–10 (cit. on p. 68).

McLeay, Robert C and Timothy L Bailey (2010). “Motif Enrichment Analysis: a unified framework and an evaluation on ChIP data”. In: *BMC bioinformatics* 11.1, p. 165 (cit. on p. 77).

McManus, Joel, Zhe Cheng, and Christine Vogel (2015). “Next-generation analysis of gene expression regulation–comparing the roles of synthesis and degradation”. In: *Molecular BioSystems* 11.10, pp. 2680–2689 (cit. on p. 2).

Mercado, Juan J et al. (1994). “The levels of yeast gluconeogenic mRNAs respond to environmental factors”. In: *The FEBS Journal* 224.2, pp. 473–481 (cit. on pp. 22, 24, 45, 47).

Merhi, Ahmad and Bruno André (2012). “Internal amino acids promote Gap1 permease ubiquitylation via TORC1/Npr1/14-3-3-dependent control of the Bul arrestin-like adaptors”. In: *Molecular and cellular biology* 32.22, pp. 4510–4522 (cit. on pp. 6, 46).

Metzl-Raz, Eyal et al. (2017). “Principles of cellular resource allocation revealed by condition-dependent proteome profiling”. In: *Elife* 6 (cit. on pp. 8, 123, 149).

Miller, Christian et al. (2011). “Dynamic transcriptome analysis measures rates of mRNA synthesis and decay in yeast”. In: *Molecular systems biology* 7.1, p. 458 (cit. on pp. 21, 26, 54, 114).

Miller, Melanie A et al. (2013). “Carbon source-dependent alteration of Puf3p activity mediates rapid changes in the stabilities of mRNAs involved in mitochondrial function”. In: *Nucleic acids research* 42.6, pp. 3954–3970 (cit. on p. 17).

Molin, Claes et al. (2009). “mRNA stability changes precede changes in steady-state mRNA amounts during hyperosmotic stress”. In: *Rna* 15.4, pp. 600–614 (cit. on p. 21).

Molina-Navarro, María Micaela et al. (2008). “Comprehensive transcriptional analysis of the oxidative response in yeast”. In: *Journal of Biological Chemistry* 283.26, pp. 17908–17918 (cit. on pp. 21, 45).

Mota, Sandra et al. (2014). “Role of the DHH1 gene in the regulation of monocarboxylic acids transporters expression in Saccharomyces cerevisiae”. In: *PloS one* 9.11, e111589 (cit. on p. 22).

Muhlrad, Denise and Roy Parker (1994). “Premature translational termination triggers mRNA decapping”. In: *Nature* 370.6490, p. 578 (cit. on p. 14).

Munchel, Sarah E et al. (2011). “Dynamic profiling of mRNA turnover reveals gene-specific and system-wide regulation of mRNA decay”. In: *Molecular biology of the cell* 22.15, pp. 2787–2795 (cit. on pp. 21, 26, 39, 53, 54, 114).

Neklesa, Taavi K and Ronald W Davis (2009). “A genome-wide screen for regulators of TORC1 in response to amino acid starvation reveals a conserved Npr2/3 complex”. In: *PLoS genetics* 5.6, e1000515 (cit. on pp. 28, 78).

Neymotin, Benjamin, Rodoniki Athanasiadou, and David Gresham (2014). “Determination of in vivo RNA kinetics using RATE-seq”. In: *Rna* 20.10, pp. 1645–1652 (cit. on pp. 16, 26, 37, 42, 53, 54, 65, 72, 114).

Neymotin, Benjamin, Victoria Ettorre, and David Gresham (2016). “Multiple transcript properties related to translation affect mRNA degradation rates in Saccharomyces cerevisiae”. In: *G3: Genes, Genomes, Genetics* 6.11, pp. 3475–3483 (cit. on pp. 16, 23, 116, 117).

Nie, Zuqin et al. (2012). “c-Myc is a universal amplifier of expressed genes in lymphocytes and embryonic stem cells”. In: *Cell* 151.1, pp. 68–79 (cit. on pp. 124, 144).

Nissan, Tracy et al. (2010). “Decapping activators in Saccharomyces cerevisiae act by multiple mechanisms”. In: *Molecular cell* 39.5, pp. 773–783 (cit. on pp. 12, 13, 46).

O’Duibhir, Eoghan et al. (2014). “Cell cycle population effects in perturbation studies”. In: *Molecular systems biology* 10.6, p. 732 (cit. on p. 123).

Oikonomou, Panos, Hani Goodarzi, and Saeed Tavazoie (2014). “Systematic identification of regulatory elements in conserved 3 UTRs of human transcripts”. In: *Cell reports* 7.1, pp. 281–292 (cit. on p. 29).

Olivas, Wendy and Roy Parker (2000). “The Puf3 protein is a transcript-specific regulator of mRNA degradation in yeast”. In: *The EMBO journal* 19.23, pp. 6602–6611 (cit. on pp. 17, 46).

Oliveira, Ana Paula et al. (2015a). “Dynamic phosphoproteomics reveals TORC1-dependent regulation of yeast nucleotide and amino acid biosynthesis”. In: *Sci. Signal.* 8.374, rs4–rs4 (cit. on p. 2).

Oliveira, Ana Paula et al. (2015b). “Inferring causal metabolic signals that regulate the dynamic TORC1-dependent transcriptome”. In: *Molecular systems biology* 11.4, p. 802 (cit. on p. 2).

Orij, Rick, Stanley Brul, and Gertien J Smits (2011). “Intracellular pH is a tightly controlled signal in yeast”. In: *Biochimica et Biophysica Acta (BBA)-General Subjects* 1810.10, pp. 933–944 (cit. on pp. 146, 147).

Parker, Roy (2012). “RNA degradation in Saccharomyces cerevisae”. In: *Genetics* 191.3, pp. 671–702 (cit. on pp. 11, 14, 23, 46).

Pelechano, Vicent and José E Pérez-Ortín (2008). “The transcriptional inhibitor thiolutin blocks mRNA degradation in yeast”. In: *Yeast* 25.2, pp. 85–92 (cit. on p. 24).

Pelechano, Vicent, Sebastián Chávez, and José E Pérez-Ortín (2010). “A complete set of nascent transcription rates for yeast genes”. In: *PloS one* 5.11, e15442 (cit. on p. 24).

Pelechano, Vicent et al. (2014). “Genome-wide identification of transcript start and end sites by transcript isoform sequencing”. In: *Nature protocols* 9.7, p. 1740 (cit. on pp. 63, 77).

Péli-Gulli, Marie-Pierre et al. (2015). “Amino acids stimulate TORC1 through Lst4-Lst7, a GTPase-activating protein complex for the Rag family GTPase Gtr2”. In: *Cell reports* 13.1, pp. 1–7 (cit. on p. 2).

Pérez-Ortín, José E et al. (2013). “Eukaryotic mRNA decay: methodologies, pathways, and links to other stages of gene expression”. In: *Journal of molecular biology* 425.20, pp. 3750–3775 (cit. on pp. 2, 21, 23, 44, 73, 74, 115, 148).

Peterman, Neil and Erel Levine (2016). “Sort-seq under the hood: implications of design choices on large-scale characterization of sequence-function relations”. In: *BMC genomics* 17.1, p. 206 (cit. on pp. 29, 78).

Petersen, NS, CS McLaughlin, and DP Nierlich (1976). “Half life of yeast messenger RNA”. In: *Nature* 260.5546, p. 70 (cit. on pp. 23, 69).

Pierrat, Benoit, François Lacroute, and Régine Losson (1993). “The 5 untranslated region of the PPR1 regulatory gene dictates rapid mRNA decay in yeast”. In: *Gene* 131.1, pp. 43–51 (cit. on p. 15).

Poornima, Gopalakrishna et al. (2016). “Arginine methylation promotes translation repression activity of eIF4G-binding protein, Scd6”. In: *Nucleic acids research* 44.19, pp. 9358–9368 (cit. on p. 13).

Powers, Ted and Peter Walter (1999). “Regulation of ribosome biogenesis by the rapamycin-sensitive TOR-signaling pathway in Saccharomyces cerevisiae”. In: *Molecular biology of the cell* 10.4, pp. 987–1000 (cit. on p. 7).

Presnyak, Vladimir et al. (2015). “Codon optimality is a major determinant of mRNA stability”. In: *Cell* 160.6, pp. 1111–1124 (cit. on pp. 12, 16, 64).

Pringle, John R et al. (1991). “[40] Immunofluorescence methods for yeast”. In: *Methods in enzymology*. Vol. 194. Elsevier, pp. 565–602 (cit. on p. 96).

Puig, Sergi, Eric Askeland, and Dennis J Thiele (2005). “Coordinated remodeling of cellular metabolism during iron deficiency through targeted mRNA degradation”. In: *Cell* 120.1, pp. 99–110 (cit. on pp. 39, 114).

Rabani, Michal et al. (2011). “Metabolic labeling of RNA uncovers principles of RNA production and degradation dynamics in mammalian cells”. In: *Nature biotechnology* 29.5, p. 436 (cit. on p. 21).

Radhakrishnan, Aditya et al. (2016). “The DEAD-box protein Dhh1p couples mRNA decay and translation by monitoring codon optimality”. In: *Cell* 167.1, pp. 122–132 (cit. on pp. 12, 16).

Raj, Arjun et al. (2008). “Imaging individual mRNA molecules using multiple singly labeled probes”. In: *Nature methods* 5.10, p. 877 (cit. on p. 79).

Rajyaguru, Purusharth, Meipei She, and Roy Parker (2012). “Scd6 targets eIF4G to repress translation: RGG motif proteins as a class of eIF4G-binding proteins”. In: *Molecular cell* 45.2, pp. 244–254 (cit. on pp. 13, 92).

Ramachandran, Vidhya, Khyati H Shah, and Paul K Herman (2011). “The cAMP-dependent protein kinase signaling pathway is a key regulator of P body foci formation”. In: *Molecular cell* 43.6, pp. 973–981 (cit. on p. 47).

Rao, Bhalchandra S and Roy Parker (2017). “Numerous interactions act redundantly to assemble a tunable size of P bodies in Saccharomyces cerevisiae”. In: *Proceedings of the National Academy of Sciences*, p. 201712396 (cit. on pp. 13, 19, 147).

Ray, Debashish et al. (2013). “A compendium of RNA-binding motifs for decoding gene regulation”. In: *Nature* 499.7457, p. 172 (cit. on p. 77).

Regenberg, Birgitte et al. (2006). “Growth-rate regulated genes have profound impact on interpretation of transcriptome profiling in Saccharomyces cerevisiae”. In: *Genome biology* 7.11, R107 (cit. on p. 3).

Reis, Mario dos, Renos Savva, and Lorenz Wernisch (2004). “Solving the riddle of codon usage preferences: a test for translational selection”. In: *Nucleic acids research* 32.17, pp. 5036–5044 (cit. on p. 16).

Riback, Joshua A et al. (2017). “Stress-triggered phase separation is an adaptive, evolutionarily tuned response”. In: *Cell* 168.6, pp. 1028–1040 (cit. on p. 147).

Risinger, April L and Chris A Kaiser (2008). “Different ubiquitin signals act at the Golgi and plasma membrane to direct GAP1 trafficking”. In: *Molecular biology of the cell* 19.7, pp. 2962–2972 (cit. on p. 6).

Risinger, April L et al. (2006). “Activity-dependent reversible inactivation of the general amino acid permease”. In: *Molecular biology of the cell* 17.10, pp. 4411–4419 (cit. on pp. 6, 46, 117, 147).

Risso, Davide et al. (2014). “Normalization of RNA-seq data using factor analysis of control genes or samples”. In: *Nature biotechnology* 32.9, p. 896 (cit. on p. 124).

Robinson, David G et al. (2014). “Design and analysis of Bar-seq experiments”. In: *G3: Genes, Genomes, Genetics* 4.1, pp. 11–18 (cit. on pp. 78, 82, 134).

Romero-Santacreu, Lorena et al. (2009). “Specific and global regulation of mRNA stability during osmotic stress in Saccharomyces cerevisiae”. In: *Rna* 15.6, pp. 1110–1120 (cit. on pp. 21, 45).

Rouhanifard, Sara H et al. (2017). “Single-molecule fluorescent amplification of RNA using clampFISH probes”. In: *bioRxiv*, p. 222794 (cit. on p. 117).

Ruano, Gualberto, Wayne Fenton, and Kenneth K Kidd (1989). “Biphasic amplification of very dilute DNA samples via’booster’PCR.” In: *Nucleic Acids Research* 17.13, p. 5407 (cit. on p. 101).

Ruiz-Echevarria, Maria J and Stuart W Peltz (1996). “Utilizing the GCN4 leader region to investigate the role of the sequence determinants in nonsense-mediated mRNA decay.” In: *The EMBO journal* 15.11, pp. 2810–2819 (cit. on p. 18).

Saito, Kazuki, Wataru Horikawa, and Koichi Ito (2015). “Inhibiting K63 polyubiquitination abolishes no-go type stalled translation surveillance in Saccharomyces cerevisiae”. In: *PLoS genetics* 11.4, e1005197 (cit. on p. 15).

Saliba, Elie et al. (2018). “The yeast H+-ATPase Pma1 promotes Rag/Gtr-dependent TORC1 activation in response to H+-coupled nutrient uptake”. In: *eLife* 7, e31981 (cit. on p. 147).

Schaechter, Moselio, Ole Maaløe, and Niels O Kjeldgaard (1958). “Dependency on medium and temperature of cell size and chemical composition during balanced growth of Salmonella typhimurium”. In: *Microbiology* 19.3, pp. 592–606 (cit. on p. 123).

Scheffler, Immo E, J Bernard, and Susana Prieto (1998). “Control of mRNA turnover as a mechanism of glucose repression in Saccharomyces cerevisiae”. In: *The international journal of biochemistry & cell biology* 30.11, pp. 1175–1193 (cit. on pp. 22, 44, 114).

Scherens, Bart et al. (2006). “Identification of direct and indirect targets of the Gln3 and Gat1 activators by transcriptional profiling in response to nitrogen availability in the short and long term”. In: *FEMS yeast research* 6.5, pp. 777–791 (cit. on pp. 5, 87).

Schmid, Manfred and Torben Heick Jensen (2008). “The exosome: a multipurpose RNA-decay machine”. In: *Trends in biochemical sciences* 33.10, pp. 501–510 (cit. on p. 14).

Schure, Eelko G ter et al. (1998). “Repression of nitrogen catabolic genes by ammonia and glutamine in nitrogen-limited continuous cultures of Saccharomyces cerevisiae”. In: *Microbiology* 144.5, pp. 1451–1462 (cit. on pp. 4, 39).

Schwartz, David C and Roy Parker (1999). “Mutations in Translation Initiation Factors Lead to Increased Rates of Deadenylation and Decapping of mRNAs inSaccharomyces cerevisiae”. In: *Molecular and cellular biology* 19.8, pp. 5247–5256 (cit. on p. 16).

— (2000). “mRNA decapping in yeast requires dissociation of the cap binding protein, eukaryotic translation initiation factor 4E”. In: *Molecular and cellular biology* 20.21, pp. 7933–7942 (cit. on p. 16).

Scott, Matthew et al. (2010). “Interdependence of cell growth and gene expression: origins and consequences”. In: *Science* 330.6007, pp. 1099–1102 (cit. on pp. 8, 123).

Scott, Matthew et al. (2014). “Emergence of robust growth laws from optimal regulation of ribosome synthesis”. In: *Molecular systems biology* 10.8, p. 747 (cit. on p. 8).

Seedorf, Matthias and Pamela A Silver (1997). “Importin/karyopherin protein family members required for mRNA export from the nucleus”. In: *Proceedings of the National Academy of Sciences* 94.16, pp. 8590–8595 (cit. on p. 137).

Shachrai, Irit et al. (2010). “Cost of unneeded proteins in E. coli is reduced after several generations in exponential growth”. In: *Molecular cell* 38.5, pp. 758–767 (cit. on pp. 8, 45).

Shah, Premal et al. (2013). “Rate-Limiting Steps in Yeast Protein Translation”. In: *Cell* 7.153, pp. 1589–1601 (cit. on pp. 7, 17).

Shalem, Ophir et al. (2008). “Transient transcriptional responses to stress are generated by opposing effects of mRNA production and degradation”. In: *Molecular systems biology* 4.1, p. 4 (cit. on pp. 21, 45, 56).

Shalem, Ophir et al. (2011). “Transcriptome kinetics is governed by a genome-wide coupling of mRNA production and degradation: a role for RNA Pol II”. In: *PLoS genetics* 7.9, e1002273 (cit. on p. 21).

Sharif, Humayun and Elena Conti (2013). “Architecture of the lsm1-7-pat1 complex: a conserved assembly in eukaryotic mRNA turnover”. In: *Cell reports* 5.2, pp. 283–291 (cit. on pp. 11, 46).

She, Richard et al. (2017). “Comprehensive and quantitative mapping of RNA–protein interactions across a transcribed eukaryotic genome”. In: *Proceedings of the National Academy of Sciences* 114.14, pp. 3619–3624 (cit. on pp. 9, 17).

Shendure, Jay et al. (2017). “DNA sequencing at 40: past, present and future”. In: *Nature* 550.7676, p. 345 (cit. on p. 27).

Sherman, James M and William R Albus (1923). “Physiological youth in bacteria”. In: *Journal of bacteriology* 8.2, p. 127 (cit. on p. 131).

Sheth, Ujwal and Roy Parker (2003). “Decapping and decay of messenger RNA occur in cytoplasmic processing bodies”. In: *Science* 300.5620, pp. 805–808 (cit. on pp. 13, 19).

Simms, Carrie L, Liewei L Yan, and Hani S Zaher (2017). “Ribosome Collision Is Critical for Quality Control during No-Go Decay”. In: *Molecular cell* 68.2, pp. 361–373 (cit. on p. 15).

Slator, Arthur (1918). “Some observations on yeast growth”. In: *Biochemical Journal* 12.3, p. 248 (cit. on pp. 2, 123).

Sliva, Anna et al. (2016). “Barcode sequencing screen identifies SUB1 as a regulator of yeast pheromone inducible genes”. In: *G3: Genes, Genomes, Genetics* 6.4, pp. 881–892 (cit. on pp. 78, 81, 117).

Smith, Andrew M et al. (2009). “Quantitative phenotyping via deep barcode sequencing”. In: *Genome research* 19.10, pp. 1836–1842 (cit. on pp. 78, 82, 105, 106).

Smith, Justin D et al. (2016). “Quantitative CRISPR interference screens in yeast identify chemical-genetic interactions and new rules for guide RNA design”. In: *Genome biology* 17.1, p. 45 (cit. on p. 144).

Smith, Tom, Andreas Heger, and Ian Sudbery (2017). “UMI-tools: modeling sequencing errors in Unique Molecular Identifiers to improve quantification accuracy”. In: *Genome research* 27.3, pp. 491–499 (cit. on pp. 69, 107).

Spealman, Pieter et al. (2017). “Conserved non-AUG uORFs revealed by a novel regression analysis of ribosome profiling data”. In: *Genome research*, gr–221507 (cit. on p. 18).

Stanbrough, Michael and Boris Magasanik (1995). “Transcriptional and posttranslational regulation of the general amino acid permease of Saccharomyces cerevisiae.” In: *Journal of Bacteriology* 177.1, pp. 94–102 (cit. on pp. 5, 6, 46).

— (1996). “Two transcription factors, Gln3p and Nil1p, use the same GATAAG sites to activate the expression of GAP1 of Saccharomyces cerevisiae.” In: *Journal of bacteriology* 178.8, pp. 2465–2468 (cit. on p. 116).

Storey, John D and Robert Tibshirani (2003). “Statistical significance for genomewide studies”. In: *Proceedings of the National Academy of Sciences* 100.16, pp. 9440–9445 (cit. on p. 53).

Storey, John D. et al. (2015). *qvalue: Q-value estimation for false discovery rate control*. R package version 2.8.0. URL: `http://github.com/jdstorey/qvalue` (cit. on p. 76).

Storici, Francesca and Michael A Resnick (2006). “The delitto perfetto approach to in vivo site-directed mutagenesis and chromosome rearrangements with synthetic oligonucleotides in yeast”. In: *Methods in enzymology* 409, pp. 329–345 (cit. on p. 94).

Stracka, Daniele et al. (2014). “Nitrogen source activates TOR (target of rapamycin) complex 1 via glutamine and independently of Gtr/Rag proteins”. In: *Journal of Biological Chemistry* 289.36, pp. 25010–25020 (cit. on pp. 2, 4).

Sweet, Thomas, Carrie Kovalak, and Jeff Coller (2012). “The DEAD-box protein Dhh1 promotes decapping by slowing ribosome movement”. In: *PLoS biology* 10.6, e1001342 (cit. on p. 12).

Tagkopoulos, Ilias, Yir-Chung Liu, and Saeed Tavazoie (2008). “Predictive behavior within microbial genetic networks”. In: *science* 320.5881, pp. 1313–1317 (cit. on p. 1).

Talarek, Nicolas et al. (2010). “Initiation of the TORC1-regulated G 0 program requires Igo1/2, which license specific mRNAs to evade degradation via the 5-3 mRNA decay pathway”. In: *Molecular cell* 38.3, pp. 345–355 (cit. on pp. 21, 47).

Tate, Jennifer J and Terrance G Cooper (2013). “Five conditions commonly used to down-regulate tor complex 1 generate different physiological situations exhibiting distinct requirements and outcomes”. In: *Journal of Biological Chemistry* 288.38, pp. 27243–27262 (cit. on pp. 6, 46, 132).

Tate, Jennifer J et al. (2015). “GATA factor regulation in excess nitrogen occurs independently of Gtr-Ego complex-dependent TorC1 activation”. In: *G3: Genes, Genomes, Genetics* 5.8, pp. 1625–1638 (cit. on p. 6).

Tate, Jennifer J et al. (2017). “General Amino Acid Control and 14-3-3 Proteins Bmh1/2 Are Required for Nitrogen Catabolite Repression-Sensitive Regulation of Gln3 and Gat1 Localization”. In: *Genetics* 205.2, pp. 633–655 (cit. on pp. 2, 6, 46).

Tesnière, Catherine et al. (2017). “Relief from nitrogen starvation triggers a transient destabilization of glycolytic mRNAs in Saccharomyces cerevisiae cells”. In: *Molecular biology of the cell*, mbc–E17 (cit. on p. 115).

Tharun, Sundaresan (2009). “Lsm1-7-Pat1 complex: A link between 3and 5-ends in mRNA decay?” In: *RNA biology* 6.3, pp. 228–232 (cit. on p. 14).

Tharun, Sundaresan and Roy Parker (1999). “Analysis of mutations in the yeast mRNA decapping enzyme”. In: *Genetics* 151.4, pp. 1273–1285 (cit. on p. 12).

— (2001). “Targeting an mRNA for decapping: displacement of translation factors and association of the Lsm1p–7p complex on deadenylated yeast mRNAs”. In: *Molecular cell* 8.5, pp. 1075–1083 (cit. on p. 12).

Tharun, Sundaresan et al. (2000). “Yeast Sm-like proteins function in mRNA decapping and decay”. In: *Nature* 404.6777, p. 515 (cit. on pp. 11, 46).

Thattai, Mukund (2016). “Universal Poisson statistics of mRNAs with complex decay pathways”. In: *Biophysical journal* 110.2, pp. 301–305 (cit. on p. 25).

Thevelein, Johan M (1994). “Signal transduction in yeast”. In: *Yeast* 10.13, pp. 1753–1790 (cit. on p. 2).

Thomas, Linda K, Daniel B Dix, and Robert C Thompson (1988). “Codon choice and gene expression: synonymous codons differ in their ability to direct aminoacylated-transfer RNA binding to ribosomes in vitro”. In: *Proceedings of the National Academy of Sciences* 85.12, pp. 4242–4246 (cit. on p. 15).

Trcek, Tatjana et al. (2011). “Single-molecule mRNA decay measurements reveal promoter-regulated mRNA stability in yeast”. In: *Cell* 147.7, pp. 1484–1497 (cit. on pp. 17, 47).

Tutucci, Evelina et al. (2017). “An improved MS2 system for accurate reporting of the mRNA life cycle”. In: *Nature methods* (cit. on p. 19).

Van Dijck, Patrick et al. (2000). “Characterization of a new set of mutants deficient in fermentation-induced loss of stress resistance for use in frozen dough applications”. In: *International journal of food microbiology* 55.1, pp. 187–192 (cit. on p. 133).

Van Zeebroeck, Griet et al. (2009). “Transport and signaling via the amino acid binding site of the yeast Gap1 amino acid transceptor”. In: *Nature chemical biology* 5.1, p. 45 (cit. on p. 6).

VanderSluis, Benjamin et al. (2014). “Broad metabolic sensitivity profiling of a prototrophic yeast deletion collection”. In: *Genome biology* 15.4, R64 (cit. on pp. 78, 82, 96, 120, 121).

Waldron, C (1977). “Synthesis of ribosomal and transfer ribonucleic acids in yeast during a nutritional shift-up”. In: *Microbiology* 98.1, pp. 215–221 (cit. on pp. 2, 4, 123).

Waldron, CLIVE and FRANQOIS Lacroute (1975). “Effect of growth rate on the amounts of ribosomal and transfer ribonucleic acids in yeast.” In: *Journal of bacteriology* 122.3, pp. 855–865 (cit. on pp. 2, 123, 124).

Waldron, CLIVE, R Jund, and F Lacroute (1977). “Evidence for a high proportion of inactive ribosomes in slow-growing yeast cells”. In: *Biochemical Journal* 168.3, pp. 409–415 (cit. on pp. 7, 8).

Walters, Robert W et al. (2017). “Identification of NAD+ capped mRNAs in Saccharomyces cerevisiae”. In: *Proceedings of the National Academy of Sciences* 114.3, pp. 480–485 (cit. on p. 18).

Wehr, CT and LW Parks (1969). “Macromolecular synthesis in Saccharomyces cerevisiae in different growth media”. In: *Journal of bacteriology* 98.2, pp. 458–466 (cit. on pp. 8, 123).

Weinberg, David E et al. (2016). “Improved ribosome-footprint and mRNA measurements provide insights into dynamics and regulation of yeast translation”. In: *Cell reports* 14.7, pp. 1787–1799 (cit. on pp. 1, 16).

West, Sean M et al. (2018). “Developmental dynamics of gene expression and alternative polyadenylation in the Caenorhabditis elegans germline”. In: *Genome Biology* 19.1, p. 8 (cit. on p. 44).

Winderickx, Joris et al. (2003). “From feast to famine; adaptation to nutrient availability in yeast”. In: *Yeast stress responses*. Springer, pp. 305–386 (cit. on p. 2).

Worley, Jeremy et al. (2016). “Genome-Wide Analysis of the TORC1 and Osmotic Stress Signaling Network in Saccharomyces cerevisiae”. In: *G3: Genes, Genomes, Genetics* 6.2, pp. 463–474 (cit. on pp. 29, 78, 145).

Yao, Gang et al. (2007). “PAB1 self-association precludes its binding to poly (A), thereby accelerating CCR4 deadenylation in vivo”. In: *Molecular and cellular biology* 27.17, pp. 6243–6253 (cit. on p. 147).

Yin, Zhikang, Lee Hatton, and Alistair JP Brown (2000). “Differential post-transcriptional regulation of yeast mRNAs in response to high and low glucose concentrations”. In: *Molecular microbiology* 35.3, pp. 553–565 (cit. on p. 22).

Yin, Zhikang et al. (2003). “Glucose triggers different global responses in yeast, depending on the strength of the signal, and transiently stabilizes ribosomal protein mRNAs”. In: *Molecular microbiology* 48.3, pp. 713–724 (cit. on pp. 22, 39, 45).

Young, Elton T et al. (2012). “The AMP-activated protein kinase Snf1 regulates transcription factor binding, RNA polymerase II activity, and mRNA stability of glucose-repressed genes in Saccharomyces cerevisiae”. In: *Journal of Biological Chemistry* 287.34, pp. 29021–29034 (cit. on p. 47).

Yu, Hong et al. (1992). “Sensitive detection of RNAs in single cells by flow cytometry”. In: *Nucleic acids research* 20.1, pp. 83–88 (cit. on p. 29).

Yu, Lijian et al. (2016). “RNA polymerase II depletion promotes transcription of alternative mRNA species”. In: *BMC molecular biology* 17.1, p. 20 (cit. on p. 24).